



---

## Computational study of the structure and optical properties of perovskite solar cells materials

---

*Student:*

Adam Abdallah Kheralla  
(218074747)

*Supervisor:*

Prof. Naven Chetty

A thesis submitted in partial the fulfillment of the requirements for  
the degree PhD in Physics

School of Chemistry and Physics

College of Agriculture, Engineering and Science

University of KwaZulu-Natal, Pietermaritzburg Campus

South Africa.

2021

# Preface

The candidate carried out the work described in this thesis under the supervision and direction of Prof. Naven Chetty in the School of Chemistry and Physics in the College of Agriculture, Engineering, and Science of the University of Kwazulu Natal. This research was funded by (Prof. Chetty) and the Ministry of Higher Education, Scientific Research-Sudan, and the University of Kordofan Sudan. This work has not been submitted for any qualification at another institute.

Signature (Student):.......... Date:2<sup>th</sup> July, 2021.

Signature (Supervisor):..... Date:.....2021.

# Abstract

Perovskite solar cells have performed a high power conversion efficiency with a credible certified value of over 25%. The perovskite materials possess a unique blend from low bulk snare concentrations, optical absorption properties, extended charge carrier diffusion and charge transport/collection properties, making them favourable for solar cell devices. Computational simulation is considered vital technology to know the properties of the different compounds, determine the operating mechanism of solar cells, predict the maximum value of controlled design, and guide the structural optimization of different devices.

This project investigates transition metal iodide perovskite  $Cs_2HfI_6$  to determine the electronic structure and optical properties. We have used Density Function Theory (DFT), as utilized in the quantum-espresso code. Our result suggests that this compound may be helpful in the future instead of the toxicity element Pb due to suitable better band gap and optical properties, representing the suitability of the  $Cs_2HfI_6$  in the solar cells.

# Dedication

*To*

*my parents*

*my wife, Jowiria*

*my son, Anas*

*Prof. Naven Chetty*

*I dedicate this study.*

# Declaration 1- Plagiarism

**I, Adam Abdalla Kheralla, declare that:**

1. The research reported in this thesis, except where otherwise indicated, is my own original research.
2. This project has not been submitted for any degree or examination at any other instation.
3. This project does not contain other persons data, pictures, graphs or other information, unless specifically acknowledged as being sourced from other persons.
4. This project does not contain other persons writing, unless specifically acknowledged as being sourced from other researchers. Where other written sources have been quoted, then:
  - Their words have been re-written but the general information attributed to them has been referenced.
  - Where their exact words have been used. then their writing has been placed in italics and inside quotation marks, and referenced.
5. This project does not contain text, graphics or tables copied and pasted from the Internet, unless specifically acknowledged, and the source being detailed the thesis and in the references sections.

Signed: \_\_\_\_\_

Date: 2<sup>th</sup> July, 2021

## Publications

### Declaration - Publications

I declare that the contents of this dissertation is based on each paper as indicated below.

1. **N. Chetty** and A. Kheralla, A review of experimental and computational attempts to remedy stability issues of perovskite solar cells, Journal of Heliyon /10.1016/j.heliyon.(2021).e06211.
2. **N. Chetty** and A. Kheralla, Investigation of the structural and electronic properties of  $Cs_2HfI_6$  using (DFT),(2021) preprint.

# Acknowledgment

I would like to thank my God for his grace. My deepest thank to my supervisor Professor Naven Chetty He always gave me excellent motivation and constructive guidelines throughout PhD journey as well as his continuous support me to reach my aim of a PhD.

I thank my family. I thank my wife for all our joys of life, I thank you for moving from Sudan to South Africa and always being there with me through my brightest days and darkest hours along this journey. You bring happiness and encouragement in the pursuit of my dreams.

My thanks extend to the Ministry of Higher Education Scientific research, University of Kordofan, Kordofan, Sudan, for their financial support. I express my thank to the University of KwaZulu-Natal (UKZN), South Africa, for offering me opportunities to conduct my Ph.D study. Moreover, I thank my colleagues, in particular, Prof. Chetty's research group for their support me.

---

# List of Abbreviation

PV	photo voltaic
A	Acceptor
OPV	organic photo voltaic cells
PSCs	Perovskite Solar Cells
DFT	Density Functional Theory
$Li_2TiO_3$	lithium Titanium Oxide
$Cs_2HfI_6$	Cesium Hafnium iodide perovskite
D	Donor
DSSCs	Dye-sensitized solar cells
Eg	Energy gap
ETL	Electron transport layer
FF	Fill factor
FTO	Fluorine-doped tin oxide
HTL	Hole transport layer
HOMO	Higher occupied molecular orbital
ITO	Indium tin oxide
$J_{sc}$	Short circuit current
J-V	Current density-voltage Curve
LUMO	Lower unoccupied molecular orbital
KS	Kohn-Sham Equations
LDA	Local Density Approximation

GGA	Generalised Gradient Approximations
Meta-GGA	Meta-Generalised Gradient Approximation
OSCs	Organic solar cells
P3HT	Poly (3-hexylthiophene)
PCE	Power conversion efficiency
PCBM	[6,6]-phenyl-C61-butyric acid methyl ester
PL	Photoluminiscence
$P_{max}$	Maximum power
QE	Quantum espresso
$\varepsilon(\omega)$	dielectric function
SCF	self-consistent calculation
nSCF	nonselself-consistent calculation
DOS	Density of state
MD	Molecular Dynamics
$n(\omega)$	refractive index
$\kappa(\omega)$	extinction coefficient
PBE	Perdew-Burke-Ernzerhof
$\alpha(\omega)$	absorption coefficient

---

# List of Figures

3.1	A flowchart that describes an SCF in QE implementation of DFT. . . .	22
3.2	Electronic band structure. . . . .	24
3.3	Calculated total DOS and Band structures. . . . .	28
3.4	complex dielectric of $Li_2TiO_3$ optical coefficients for all direction . . .	29
3.5	Reflectivity index of $Li_2TiO_3$ . . . . .	30
4.1	Gradual increase of efficiency (a) and (b) research output of perovskite based solar cells [8, 9]. . . . .	37
4.2	Architectures of perovskite solar cells (a) device structure and (b) band diagram. . . . .	39
4.3	Work principles of Perovskite Solar Cells [20]. . . . .	40
4.4	Sun irradiance and bandgap of PSCs with permission from [39, 108].	43
4.5	Relationship between solar cell efficiency limits and band gap with Shockley-Queisser wide balance range [48]. . . . .	46
4.6	UPS with IPES spectrum of $MAPbI_3$ in(a) linear (B) Semi-logarithmic graph. Compare this with the case density calculated by <i>DFT</i> [51]. . .	47
4.7	J-V characteristics produced by vapour deposition and solution deposition of the PSCs [3]. . . . .	49

4.8	Different perovskite film preparation methods [81]. . . . .	49
4.9	Number of <i>DFT</i> papers published based approximation function with citations [85]. . . . .	52
4.10	Calculated goldsmiths tolerance factor for some materials [112], Copyright 2015, The Royal Society of Chemistry . . . . .	55
4.11	Exfoliated montmorillonite nanosheets to improve the environmental stability of <i>MAPbI<sub>3</sub></i> (b) Relative humidity of the <i>MAPbI<sub>3</sub></i> with the environmental condition around the film (c) Relative humidity of the <i>MAPbI<sub>3</sub></i> at room temperature with constant sunlight [114]. . . . .	56
4.12	(A) LBIC mapping development of perovskite/SWCNT devices under high humidity conditions, (b) stability testing of perovskite/SWCNT devices under high humidity conditions [123]. . . . .	58
4.13	Simulation results of Thermal instability of <i>PSCs</i> [126, 127]. . . . .	60
4.14	(a) operating device temperature curve, (b) a temperature-time graph under the sun [129]. . . . .	61
4.15	<i>UV</i> degradation/recovery cycle of perovskite device performance [141].	62
4.16	Diagram of ion migration in perovskites solar cells [141]. . . . .	64
5.1	DOS and PDOS for <i>Cs<sub>2</sub>HfI<sub>6</sub></i> . . . . .	85
5.2	Band gap structure of <i>Cs<sub>2</sub>HfI<sub>6</sub></i> perovskite. . . . .	85
5.3	The real and imaginary parts of dielectric function of <i>Cs<sub>2</sub>HfI<sub>6</sub></i> per- ovskite as a function of Photon energy. . . . .	87

5.4	The absorption coefficient of $Cs_2HfI_6$ perovskite as a function Photon energy. . . . .	87
5.5	Refractive index real part of $Cs_2HfI_6$ . . . . .	88
5.6	Reflectivity index of $Cs_2HfI_6$ . . . . .	88

---

# List of Tables

4.1	Summary of reported calculated band gap by computational of perovskite solar cell materials ( $ABX_3$ , X= S, Se) . . . . .	47
-----	---	----

---

# Contents

<b>List of Figures</b> . . . . .	<b>x</b>
<b>List of Tables</b> . . . . .	<b>xiii</b>
<b>1 Solar Energy</b> . . . . .	<b>2</b>
1.1 Challenges and opportunities . . . . .	2
1.2 Aim of the thesis . . . . .	4
1.3 Objectives of the thesis . . . . .	4
1.4 Outline of this thesis . . . . .	5
<b>References</b> . . . . .	<b>6</b>
<b>2 Computational Approaches</b> . . . . .	<b>8</b>
2.1 Density Function Theory ( <i>DFT</i> ) . . . . .	8
2.2 Schrodinger Equation . . . . .	9
2.2.1 Energy Functional . . . . .	10
2.3 Born-Oppenheimer approximation . . . . .	12

2.3.1	External Potential . . . . .	12
2.4	Hohenberg-Kohn theorem . . . . .	13
2.5	Kohn-Sham equations (KS) . . . . .	14
2.6	The Exchange-Correlation Functional . . . . .	15
2.6.1	Local Density Approximation . . . . .	15
2.6.2	The Generalised Gradient Approximations . . . . .	16
2.6.3	Meta-Generalised Gradient Approximation . . . . .	16
2.7	Summary . . . . .	17
<b>References . . . . .</b>		<b>18</b>
<b>3</b>	<b>Plan of the Calculations . . . . .</b>	<b>20</b>
3.1	Quantum Espresso (QE) . . . . .	20
3.2	Pseudopotentials . . . . .	21
3.3	Fermi energy . . . . .	23
3.4	Electronic band structure . . . . .	23
3.5	Density of states (DOS) . . . . .	24
3.6	Optical properties . . . . .	25
3.7	Introduction to the properties of lithium titanium oxide $Li_2TiO_3$ . . . . .	26

3.8	Computational Details . . . . .	27
3.8.1	Methodology . . . . .	27
3.9	Results and Discussions . . . . .	28
3.9.1	Density of States of $Li_2TiO_3$ . . . . .	28
3.9.2	Band Structures . . . . .	28
3.10	Optical properties of $Li_2TiO_3$ . . . . .	29
3.11	Conclusion . . . . .	30
	<b>References . . . . .</b>	<b>32</b>
<b>4</b>	<b>A review of experimental and computational attempts to remedy stability issues of perovskite solar cells . . . . .</b>	<b>35</b>
4.1	Abstract . . . . .	35
4.2	Introduction . . . . .	36
4.3	Architectures of perovskite solar cells . . . . .	38
4.4	Working principles of perovskite solar absorber . . . . .	39
4.5	Perovskite based solar cells evolution . . . . .	41
4.6	Band Gap of Perovskites . . . . .	42
4.6.1	Binding Energy . . . . .	45
4.7	Perovskite Chalcogenide . . . . .	46

4.8	Design/Fabrication Approaches . . . . .	48
4.8.1	Experimental Approach . . . . .	48
4.8.2	Computational Approach . . . . .	50
4.8.3	Density Function Theory . . . . .	51
4.9	Stability of Perovskite Solar Cells . . . . .	53
4.9.1	Moisture instability . . . . .	54
4.9.2	UV instability . . . . .	61
4.10	Hysteresis Effects . . . . .	63
4.11	Conclusions and perspectives . . . . .	65
	<b>References . . . . .</b>	<b>66</b>
<b>5</b>	<b>Investigation of the structural and electronic properties of <math>Cs_2HfI_6</math> using (DFT) . . . . .</b>	<b>81</b>
5.1	Abstract . . . . .	81
5.2	Introduction . . . . .	81
5.3	Computational Details . . . . .	84
5.3.1	Methodology . . . . .	84
5.4	Results and Discussions . . . . .	84
5.5	Geometric Structure . . . . .	84

5.6	Band structure of $Cs_2HfI_6$ and Density of State . . . . .	86
5.7	Optical Properties of $Cs_2HfI_6$ . . . . .	86
	<b>References . . . . .</b>	<b>90</b>
<b>6</b>	<b>Summary and future work . . . . .</b>	<b>93</b>
6.1	Summary . . . . .	93
6.2	Future work . . . . .	94

---

# CHAPTER 1

## Solar Energy

### 1.1 Challenges and opportunities

The main challenges in energy supply are the increasing ever demand energy due to the rapid development of the economy and increasing world population. Using fossil fuels has caused global environmental degradation, climate change and global warming, and carbon dioxide emission into the atmosphere [1]. Currently, the world counts heavily on non-renewable and polluting energy sources, including coal, natural gas, and oil which will be depleted in the near future [2]. These resources have unsustainable consequences on social, economic, geopolitical and environmental issues. Therefore, we need to focus on alternative energy sources to prevent the future incidence of energy crises. One of the alternative green energy sources is solar energy, which remains an untapped potential at present [3]. Since implementing the concept of using solar energy, it has been a challenge to find a mechanism to convert solar energy into electricity. The premier generation solar cells were manufactured based on crystalline silicon and have dominated the photovoltaic (PV) market for the past half-century [4]. However, the processing cost of crystalline silicon-based solar cells is high, and silicon wafers' processing residues are not environmentally friendly [4]. The second generation of photovoltaic technology utilizes thin-film inorganic compounds and usually requires vacuum vapour deposition to prepare high-energy thin films [5]. The third generation of photovoltaic technology is solution-processable thin-film solar cells, including concentrator cells, organic photovoltaic cells (OPV) and dye-Sensitized solar cells (DSSC) [6]. Recently, perovskite-based solar cells have become the fourth generation of photovoltaic tech-

nology, originating from the concept of dye-sensitized solar cells. Due to their high power conversion efficiency and low cost in a short period, they have attracted much attention in a concise period [7]. The current demand for power worldwide is increasing dramatically. Future projection of energy consumption in the United States shows that the demand will increase with time progress, and energy consumption will be greater than energy production [8]. There are plenty of renewable energy sources, including wind, hydro, nuclear, solar energy, etc. Solar energy is the first renewable energy source, which is considered a great solution to meet the growing energy demand [9]. Most research currently focuses on the Perovskite Solar Cells (PSCs), where the conversion of light into electricity begins. We use computational way, density functional theory approach (DFT), to study perovskite materials and understand their structural, electronic, and optical properties.

## 1.2 Aim of the thesis

This PhD thesis aims to investigate the properties of perovskite materials. The investigation is dependent on a systematic computational study to provide information about the perovskite compounds structure and optical properties as promising materials for solar cells applications.

## 1.3 Objectives of the thesis

Motivated by their potential perovskite solar cells applications, the project study focused on perovskite materials.

- Computational study of the  $Li_2TiO_3$ ,  $Cs_2HfI_6$  to determine the optical properties.
- To understand and estimate the electronic and optical properties of the perovskite solar cells based on the density functional theory approach.

## 1.4 Outline of this thesis

We briefly summarize the topics covered in the theses to follow (chapters 1-6).

**Chapter One** : Introduces current challenges and opportunities of solar energy and the aims of this study and outlines.

**Chapter Two** : Provides a theoretical background, of the Density Functional Theory (DFT) and exchange-correlation approximations.

**Chapter Three** : Provides the plan of calculation methods and example of the electronic structure and optical properties of  $Li_2TiO_3$ .

**Chapter Four** : Literature review of the evolution in the perovskite. Details of the structures in the current work, the experimental and computational approaches. Recent progress in resolving the stability challenges that influence device performance is considered and discussed in this chapter's main body as emerged from a published paper.

**Chapter Five** : The use of (DFT) to determine the structure and electronic properties of transition metal iodide perovskite  $CS_2XI_6$  ( $X = Hf$ ) as promising compound for perovskite devices.

**Chapter Six** : Outlines the conclusions made from this work and possible future work of the study.

---

## References

- [1] N. Saiqa, R. Sultan, K. Zaman, A. Mohammed Aldakhil, Abdelmohsen A Nassani. *Moderating and mediating role of renewable energy consumption, fdi inflows, and economic growth on carbon dioxide emissions: evidence from robust least square estimator. Environmental Science and Pollution Research*, 26(3):2806–2819,(2019).
- [2] Shahriar Shafiee and Erkan Topal. *When will fossil fuel reserves be diminished. Energy policy*, 37(1):181–189,(2009).
- [3] Sunita Satyapal. *Hydrogen fuel cells program overview. In 2011 Annual Merit Review and Peer Evaluation Meeting, Fuel Cell Technology Program, Office of Energy Efficiency and Renewable Energy, US Department of Energy, Washington, DC,(2011).*
- [4] Daryl M. Chapin, C.S Fuller, and G.L Pearson. *A new silicon p-n junction photo-cell for converting solar radiation into electrical power. Journal of Applied Physics*, 25(5):676–677(1954).
- [5] Taher M El-Agez, Ahmed A El Tayyan, Amal Al-Kahlout, Sofyan A Taya, and Monzir S Abdel-Latif. *Dye-sensitized solar cells based on zno films and natural dyes. International Journal of Materials and Chemistry*, 2(3):105–110,(2012).
- [6] Jin Cui, Huailiang Yuan, Junpeng Li, Xiaobao Xu, Yan Shen, Hong Lin, and Mingkui Wang. *Recent progress in efficient hybrid lead halide perovskite solar cells. Science and technology of advanced materials*, 16(3):036004,(2015).
- [7] Samrana Kazim, Mohammad Khaja Nazeeruddin, Michael Grätzel, and Shahzada Ahmad. *Perovskite as light harvester: a game changer in photovoltaics. Angewandte Chemie International Edition*, 53(11):2812–2824,(2014).
- [8] US Energy Information Administration et al. *Annual Energy Outlook 2011: With Projections to 2035. Government Printing Office, (2011).*

- [9] *Luyao Lu, Tianyue Zheng, Qinghe Wu, Alexander M Schneider, Donglin Zhao, and Luping Yu. Recent advances in bulk heterojunction polymer solar cells. Chemical reviews, 115(23):12666–12731, 2015.*

---

## CHAPTER 2

# Computational Approaches

This chapter aims to outline theoretical background of the Density Function Theory (*DFT*) and summarize its different approximations methods

### 2.1 Density Function Theory (*DFT*)

Predicting the behavior of many numbers of reactive particles for the scientific community is still difficult to verify their properties. The principles of density functional theory are explained in detail by referring to wave theory [1]. Wave theory has been used in quantum mechanics to describe the behavior of particles called quantum particles [2]. Thus we use quantum mechanics principles to build to density functional theory due to the wave function expressing particle, which can be reacting with other electrons and nuclei in the system. To solve this complex problem, scientists have adopted a method to circumvent the electrons more massive nuclei from that of the electron. Most electronic problems are often referred to as the study of electronic structures, these studies can help predict properties of materials structure, mechanics, dynamics, thermodynamics, electronics, and optic. Recently density function theory shows that it is a popular and effective quantum mechanics approaches to solve these problems [3]. If we consider a simple system like the hydrogen atom, the wave function and quantum mechanics consist of all the information required for the system [4]. Solving a Schrodinger equation we can determine the permitted energy state of the system. Regrettably, it is unattainable to solve the Schrodinger equation for an N-body system [5]. Therefore which is the the quantum mechanics principle can be used to build density functional theory

with an approximation. Density function theory is an approach to obtaining the approximation solution of the Schrodinger equation [6].

## 2.2 Schrodinger Equation

Solving the Schrodinger equation of the N-body system is a problem due to many atoms and electrons [7]. Schrodinger equation is given by:

$$\hat{H}\Psi(r_1, r_2, \dots, r_N) = E\Psi(r_1, r_2, \dots, r_N), \quad (2.1)$$

where  $\hat{H}$  is Hamiltonian that represents the total of the kinetic energy,  $E$  is the energy  $\Psi$  is wave function is given by [7]:

$$\Psi = \Psi(r_1, r_2, \dots, r_N), \quad (2.2)$$

and  $\hat{H}$  is given by [7]:

$$\hat{H} = \hat{T} + \hat{V}_{ee} + \hat{U}_{ei}, \quad (2.3)$$

where  $T$  is Kinetic energy:

$$\hat{T} = \frac{-\hbar^2}{2m} \sum_i \nabla_i^2, \quad (2.4)$$

$V_{ee}$  is represent the electron-electron interaction:

$$V_{ee} = \frac{1}{2} \sum_i \frac{e^2}{|r_i - r_j|}, \quad (2.5)$$

and  $V_{ext}$  is represent the interaction with the external potential:

$$V_{ei} = \frac{-\hbar^2}{2m} \sum_{i,j} \frac{(Z_i)e^2}{|\hat{R}_i - r_j|}. \quad (2.6)$$

The total energy is given by:

$$E[\Psi] = \langle \Psi | \hat{H} | \Psi \rangle, \quad (2.7)$$

where

$$E[\Psi] \geq E_0,$$

$E_0$  is the ground state energy. The ground state wave function and energy may be found by searching all possible wave functions for the one that minimizes the total energy [8]. We will deal with minimization of the functional later. Our goal is to write the functional as a function of the electron density  $n(r)$ . For an  $N$ -body system

$$n(\bar{r}) = N \int d^3\bar{r}_2 \dots \int d^3\bar{r}_N \Psi^*(\bar{r}, \bar{r}_2 \dots \bar{r}_N) \Psi(\bar{r}, \bar{r}_2 \dots \bar{r}_N). \quad (2.8)$$

We assume that we can invert the expression in the case of the ground state so that the wave function as a function of the ground-state electron density.

$$\Psi_0 = \Psi_0[n_0(\bar{r})], \quad (2.9)$$

where  $n_0(\bar{r})$  or  $n_0$  is the ground state. The ground state energy is then written as

$$E_0 = \langle \Psi_0 | \hat{H} | \Psi_0 \rangle, \quad (2.10)$$

or

$$E_0 = \langle \Psi_0[n_0] | \hat{H} | \Psi_0[n_0] \rangle, \quad (2.11)$$

usually (not necessarily the  $E_0$  of the system), yields [1]

$$E = \langle \Psi[n] | \hat{H} | \Psi[n] \rangle. \quad (2.12)$$

## 2.2.1 Energy Functional

Since  $\Psi$  can be expressed as a function of  $n(r)$ , it follows that the energy functional which was expressed in terms of  $\Psi$  can be expressed in terms of  $n(r)$ . Thus we will have [8]:

$$E[n] = T[n] + V[n] + U[n], \quad (2.13)$$

where the  $T[n]$  is the kinetic energy,  $V[n]$  is the interaction with the external potential, and  $U[n]$  is the electron-electron interaction [8]:

$$V[n] = \int d^3r \hat{V}(r)n(r), \quad (2.14)$$

then

$$E[n] = T[n] + \int d^3r \hat{V}(r)n(r) + U[n]. \quad (2.15)$$

Now, we do not know the explicit expression of kinetic and electron-electron interaction functional. Kohn and Shan [9]. proposed to map the original system to a non-interacting electronic system with effective potential which simulates the real system. Since electrons are non-interactive and their coordinates are decoupled, their wave function is the output of the single-electron wave function  $\phi_i(r_i)$  called orbitals. The kinetic energy and the density of such a system are given by [9]:

$$T_s[n] = -\frac{1}{2} \sum_i^N \langle \phi_i | \nabla^2 | \phi_i \rangle, \quad (2.16)$$

$$n_s(r) = n(r) = \sum_{i=1}^N |\phi_i(r)|^2, \quad (2.17)$$

where the subscripts s show that its not the real system, and we have

$$\phi(r_1, r_2 \dots r_N) = \phi_1(r_1)\phi_2(r_2)\dots\phi_N(r_N), \quad (2.18)$$

Since the most crucial section of electron-electron interaction comes from Coulomb interaction (Hartree energy), it is physically correct to separate electron-electron interaction into Hartree energy and exchange-correlation contribution. This is because we can correlate exchange contribution is regarded as a disturbance to the total electron-electron energy [2]

$$E[n] = T[n] + V[n] + V_H[n] + E_{xc}[n], \quad (2.19)$$

where

$$V_H[n] = \frac{1}{2} \int \frac{n(r_1)n(r_2)}{|r_1 - r_2|} dr_1 dr_2. \quad (2.20)$$

where  $E_{xc}[n]$  is the exchange-correlation function. It represents the difference between the energy of the original system and the energy of a system of electrons interacting classically through a pairwise Coulomb potential and subject to an external potential. Over the years many approaches advanced to a solution to the challenges of electronic structure, such as the Hartree and Fock approach, the Thomas and Fermi approach, and DFT [8].

## 2.3 Born-Oppenheimer approximation

All *DFT* calculations for solids are made assuming the Born-Oppenheimer approximation. We will discuss this approximation from Newton law:

$$F_1 = F_2 = Fa_1 = \frac{F}{M}a_2 = \frac{-F}{m}V_1 = \frac{F\Delta t}{M}V_2 = \frac{F\Delta t}{m} \Rightarrow V_1 \ll V_2 \quad (2.21)$$

If we freeze the nuclear position equal to the Born-Oppenheimer approximation, we can express it as a variable of function with a parameter [12]

$$\Psi(X_1, Y_1, Z_1, \alpha_1, \dots, X_N, Y_N, Z_N, \alpha_N; \hat{R}_1, \dots, \hat{R}_N) \quad (2.22)$$

simplified Hamiltonian the Born-Oppenheimer approximation is major simplified, but still the resulting the equation is way too hard to solve [10]:

$$\hat{H} = -\sum_i \frac{\nabla^2}{M_i} - \sum_i \frac{\nabla^2}{m_i} - \sum_{i,j} \frac{(Z_i)e}{|\bar{R}_i - \bar{r}_j|} + \frac{1}{2} \sum_{ij} \frac{e^2}{|\bar{r}_i - \bar{r}_j|} + \frac{1}{2} \sum_{ij} \frac{(eZ_i)(eZ_j)}{|\bar{R}_i - \bar{R}_j|}. \quad (2.23)$$

### 2.3.1 External Potential

The following equations give the electron density operator for one electron [11].

$$\hat{\rho}(\hat{r}) = \hat{\delta}(\hat{r}'\hat{r}), \quad (2.24)$$

the electron density for one electron is [11]

$$\hat{\rho}(\hat{r}) = \langle \Psi | \hat{\rho}(\hat{r}) | \Psi \rangle = \int \Psi^*(\hat{r}) \Psi(\hat{r}) \delta(\hat{r}' - \hat{r}) d\hat{r}' = \Psi^* \hat{r} \Psi \hat{r} = |\Psi(\hat{r})|^2. \quad (2.25)$$

This is interpretation probability to find the electron at  $r$  position for many  $N$  electron.

$$\hat{\rho}(\hat{r}) = \sum_i = 2^N \delta(\hat{r}' - \hat{r}), \quad (2.26)$$

$$\hat{\rho}(\hat{r}) = \sum_i \int \Psi^*(\hat{r}_1, \dots, \hat{r}_i = \hat{r}, \dots, \hat{r}_N) \Psi(\hat{r}_1, \dots, \hat{r}_i = (\hat{r}_1, \dots, \hat{r}_N)) d\hat{r}_1, \dots, d\hat{r}_N = \sum_i |\Psi(\hat{r}_i)|^2. \quad (2.27)$$

The probability of finding any electron, can only be written by one-electron with function as show in (Eq.2.27).

## 2.4 Hohenberg-Kohn theorem

An alternative to the ground state solution in two theorems consider as the cornerstone of DFT by Hohenberg and Kohn [10]. The first theorem is the external potential  $V_{ext}(r)$  and, therefore, the total energy is a unique function of the state. This electron determines the position of the atomic nucleus in the system and all the electronic properties of ground states because the number of electrons  $N$  defines the Hamiltonian of the system  $V_{ext}(r)$  [10]. Second theorem is variable  $E_0$  can acquire the density that minimizes the total energy is the exact ground-state density. Then the correct intensity that minimizes energy is then the density of the ground state [11, 12].

$$E_0 = \langle \Psi_0 | H | \Psi_0 \rangle, \quad (2.28)$$

$$E'_0 = \langle \Psi'_0 | H' | \Psi'_0 \rangle, \quad (2.29)$$

$$E_0 = \langle \Psi_0 | H | \Psi_0 \rangle \langle \Psi'_0 | H' - (V'_{ei} - V_{ei}) | \Psi'_0 \rangle = E'_0 - \langle \Psi'_0 | V'_{ei} - V_{ei} \rangle, \quad (2.30)$$

$$\langle \Psi'_0 | V'_{ei} - V_{ei} | \Psi'_0 \rangle = \sum_i \langle \Psi'_0 | V'_{ion}(r_i) - V_{ion}(r_i) | \Psi'_0 \rangle = \int dr n_0(r) (V'_{ion}(r) - V_{ion}(r)), \quad (2.31)$$

$$E_0 < E'_0 - \int dr n_0(r)(V'_{ion}(r) - V_{ion}(r)), \quad (2.32)$$

$$E'_0 < E_0 - \int dr n_0(r)(V_{ion}(r) - V'_{ion}(r)), \quad (2.33)$$

$$E_0 + E'_0 < E'_0 + E_0, \quad (2.34)$$

$$F[n] = \Psi_0[n]|T + V_{ee}|\Psi_0[n], \quad (2.35)$$

$$E[n] = \int dr n(r)V_{ext}(r) - V_{ion}(r) + F[n], \quad (2.36)$$

$$E_0 = E[n_0(r)] = \langle \Psi_0[n_0]|H|\Psi_0[n_0] \rangle \leq \langle \Psi_0[n]|H|\Psi_0[n] \rangle. \quad (2.37)$$

From the above first theorem one can conclude that if we know the ground state particle density its possible to reconstruct the new Hamiltonian. Schrodinger equation was used to solve the new many body wave functions for new Hamiltonian. They are independent of number of particles and purely dependent on electron density, the Second theorem states that the exact ground state is the global minimum value of the functional.

## 2.5 Kohn-Sham equations (KS)

Kohn and Sham introduced one-particle orbitals to approximate the kinetic and exchange-correlation energies; it is a widely applied electronic structure theory, which attains the best adjustment between precision and cost [9]. Practical *DFT* is nearly always done within the framework established by Kohn-Sham in 1965, the exact ground state density of N-electron [9] given by:

$$\hat{H}_{(KS)}\varphi_i = \varepsilon_i\varphi_i, \quad (2.38)$$

$$\hat{H}_{(KS)} = \hat{T}_0 + \hat{V}_H + \hat{V}_{ext} + \hat{V}_{xc}, \quad (2.39)$$

$$\hat{H}_{(KS)} = \frac{-\hbar^2}{2m} \nabla_i^2 + \frac{e^2}{4\pi\epsilon_0} \int \frac{\rho(\vec{r}')}{|\vec{r} - \vec{r}'|} d\vec{r}' + \hat{V}_{ext} + \hat{V}_{xc}, \quad (2.40)$$

$$\hat{V}_{xc} = \frac{\delta V_{xc}\rho}{\delta p}. \quad (2.41)$$

The Kohn-Sham equation is an exact transformation of the original problem, which coupled differential equation, in the single-particle equation, means uncoupled. If we compare Kohn-Sham equation with Schrodinger equation; we will find the Kohn-Sham equation is much easier mathematically. Still, it has to know this term to discuss this, such as in the section of exchange-correlation functional.

## 2.6 The Exchange-Correlation Functional

Thus the electron correlation is another important concept and it is the property that rises most of the hurdles for finding the exact solution of the quantum system molecule or solid [13]. However, the biggest challenge density-functional theory face is that the exchange-correlation term doesn't have an exact expression. It is that reason that forces the use of approximations.

### 2.6.1 Local Density Approximation

*LDA* is considered as the most utilizing approximations is the simplest  $V_{xc}$  approximations and has proven to be very successful in many systems, here the exchange correlation function is given by [14]:

$$E_{xc} = \int E_{xc}(n)n(r)d^3r, \quad (2.42)$$

where  $E_{xc}(n)$  is the exchange and correlation energy density of the uniform electron gas. Properties such as structure, vibration frequencies, elastic moduli, and phase stability are described reliably for many systems. However, in computing energy differences between rather different structures, the *LDA* can bring significant errors.  $E_{xc}(n)$  is the exchange-correlation function density of the uniform electron gas. The term doesn't have an exact expression, and this has led to the use of approximations such as the Local Density Approximation (*LDA*) considered the first and most used approximation transforming the problem into a non-interacting sys-

tem in an effective potential [16]. These approximations are used to calculate the electron structure, From which different ground-state properties such as structural, magnetic, optical, mechanical, etc. of materials can be calculated [14]. The *LDA* can have significant errors, in computing energy differences between rather different structures.

## 2.6.2 The Generalised Gradient Approximations

The Generalised gradient approximation *GGA* is an exchange-correlation function that depends on the density and its derivative, and it is given by. The local density approximation can be considered to be the zeroth order approximation to the semi-classical expansion of the density matrix in terms of the density and its derivatives. A natural progression beyond the *LDA* is thus to the gradient expansion approximation (*GGA*) in which first-order gradient terms in the expansion are included [15, 17]. This leads to an exchange-correlation functional that depends on the density and its derivative, given by:

$$E_{xc} = \int \epsilon_{xc}(n, \nabla n) n(r) d^3 r, \quad (2.43)$$

This approximation it is improves significantly on the *LDA* description by determine the binding energy of molecules.

## 2.6.3 Meta-Generalised Gradient Approximation

The is another functional called *Meta – GGA* functional, which includes the second derivative of the electron density [17]. it is written as:

$$E_{xc} = \int \epsilon_{xc}(n, |\nabla n|, \nabla^2 n, \tau) n(r) d^3 r, \quad (2.44)$$

$\tau$  is:

$$\tau = \frac{1}{2} \sum_i |\nabla \phi_i|^2. \quad (2.45)$$

## 2.7 Summary

This chapter aimed to provide a detailed theoretical background on the density functional theory and approximation. Density function theory is considered an efficient tool to compute the ground state energy in realistic models of bulk materials and their surfaces. The use of *DFT* in materials science has recently increased many folds and is now one of the preferred methods for examining materials. In implementations of *DFT*, different approximations are used to calculate the electron structure. All electronic structure properties can be calculated when determining the ground state energy for materials, e.g. structural, magnetic, optical, mechanical. Significant advances have been made in the quality of exchange-correlation functional as follows. *LDA* was the first and simplest approximation for the exchange and correlation functional, were to assume that the electrons would behave like a homogeneous gas. In this case, the effects of the exchange and correlation are local. Kohn and Sham made *LDA*. Their  $E_{xc}$  is an overall integral space, assuming that the exchange-correlation energy density is the same as a homogeneous electron gas at each point. It underestimates the band gap by up to 50%, and it wrongly predicts the magnetic properties of bulk materials. *GGA* it has marked improvements over *LDA* for many reasons describes an in homogeneous electron system. However, *GGA* gives better results for the ground state energies, for predicting molecular geometries, and predicting the magnetic properties of three domination transition metals [14, 15, 17].

---

# References

- [1] Robert G Parr. *W. yang density functional theory of atoms and molecules*. Oxford University Press, 1:989, 1989.
- [2] Anthony C Phillips. *Introduction to quantum mechanics*. John Wiley Sons, 2013.
- [3] Richard C Remsing, Michael L Klein, and Jianwei Sun. *Dependence of the structure and dynamics of liquid silicon on the choice of density functional approximation*. *Physical Review B*, 96(2):024203, 2017.
- [4] Kieron Burke. *Perspective on density functional theory*. *The Journal of chemical physics*, 136(15):150901, 2012.
- [5] K.I Ramachandran, Gopakumar Deepa, and Krishnan Namboori. *Computational chemistry and molecular modeling: principles and applications*. Springer Science Business Media, 2008.
- [6] Walter Kohn, Axel D Becke, and Robert G Parr. *Density functional theory of electronic structure*. *The Journal of Physical Chemistry*, 100(31):12974–12980, 1996.
- [7] John S Briggs and Jan M Rost. *On the derivation of the time-dependent equation of schrödinger*. *Foundations of Physics*, 31(4):693–712, 2001.
- [8] N.M Harrison. *An introduction to density functional theory*. *Nato Science Series Sub Series III Computer and Systems Sciences*, 187:45–70, 2003.
- [9] Walter Kohn and Lu. Jeu Sham. *Self-consistent equations including exchange and correlation effects*. *Physical review*, 140(4A):A1133, 1965.
- [10] P Hohenberg and WKohn. *Inhomogeneous electron gas* *physical review* 136. B864, 1964.
- [11] David Sholl and Janice A Steckel. *Density functional theory: a practical introduction*. John Wiley Sons, 2011.

- [12] *Richard M Martin and Richard Milton Martin. Electronic structure: basic theory and practical methods. Cambridge university press, 2004.*
- [13] *Klaus Capelle. A bird's-eye view of density-functional theory. Brazilian journal of physics, 36(4A):1318–1343, 2006.*
- [14] *Walter Kohn. Nobel lecture: Electronic structure of matter—wave functions and density functionals. Reviews of Modern Physics, 71(5):1253, 1999.*
- [15] *P. Hohenberg and W. Kohn. Inhomogeneous electron gas physical review 136.B864, 1964.*
- [16] *Fabien Tran, Julia Stelzl, and Peter Blaha. Rungs 1 to 4 of dft jacob's ladder: Extensive test on the lattice constant, bulk modulus, and cohesive energy of solids. The Journal of chemical physics, 144(20):204120, 2016.*
- [17] *Jianmin Tao, John P. Perdew, Viktor N Staroverov, and Gustavo E Scuseria. Climbing the density functional ladder: Nonempirical meta-generalized gradient approximation designed for molecules and solids. Physical Review Letters, 91(14):146401, 2003.*

---

## CHAPTER 3

# Plan of the Calculations

Chapter Three summarizes the steps and software utilized in the calculations from this study and investigates the geometry optimization, electronic structure and optical properties.

### 3.1 Quantum Espresso (QE)

Quantum Espresso is one of the many open-source software computer program packages for calculating and modelling material parameters. These procedures are based on *DFT* using plane waves and pseudopotentials. Quantum espresso developed around *PWscf*, one of the two main programs used to perform self-consistent calculations, and *CP* is used to perform molecular dynamics calculations. The quantum espresso project allows modules developed by scientists to be included in the field [1]. The input file of Quantum Espresso contains three main parts (Control, System, and Electronics) and two optional partitions (ions and cells), depending on the type of calculation performed. Basic types of calculations in quantum espresso include:

1. Single point energy calculation (SCF) without changing atomic coordinates or the cell parameters, i.e., no structure relaxation
2. Non-self-consistency calculation (NSCF) ) conducted to extract the desired properties (e.g., DOS) if needed a denser electronic momentum mesh (k-mesh) based on self-consistency calculation.

3. BANDS - Calculation of electronic bands along a path of high-symmetry k-points based on self-consistency calculation.
4. RELAX - Optimize the atomic coordinates and minimize the forces while keeping the cell fixed. This calculation requires sections ions. All options for a single SCF calculation apply, plus a few others.
5. VC-RELAX - Optimization of both atomic coordinates and the cell parameters. Structure relaxation is vital to minimize forces acting on the atoms and reduce the stress in the cell. This calculation requires section and cell.

Parameters Convergence: In order to obtain accurate results, the calculated density function theory (DFT) requires specific parameters of relevant materials and convergence. These parameters used in any DFT calculation include:

- Threshold of plane wave energy.
- Brillouin area sampling.
- Self-consistent energy convergence threshold.

It is necessary to optimize these parameters by minimizing energy. The equilibrium structure at zero temperature and pressure is found among all possible structures by minimizing the DFT energy. Suppose we have to calculate the energy-band structure(non-self-consistent calculation), the ground-state electron density Hartree and the determined changes and related potentials. In a non-self-consistent calculation, the code pw.x determines the Kohn-Sham. The eigenfunctions and eigenvalues do not increase Kohn-Sham Hamiltonian at every step Fig.(3.1).

## 3.2 Pseudopotentials

The nucleus electrons closest to the core have higher kinetic energy, so multiple plane waves are impractically required. However, these electrons rarely participate

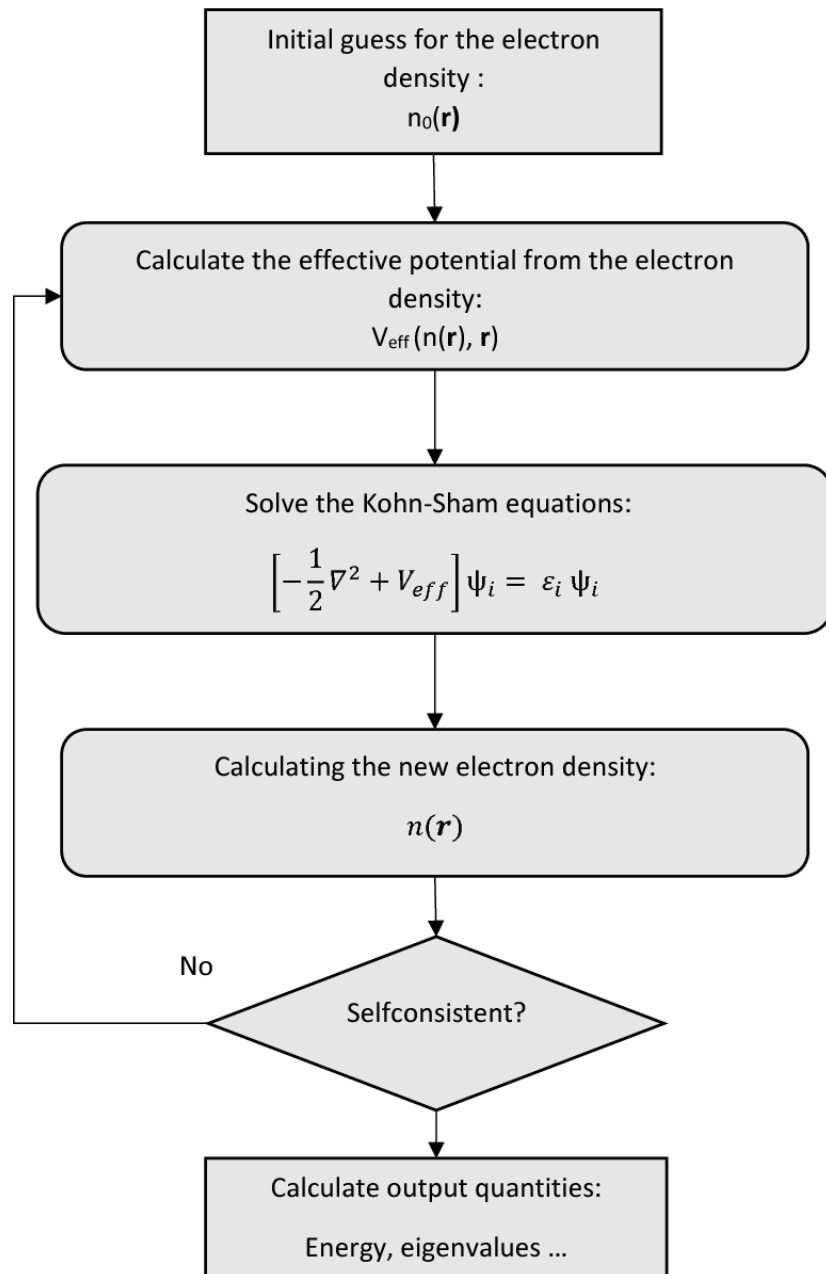


Figure 3.1: A flowchart that describes an SCF in QE implementation of DFT.

in adhesion and have negligible influence on the characteristic of the material, and the features material almost entirely depend on the valence electrons. The plane wave pseudopotential theory replaces the wave function of the core electron with a weaker and slower. In the pseudopotential method, the system considered to be composed of ion nuclei and valence electrons. The force on an ion is the sum of the electrostatic force combined with other ion nuclei plus the force exerted by its valence electrons. The false potential acts on a series of pseudo wave functions that quickly represent the wrong potential. The oscillatory wave function of valence

electrons. The potential for error is a core orbitals method of freezing; the nucleus assumed to be the same in free atoms and any chemical medium. This assumption, the Kohn-Sham equation, is solved only for the valence electrons and interacts with the nucleus's pseudo value. In the primary, the infinite plane wave set is desired to model the energy precisely. The basic set is truncated at the finite shear value of the plane wave energy, then select the "contains" cut so that the modelled properties are close to acceptable accuracy [2].

### **3.3 Fermi energy**

For every N-electron system, only a part of the band structure will be occupied. Since electrons follow the principle of Pauli repulsion, two electrons cannot hold the same position, which means that these energy bands will start filling electrons from the lowest energy. Fermi energy defines as the difference between the highest energy level occupied and the lowest energy level empty. Depending on the system, there are two main ways to fill the bands. Firstly, a band that can partially fill allows Fermi energy to intersect with one or more bands. Second, all occupied bands can fill an energy gap between the highest and lowest occupied bands. Depending on how the bands are filled and whether the energy gap is large compared to KBT at room temperature, the material will have different electronic properties, such as metallic properties, semiconductor properties, or an insulator [3].

### **3.4 Electronic band structure**

An atom has a positively charged nucleus surrounded by negatively charged electrons. The electrons in an atom have only a certain amount of energy. . Therefore, they can only occupy certain allowable energy levels. An illustration of the electronic band structure of a material is shown in Fig.(3.2). Generally, the lowest energy level available is called the ground state. Atoms can sometimes absorb ex-

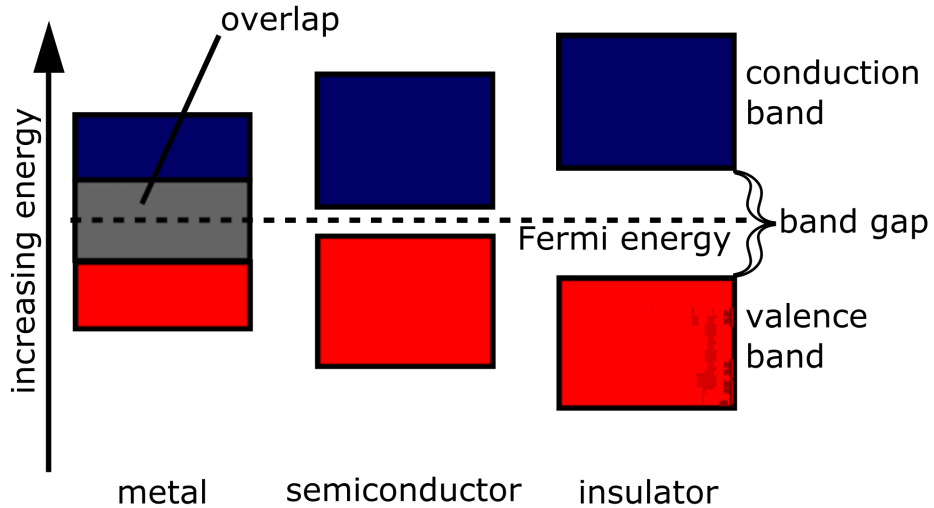


Figure 3.2: Electronic band structure.

ternal energy; if sufficient, they can shift the electron to a higher energy level, and then the atom is in an excited state. Other wise the electron can absorb much energy, and it will no longer be combined with the atom but will be free. When atoms are apart, they have similar energy levels and wave functions; when they are imparted closer together, their wave functions are superposed according to the Paulie principle. The atoms energy level is altered by other atoms electric field, creating a split in the energy levels. When more atoms interact, the energy levels are closely spaced to appear as energy bands. According to the size of the bandgap, materials can be classified as insulators, semiconductors, or metals. When the conductivity is empty for insulators and semiconductors, the valence band is filled. The band-gap of insulators is more than semiconductors, while metals do not have a bandgap [4].

### 3.5 Density of states (DOS)

DOS is a quantity of importance and can be defined as the number of states per unit of energy and per unit volume. The state of complex materials with different atom types, the donating of a given atom is achieved by the projected density of states [5].

### 3.6 Optical properties

The dielectric function is the principal magnitude applied to determine the characteristics of materials, and it defines the material's response to electromagnetic rays. When the external electric field  $E_{ext}$  is used in the electronic system, the total electric field acting on the system will generate the induced electric field. The optical processes such as absorption, reflection, and transmission observed in solids are quantified by several parameters. The properties of the solids can describe the parameters at microscopic and macroscopic levels. At microscopic or quantum mechanical level in bulk solids the complex dielectric function is closely connected with the band structure. The expression for the complex imaginary dielectric function are connected by the Kramers-Kronig eq.(3.1) [25]:

$$\epsilon_{\alpha\beta}^1(\omega) = 1 + \frac{2}{\pi} P \int \frac{\epsilon_{\alpha\beta}^1(\omega')\omega'}{\omega'^2 - \omega^2 + i\eta} d\omega'. \quad (3.1)$$

The reflective equation is given by,

$$R(\omega) = \left| \frac{\sqrt{\epsilon(\omega)} - 1}{\sqrt{\epsilon(\omega)} + 1} \right|^2. \quad (3.2)$$

The Energy-loss spectrum, Refractive index and extinction coefficient formula are presented below:

$$L(\omega) = \frac{\epsilon_2(\omega)}{\epsilon_1^2(\omega) + \epsilon_2^2(\omega)}. \quad (3.3)$$

$$n = \left| \frac{\sqrt{\epsilon_1^2 + \epsilon_2^2} + \epsilon_1}{2} \right|^{\frac{1}{2}}. \quad (3.4)$$

$$K = \left| \frac{\sqrt{\epsilon_1^2 + \epsilon_2^2} - \epsilon_1}{2} \right|^{\frac{1}{2}}. \quad (3.5)$$

### 3.7 Introduction to the properties of lithium titanium oxide $Li_2TiO_3$

Recently, many studies have focused on modern semiconductor-based technological applications with a lot of attention to perovskite compounds. The initial meaning of perovskite was discovered in 1839 by a German scientist called Gustav Rose with another scientist Russian mineralogist named Lev Perovski [6]. Perovskite is generally described in the form  $ABO_3$  [7]. Knowledge of material properties is vital in scientific research because it facilitates its use in many applications.  $Li_2TiO_3$  is a perovskite with semiconductor properties overly applied a tritium-based candidate in fusion reactors. They have good tritium emission characteristics such as good thermal conductivity than other breeder materials, as well as rising chemical stability, higher thermal stability, mechanical resistance, and smaller reactivity to humidity compared to other ceramics breeders [8, 9]. Furthermore,  $Li_2TiO_3$  are often considered electromagnetic materials with perovskite structures [10]. Thus, they found magnificent interest in futuristic function materials because of their perfect photoelectric and infrared sensors applications, high insulation constant and low leakage current [11]. Photovoltaic materials are important for technological applications in electronics, optical, waveguides, laser frequency multiplication, fusion power, and solar cells. Optical damage from lasers was first observed in  $Li_2TiO_3$  crystal in bell laboratories [12, 22]. Consequently, various studies to understand their properties have been conducted by many researchers on  $Li_2TiO_3$  [13, 17–19]. This work studied the band gap and optical properties of cubic perovskites lithium Titanium Oxide  $Li_2TiO_3$ , crystal configurations applying (DFT) as performed in quantum espresso code.

## 3.8 Computational Details

### 3.8.1 Methodology

This calculation was done by applying (*DFT*) within the plane-wave pseudopotential approaches applied in the Quantum Espresso code [14, 20, 21]. Our analyses were performed using the Perdew-Burke-Ernzerhof *PBE* for exchange-correlation and the Local Density Approximation (*LDA*) with Generalized gradient approximation (*GGA*) [15]. A plane wave cut-off of 520 eV as a basis set and geometrically relaxed such that the maximum force on each atom was less than  $0.05 \text{ eV } \text{\AA}^{-1}$ . Their DOS patterns were obtained after a geometry optimization process. We focused on the local DOS of the d orbitals in metals for simplicity, and every DOS normalized by the number of atoms in a periodic system was described as  $\text{DOS} = f(E E_f)$ , where  $E E_f$  is the relative energy shift from the Fermi level ( $E_f$ ). In addition, during the *DFT* calculations, we turned on the spin polarization effect to consider the magnetic properties of the metals. In representing the DOS patterns via our learning model, we applied our model separately for the up spin and the down spin. We applied the tetrahedron method to compute DOS calculations in PBE calculation. We use the materials project as an open application programming interface (*API*) to prepare an input file for the materials cubic structure mp-36864-LTO [16]. The geometry optimization calculations are carried out to determine energy minimize in the system and atomic locations. The self-consistent calculation (*SCF*) was done to find the total energy calculation and the atomic positions of different atoms. Also, non-self-consistent calculation (*nSCF*) was done for the density of states calculations, for the perovskites structure unit cell of both materials, the k-point grid of  $6 \times 6 \times 6$  was used.

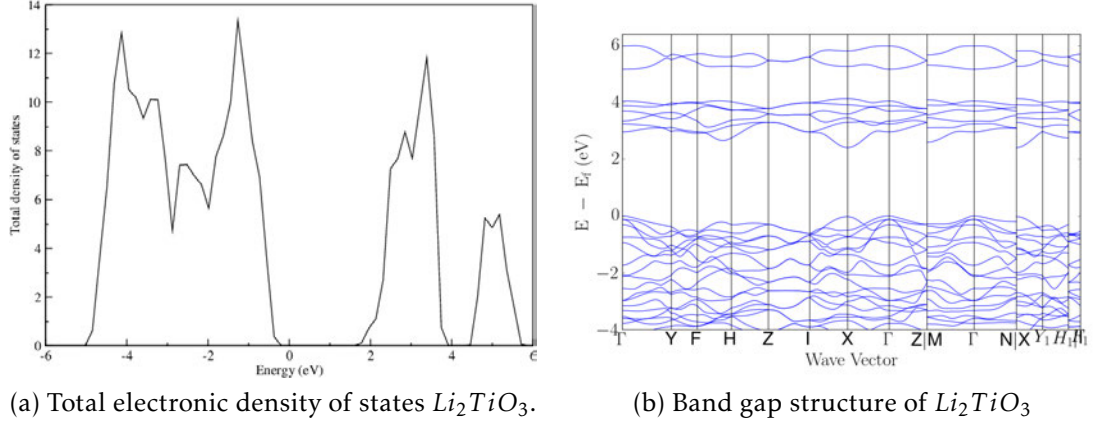


Figure 3.3: Calculated total DOS and Band structures.

## 3.9 Results and Discussions

### 3.9.1 Density of States of $Li_2TiO_3$

The electronic density of states (*DOS*) plays a vital role in determining the properties of metals. In the field of solid and condensed matter physics, it carefully diagnoses the density distribution of free electrons in metals to understand the scientific concepts hidden in the density distribution (such as the d-band centre theory). (Fig.3.3a) displayed electronic structures when the system was at zero pressure.

### 3.9.2 Band Structures

The bandgap is considered one of the most valuable sides of the band structure, as it strongly affects the electrical and optical properties of the materials. Therefore, it is essential to be specific when studying the material's properties. The energy band structure was computed applying the *DFT* with (*LDA*), at zero energy is determine Fermi level. Our calculated results agree with earlier published theoretical and experimental works [23, 24]. The calculated relaxed lattice parameters are  $A = 5.061 \text{ \AA}$  and  $C = 5.086 \text{ \AA}$ , yielding the ratio by 1:005. This refers to a change in structure from cubic to a monoclinic structure. We find indirect band energy of 2.41 eV. and structure as shown in (Fig.3.3b)

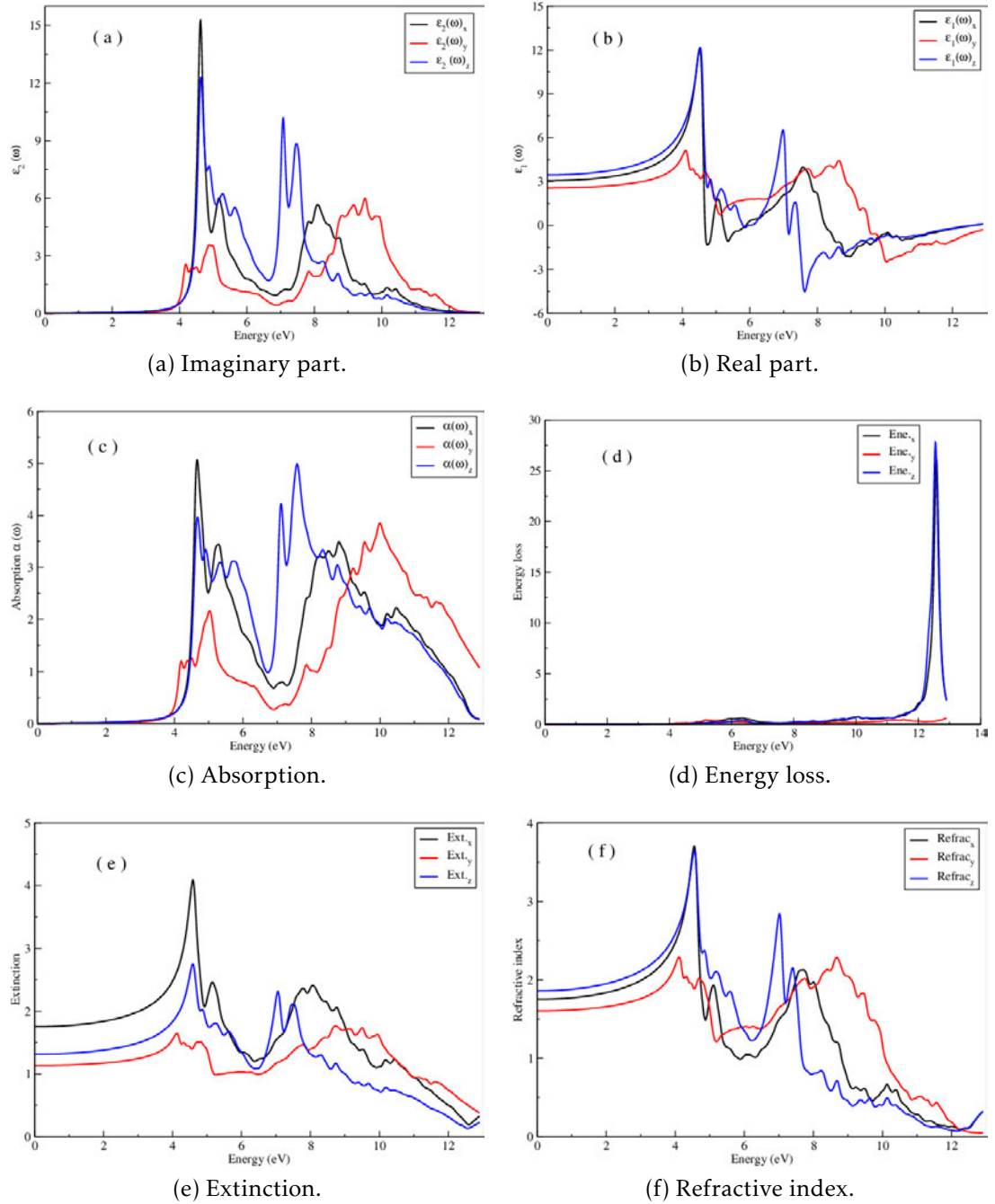


Figure 3.4: complex dielectric of  $Li_2TiO_3$  optical coefficients for all direction

### 3.10 Optical properties of $Li_2TiO_3$

The investigation of the optical properties of a material is essential for various applications like absorbers, optical coatings, reflectors, and different optoelectronic devices. It is measured by the various optical parameters concerning photon energy, such as dielectric constant.

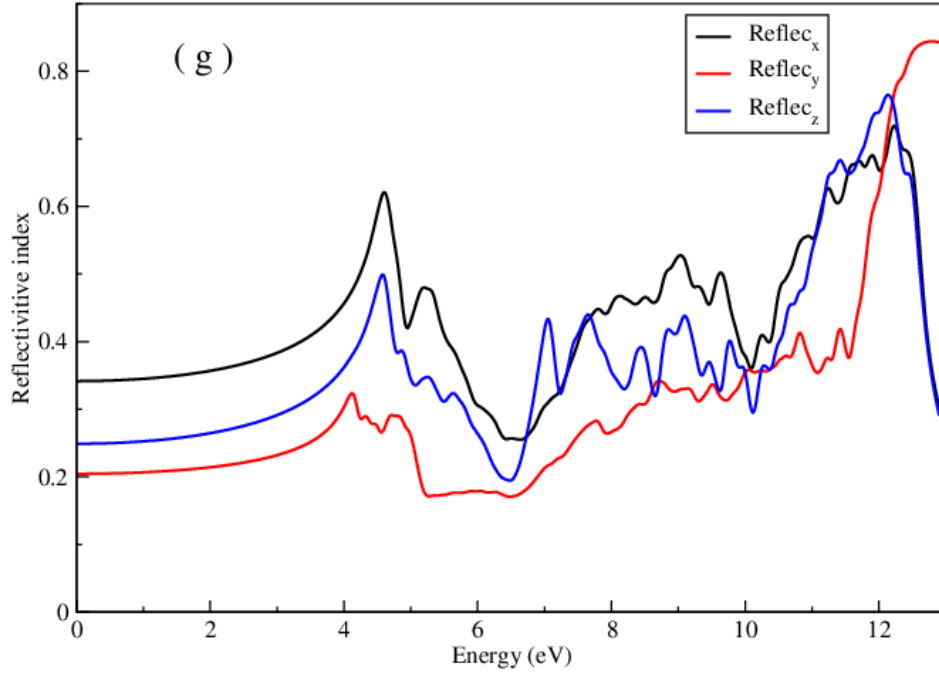


Figure 3.5: Reflectivity index of  $Li_2TiO_3$ .

Optical parameters of  $Li_2TiO_3$  is calculated for energies up to 20 eV as shown in (Fig.3.4). The real and the imaginary parts of the complex dielectric constant are shown in Figure. (3.4a, 3.4b), displayed properties for these materials as a semiconductor. The complex refractive index as a function of energy in eV is displayed in Fig.(3.4c, 3.4d). ). The absorption coefficient can determine the energy conversion efficiency, which indicates the distance that light of specific energy (frequency) can penetrate the material before being absorbed Fig.(3.4e) depicts the absorption. The reflective spectrum as a function of photon energy is shown in Fig.(3.4f) and Figure.(3.5) shows the Reflectivity index, which determines the loss of energy of fast electron when it traverses through the medium.

### 3.11 Conclusion

In this work, was studied the electronic structure and optical characteristics of  $Li_2TiO_3$  found band gaps as to 2.41 eV calculated using (QE) package, which has successful capabilities to find the bandgap in perovskite structure; we have examined the optical properties based on dielectrics function such as refractive index

$n(\omega)$  and the extinction coefficient  $k(\omega)$ , which have best properties make them as excellent in many applications.

---

# References

- [1] P. Giannozzi, S. Baroni, N. Bonini, Matteo Calandra, Roberto Matteo Cococcioni, Ismaila Dabo, et al. *Quantum espresso: a modular and open-source software project for quantum simulations of materials. Journal of physics: Condensed matter*, 21(39):395502, 2009.
- [2] DR Hamann, M. Schlüter, and C. Chiang. *Norm-conserving pseudopotentials. Physical Review Letters*, 43(20):1494, 1979.
- [3] Takeo Fujiwara and Takeshi Yokokawa. *Universal pseudogap at fermi energy in quasicrystals. Physical review letters*, 66(3):333, 1991.
- [4] Mike C. Payne, Michael P. Teter, Douglas C. Allan, T.A Arias, and ad JD Joannopoulos. *Iterative minimization techniques for ab initio total-energy calculations: molecular dynamics and conjugate gradients. Reviews of modern physics*, 64(4):1045, 1992.
- [5] Joseph P. Heremans, Vladimir Jovovic, Eric S. Toberer, Ali Saramat, Ken Kurosaki, Anek Charoenphakdee, Shinsuke Yamanaka, and G Jeffrey Snyder. *Enhancement of thermoelectric efficiency in pbte by distortion of the electronic density of states. Science*, 321(5888):554–557, 2008.
- [6] Mark Fox. *Optical properties of solids*, 2002.
- [7] Zhengqi Shi and Ahalapitiya Jayatissa. *Perovskites-based solar cells: A review of recent progress, materials and processing methods. Materials*, 11(5):729, 2018.
- [8] Faruk Sani, Suhaidi Shafie, Hong Ngee Lim, and Abubakar Ohinoyi Musa. *Advancement on lead-free organic-inorganic halide perovskite solar cells: a review. Materials*, 11(6):1008, 2018.

- [9] H Ohno, S Konishi, T Nagasaki, T Kurasawa, H Katsuta, and H Watanabe. Correlation behavior of lithium and tritium in some solid breeder materials. *Journal of nuclear materials*, 133:181–185, 1985.
- [10] Daniel Popovici, Masanori Okuyama, and Jun Akedo. Barium titanate-based materials—a window of application opportunities. *Ferroelectrics-Material Aspects*, by Mickaël Lallart, IntechOpen, London, pages 279–304, 2011.
- [11] Kunimitsu Kataoka, Yasuhiko Takahashi, Norihito Kijima, Hideaki Nagai, Junji Akimoto, Yasushi Idemoto, and Ken-ichi Ohshima. Crystal growth and structure refinement of monoclinic  $\text{Li}_2\text{TiO}_3$ . *Materials Research Bulletin*, 44(1):168–172, 2009.
- [12] Mickaël Lallart. *Ferroelectrics: Applications*. BoD—Books on Demand, 2011.
- [13] J Zhuang, G.S Li, X.C Gao, X.B Guo, Y-H Huang, Z.Z Shi, Y-Y Weng, and J Lu. Preparation and photorefractive properties of barium strontium titanate ( $\text{Ba}_{1-x}\text{Sr}_x\text{TiO}_3$ ). *Optics communications*, 82(1-2):69–72, 1991.
- [14] Jürgen Hafner. Materials simulations using vasp—a quantum perspective to materials science. *Computer physics communications*, 177(1-2):6–13, 2007.
- [15] Robert O Jones and Olle Gunnarsson. The density functional formalism, its applications and prospects. *Reviews of Modern Physics*, 61(3):689, 1989.
- [16] A. Jain, Shyue P. Ong, G. Hautier, Dan Gunter, David Skinner, Gerbrand Ceder, and Kristin a. Persson. The Materials Project: A materials genome approach to accelerating materials innovation. *APL Materials*, 1(1):011002, 2013.
- [17] Z. Wan, Y. Yu, HF Zhang, T Gao, XJ Chen, and CJ Xiao. First-principles study of electronic, dynamical and thermodynamic properties of  $\text{Li}_2\text{TiO}_3$ . *The European Physical Journal B*, 85(6):181, 2012.
- [18] Samuel T. Murphy, Philippe Zeller, Alain Chartier, and Laurent Van Brutzel. Atomistic simulation of the structural, thermodynamic, and elastic properties of  $\text{Li}_2\text{TiO}_3$ . *The Journal of Physical Chemistry C*, 115(44):21874–21881, 2011.
- [19] E. Proust, L. Anzidei, G. Casini, M. Donne, L Giancarli, and S Malang. Breeding blanket for demo. In *Fusion Technology 1992*, pages 19–33. Elsevier, 1993.

- [20] L. Huang, Z. Chen, D. Wilson, and Stephen O'Brien. *Barium titanate nanocrystals and nanocrystal thin films: Synthesis, ferroelectricity, and dielectric properties*. *Journal of Applied Physics*, 100(3):034316, 2006.
- [21] JM Miller, HB Hamilton, and JD Sullivan. *Testing of lithium titanate as an alternate blanket material*. *Journal of nuclear materials*, 212:877–880, 1994.
- [22] P. Gierszewski. *Review of properties of lithium metatitanate*. *Fusion Engineering and Design*, 39:739–743, 1998.
- [23] Vivek Kumar Shukla. *Electronic structure of pbtio3 perovskite based on density functional calculation*. In *AIP Conference Proceedings*, volume 1953, page 110035. AIP Publishing, 2018.
- [24] Qilai Zhou, Lihong Xue, YaWang, Heping Li, Takumi Chikada, Yasuhisa Oya, and Youwei Yan. *Preparation of li2tio3 ceramic with nano-sized pores by ultrasonic-assisted solution combustion*. *Journal of the European Ceramic Society*, 37(11):3595–3602, 2017.
- [25] C. Kittel, Paul McEuen, and Paul McEuen. *Introduction to solid state physics*, volume 8. Wiley New York, 1996.

---

## CHAPTER 4

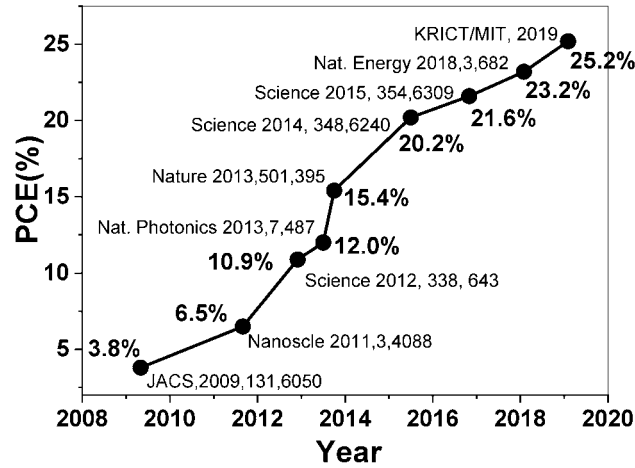
# A review of experimental and computational attempts to remedy stability issues of perovskite solar cells

### 4.1 Abstract

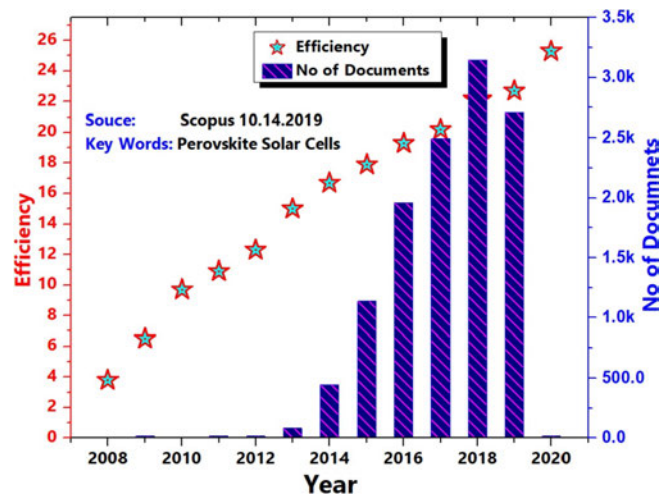
Photovoltaic technology using perovskite solar cells has emerged as a potential solution in the photo-voltaic makings for cost-effective manufacturing solutions deposition/coating solar cells. The hybrid perovskite-based materials possess a unique blend from low bulk snare concentrations, ambipolar, broad optical absorption properties, extended charge carrier diffusion, and charge transport/collection properties, making them favourable for solar cell applications. However, perovskite solar cells devices suffer from the effects of natural instability, leading to their rapid degradation while bared to water, oxygen, as well as ultraviolet rays, are irradiated and in case of high temperatures. It is essential to shield the perovskite film from damage, extend lifetime, and make it suitable for device fabrications. This paper focuses on various device strategies and computational attempts to address perovskite-based solar cells environmental stability issues.

## 4.2 Introduction

One of the critical problems confronting our community today is the need for ecofriendly and renewable energy sources to overcome the increasing energy demand regarding the swelling population and manufacturing. One of the promising technologies is solar cell technology, which is considered efficient for clean energy at low cost and minimal pollution [1]. The mineral perovskite was discovered and named after the Russian mineralogist Kon Lev Aleksevich von Perovski by Gustav Rose in 1839 after a sample was found in the Ural Mountains [2]. The compound named Calcium Titanium Oxide ( $CaTiO_3$ ) describes a joint oxide group with a similar structure with the general formula  $ABO_3$ . Goldschmidt (1926) produced the first synthetic perovskites at the University of Oslo, leading to the term perovskite, which describes a class of compounds with the same general stoichiometry linkages as in  $CaTiO_3$  [3]. Recently, with appeared the fourth generation of photovoltaic technology, Perovskite Solar Cells (*PSCs*) have appeared, which exceeded expectations for Power Conversion Efficiency (*PCE*) within short term [4]. They attracted widespread attention from the solar cell research community due to their fantastic improvement in device efficiency with a significant increase from an initial value of 3.8% in 2009 [5], to 15% in 2013 [6], up to 23.3-25.2% recently [7, 8]. As of 2020, a simple search on Science Direct on the titled perovskite-type solar cell production and characterization revealed a total of 1606 published papers. This indicates the high volume of the investigation carried out in the research field as shown in (Fig.4.1). Despite the research efforts, a tiny fraction of the total research on the *PSC* has reported power conversion efficiency greater than 25%. This is partly due to the instability of the perovskite medium and problems associated with the reproducibility of the devices [7, 10]. However, the perovskite solar cell is a type of solar cell includes a perovskite structured compound [11], with distinctive properties such as effective electroluminescence, effective electrolysis from visible to the near-infrared range, photodetector applications. It has a highly adjustable bandgap, a broad absorption spectrum, and simple fabrication [103]. This makes them promising for solid-state solar cells. Compared to other silicon devices, low cost and useful manufacturing techniques these are also advantage of perovskite



(a) Efficiency of perovskite based solar cell.



(b) The number of research outputs in the field from reported years based on science direct.

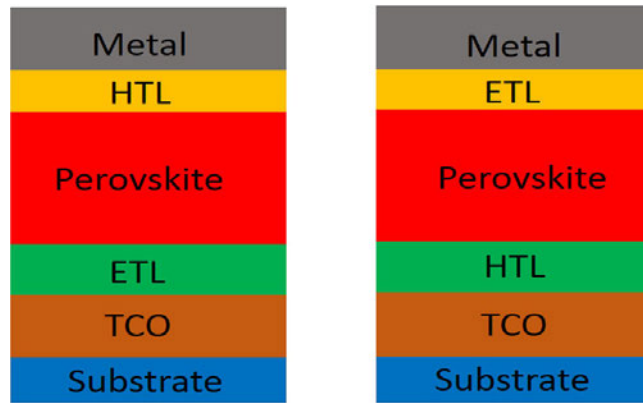
Figure 4.1: Gradual increase of efficiency (a) and (b) research output of perovskite based solar cells [8, 9].

devices [13]. Perovskite has attracted widespread attention as a potential alternative to silicon photovoltaic (*PV*) devices currently dominate the *PV* market [14]. The instability of the perovskite in the open-air environment is the main drawback to its large-scale realization and commercialization. In recent years, researchers have made considerable experimental and computational efforts to study the performance and control the size, morphology, and crystallinity of the perovskite films. In this review, we inclusively discuss the evolution in the perovskite based solar cells, details with structures and working principle by experimental and computational design/fabrication approaches of perovskite are will discuss. Besides,

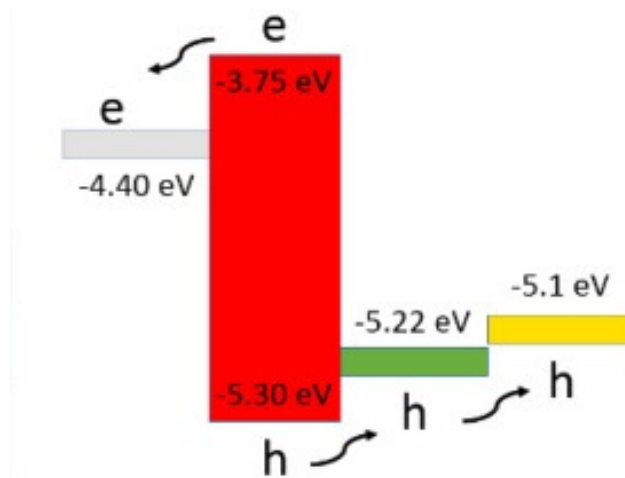
we discuss some recent progress to resolve the stability challenges that affect the performance of perovskites devices.

### 4.3 Architectures of perovskite solar cells

The comprehensive chemical structure of PCS are  $ABX_3$ ,  $A_2BB'X_6$  where  $A$  is an organic molecule  $CH_3NH_3$  or  $NH_2CHNH_2$ ,  $B$  is a divalent metal ( $Pb, Sn$ ),  $X$  is a halide ( $Cl, Br, or I$ ), makes this material important for more applications [15]. PCSs include a perovskite photosensitive film confined between two electrodes. A surface buffer layer is usually used among the active and electrode layers to make easy charge processing. The device structure has two types of interface layers: Electron Transport Materials (*ETM*) and hole transport materials (*HTM*). In fundamental, one of the electrodes should be a transparent conductive oxide, such as a nitride containing indium. (Fig.4.2a), displayed the device structure of the tow types of (*PSC*). The structure of the device by the deposition to show the two *PCSs* device structure. The structure of the device is widely used by depositing metal (top) electrodes of aluminum, silver or gold. There are two essential device architectures are used to prepare *PCSs*, mesoporous and planar *PCS* compositions. Therefore, the *PSC* charge transport channel is often discussed based on the kind of the device structure [15]. The perovskite layers have a mesoporous structure and are formed by a layer of porous semiconductor metal oxide such as titanium oxide  $TiO_2$ , which forms an interlocking network between the two-phase interfaces. Therefore, light-induced electrons can be transported to the cathode through the  $TiO_2$ , channel, and the pores are transported to the anode via the perovskite channel (Fig.4.2b). At the planar structure, the interface hole layer and electron transport material are used to produce the cell. Excitation generated in the perovskite layer drifted into the electrode by an established electric potential or an externally imposed electric field [15].



(a) The device structure of the two types *PSC* [16].



(b) Energy band diagram of the planar *PSC* showing the separation and collection of photogenerated carriers [17].

Figure 4.2: Architectures of perovskite solar cells (a) device structure and (b) band diagram.

## 4.4 Working principles of perovskite solar absorber

Over the past a few years, several studies on charge transport kinetics in *PSC* have explained that light excitation in a perovskite medium will immediately generate electron-hole excitons in less than 2-picoseconds at electric field caused by the difference of function between anode and cathode and then splits it into delocalized charge carriers [18]. Besides, the success of perovskite solar absorbers mainly due to rising carrier mobility at the thin film medium, as well as charge spread the length of electrons and holes in the perovskite medium around  $1 \mu m$  this is sufficient for the photogenerated charges reach into the interface layer and electrode without recom-

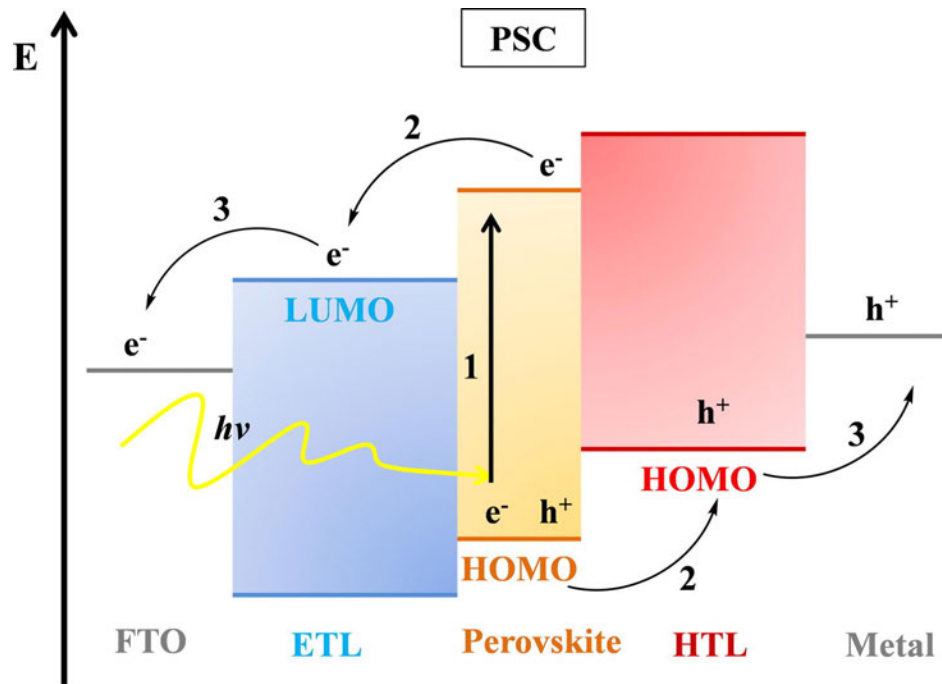


Figure 4.3: Work principles of Perovskite Solar Cells [20].

bination [18]. Due to the complex nature of perovskite environment, researchers still do not know much about the process of generating and collecting charges in perovskite solar cells. So, the principle applied to characterize silicon solar cells is as yet used to describe *PCSs* characteristics [19]. Typically, perovskite solar cells device can be described in four fundamental steps :-

1. Photon absorption and exciton formation
2. Exciton diffusion and splitting
3. Charge transportation
4. Charge collection

Once sunlight drop on the perovskite layer, it absorbs photons excitons. Owing to the difference in the excites' binding energies in the perovskite material, the exciton can form electrons and holes when the excitons are separated. Exciton separation happens at the interface between the hole transport layer and the charge transport layer. Electrons are separated from the holes and injected into the electron transport layer, typically migrating to the Fluorine-doped Tin Oxide (*FTO*) anode, at the same

moment, holes are mainlines into the holes transport layer and then transferred to the cathode, usually a metal as displayed in (Fig.4.3) [21]. The metal electrode collects electrons and holes, and the counter electrode is transferred to an external circuit to generate a current.

## 4.5 Perovskite based solar cells evolution

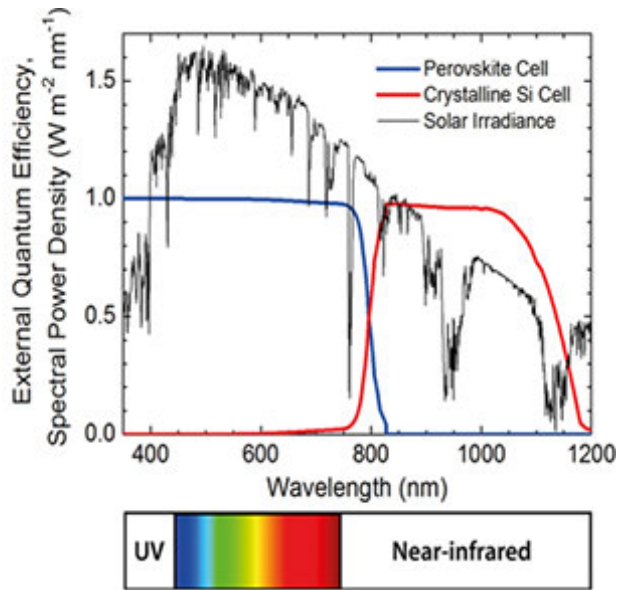
The has been the development of perovskites to achieved high efficiency as solar cells devices. Miyasaka *et al.* [22] reported the first *PSC* in 2006 regarded many as a benchmark towards achieving perovskite solar cells. Using  $CH_3NH_3PbBr_3$  as the solar sensitive material, they obtained a solar cell with an efficiency of 2.2% [23]. The first device from perovskite using  $TiO_2$  as sensitized solar cells was achieved by fluid electrolyte based on iodide [24]. Three years later, in 2009, Kojima *et al* [25]. reported the first organic lead halide synthesis  $CH_3NH_3PbBr_3$ ,  $CH_3NH_3PbI_3$  as sensitizers in the cell. The measurement of *PSCs* increased *PCE* approximately 3.81% into the  $CH_3NH_3PbBr_3$ as well as 3.13% into an  $CH_3NH_3PbI_3$ -based cells, respectively, but with improved fabrication conditions. However, they found limitations produced by the nanocrystals' decomposition in the iodide fluid that led to quick device degradation. The device lasted only about 10 min [25]. In 2011, Park and colleagues produced the  $MAPbI_3$  perovskite as quantum dots, resulting in enhanced productivity to 6.5% through  $TiO_2$  surface treatment. By mid-2012, Park *et al.* [26]. tried to use solid organic molecules or polymers as an *HTM* and absorber ( $CH_3NH_3PbI_3$ ) into avoid an effects of electrolytes manufacture with a significantly increased the *PCE* of 9.7%. The above results Demonstrates that a solid-state *HTM* highly increased the device's stability compared with liquid electrolytes. Nevertheless, instability challenge remained the major limitation impeding manufacturing and photovoltaic marketing of *PSCs* [19]. In the same year, Snaith *et al.* [27] reported fabrications perovskite solar cells using Spiro-OMeTAD based *HTM* and  $Al_2O_3$  as supports. The efficiency of the device was 10.9%. In their report, they showed that the use of mixed halides ( $CH_3NH_3PbI_3xCl_x$ ) can improve performance because of its higher charge carrying capacity. They also

showed that perovskite has bipolar charge transport electrons and hole transport. In March 2013, Seok *et al* [30]. they found promising results from using the structures of nanoporous  $TiO_2$  infiltrated by mixed-halides PSC through optimization the halides in  $CH_3NH_3Pb(I_{1-x}Br_x)_3$  compound certified efficiency of 12.3%. Paves the way for reaching a *PCE* milestone that has been designed for many years. In 2013, *PCE* production of well-designed solar cells was 12.3% and 15%, Increased to 19.3% in the first half of 2014 [29]. Seok *et al.* [30] reported an efficiency using  $CH_3NH_3PbI_{3-x}Cl_x$  and poly-triarylamine *HTM* of 16.2% and 17.9%, respectively. Subsequently, Saliba *et al.* [31] introduced a perovskite solar cell using a trication (Cs, MA, FA) mixture with 21.1% efficiency showed high stability and respectability. Yang *et al.* [98] introduced a method to reduce defects in the perovskite layer using an intermolecular exchange process in 2017, which helps reduce the concentration of defects and achieve an efficiency of more than 22%. In 2018 Zhao *et al.* [33] all production reports of 4-terminal perovskite tandem solar cells with power conversion efficiency of over 23%. In 2019, Jiang *et al.* [34] produced a cell with an efficiency of 23.32% using organic halide  $HC(NH_2)_2CH_3NH_3$  to prepared solar cells with surface defects. Sahil *et al.* [36] prepared fully textured monolithic perovskite-silicon tandem solar cell, and it achieved efficiency around 25.2%. Besides, to improving efficiency, a new design of device architecture has developed for low-cost and highly stable *DSSCs* and *PSC*.

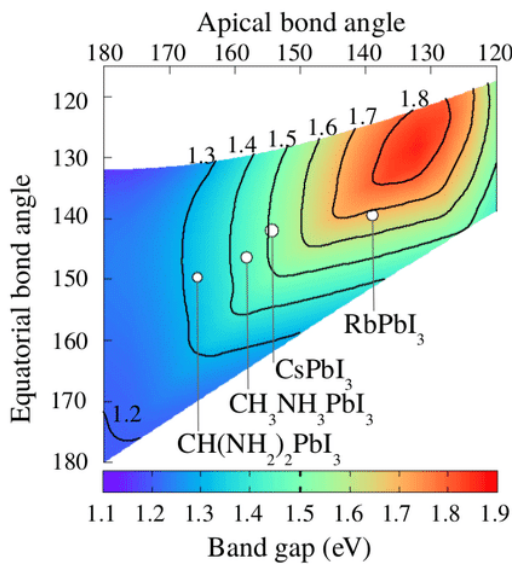
## 4.6 Band Gap of Perovskites

The design of solar cell technology strongly depends on the knowledge of the energy from the sun. The sun releases a considerable amount of energy  $\approx 174PW$ , which is roughly 6000 times worldwide energy usage [37]. This energy is estimated to be  $1366 W/m^2$  just outside the atmosphere. Standard Air Mass (A.M 1.5) solar spectrum at ground level (Fig.4.4a) shows that upon integration, the range gives  $1000 W/m^2$  [38].

$$E = \frac{hc}{\lambda} \quad (4.1)$$



(a) The complementation of EQE in Si and perovskite tandem solar cell



(b) Band-gap and electronic-structure-tunability of PSC Materials

Figure 4.4: Sun irradiance and bandgap of PSCs with permission from [39, 108].

Where  $E$  is the energy of the photon,  $h$  is Planks constant,  $C$  constant of light, and  $\lambda$  is the wavelength. The (Fig.4.4b) showed bandgap and the relation between bond angles. The angular coordinates' variation induced a substantial modulation of the bandgap from the top of the mid-infrared (1.1 eV) to the beginning of the visible spectrum (1.9 eV). This trend is in line with calculations on simpler two-dimensional (2D)  $Sn - I$  perovskites for solution-processable electronics. Photons

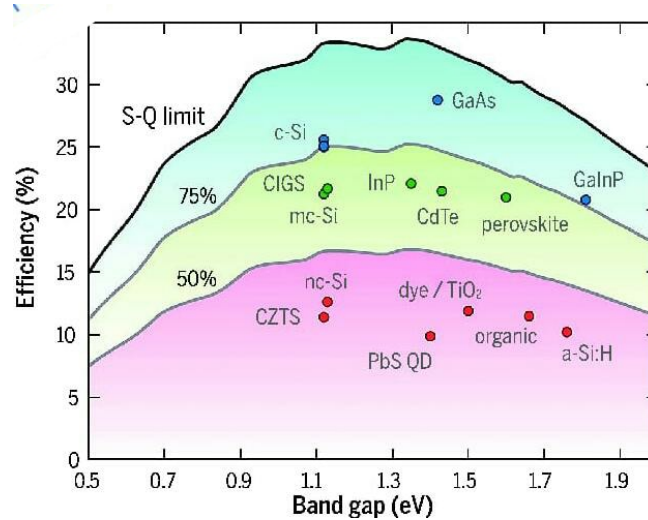
that get absorbed are those with energy greater than the band gap of the material. The band gap has an important impact on the optical properties of perovskite material. In a systematic study, Shockley and co, the bandgap has an essential effect on the material's optical properties. Workers found that the most favourable bandgap should be near the Shockley-Queisser limit 1.34 eV [35]. An important feature of solar absorbers is the bandgap, its determines the maximum theoretical power conversion efficiency, which is an inherent characteristic and ultimately directly affects the true performance of photovoltaic cells. In recent years, methylammonium lead iodide ( $MAPbI_3$ ) is the most widely used as a light absorber in perovskite solar cells, for optimal bandgap and long-term stability are currently many studies were currently being to replace methylammonium (MA) in  $MAPbI_3$ , the optimal bandgap for a single-junction solar cell is between 1.1 and 1.4 eV while the reported band gaps of  $MAPbI_3$  are between 1.50 and 1.61 eV, solar light-harvesting efficiency of PSC's can be further by using a lower bandgap than  $MAPbI_3$  [43]. Replacing MA ions with larger organic formamidinium (FA) ions will result in a cubic structure with a slightly larger lattice, and thus the bandgap will be slightly reduced from 1.59 eV for  $MAPbI_3$  to 1.45 – 1.52 eV for  $FAPbI_3$  Closer to the optimal bandgap of a single link Solar cells, so can harvest more light [44]. They found that when halogen substitution occurs between Cl, Br, and I, the absorbance changes significantly, as the halide ion size increases, the bandgap energy decreases, that is, for single crystals, the bandgap is 2.97, 2.24, and 1.53 eV for the Cl, Br, and I perovskite, respectively. In addition, compared with the absorption starter group, the smaller PL peak makes it to be applied in solar cells advantageous [45]. Recently, the effects of cation exchange with  $MA^+$ ,  $Cs^+$ , and  $Rb^+$  on the properties of  $FAPbI_3$  perovskite have been studied through first principles calculations, it was found that these additives can slightly increase the energy band gap of  $FAPbI_3$  [46]. Liu *et al.* [47] studied by first-principles calculations the electronic and optical properties of Rb-incorporated methylammonium lead halide perovskite ( $MAPbI_3$ ), they find that the band gaps of Rb-doped  $MAPbI_3$ , between (1.53 – 1.49) eV. For  $MAPbI_3$ , Rb-doped systems, the band-gap is 1.49 eV. Besides that, show Rb doping can degrade the structural stability of  $MAPbI_3$ , which can be attributed to the close band gaps of them, if the perovskites solar absorber has the band gap of a solar absorber is too

small  $< 1$  eV, the device will be able to collect extra current from infrared emission, but the open-circuit voltage will be too small. In addition, when the band gap is too large ( $> 2$  eV), only a tiny amount of solar radiation can be trapped. Hence, a semiconductor with a band gap approximately 1.2 – 1.6 eV is the perfect material for solar cell preparation in the configuration design of a single junction system (Fig.4.5). The hybrid perovskite films are composed of direct band gap semiconductors with low bulk trap densities, which have shown remarkable luminous properties. One advantage of using the band gap of the hybrid perovskites can be tuned by molecular geometry, i.e. by adjusting the composition of the compounds.

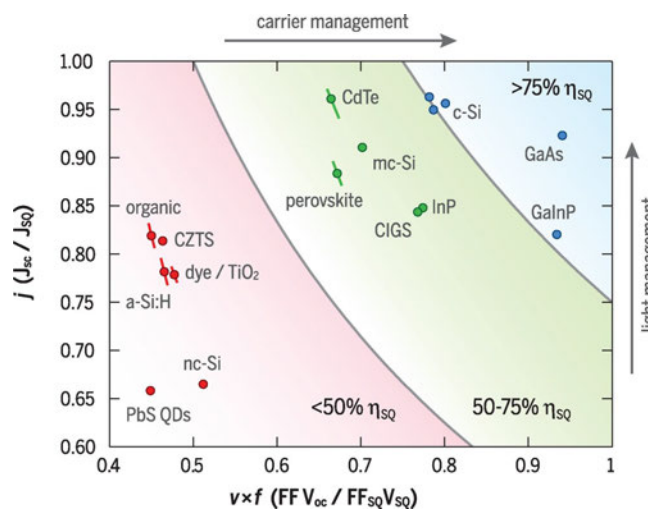
### 4.6.1 Binding Energy

It has already been mentioned that upon absorption of photons, *PSC* devices produce an exciton electrical bound pair. This exciton has to dissociate into electron and hole. Thus, the magnitude of exciton binding energy has a direct influence on the *PCE* of *PSC* devices performance. If the bending energy is low, excitons are loosely bound, and dissociation is favored. While if band energy is high, excitons are tightly bound. Thus, recombination is favored [49]. The evaluation of the bending energy can be performed by carefully aligning the spectra obtained from the *PES* and *IPES* measurements with the simulated spectra calculated from the *DFT*, (Fig.4.6) [50]. Endres *et al.* [51] have reported many significant improvements in the measurement of band onset a range by hybrid perovskite films, the band gap of *MAPbI<sub>3</sub>* is determined to be  $1.6 \pm 0.1$  eV. Another property that enhances charge dissociation is the degree of the change in dipole moment from the ground state to the excited state [67]. The bigger the change, the higher the dissociation rate and the inverse is true. The calculation is done by finding the dipole moment of molecules at ground state ( $\mu_g$ ) and also at excited state ( $\mu_e$ ) then, using equation (4.2), the change in dipole moment can determine.

$$\nabla\mu = \left[ (\mu_{gx} - \mu_{ex})^2 + (\mu_{gy} - \mu_{ey})^2 + (\mu_{gz} - \mu_{ez})^2 \right]^{1/2} \quad (4.2)$$



(a) Relationship between maximum efficiency limit and energy band gap of solar absorber



(b) Relationship between wide balance efficiency range and theoretical Shockley-Queisser bandgap.

Figure 4.5: Relationship between solar cell efficiency limits and band gap with Shockley-Queisser wide balance range [48].

## 4.7 Perovskite Chalcogenide

Transition metal perovskite chalcogenides have emerged as a new class of versatile semiconductors, with large chemical and structural tunability, that translates to a tenable band gap in the visible to the infrared of the electromagnetic spectrum [53]. In addition, this band gap tunability provides a unique opportunity to realizing multi-state semiconductors with high carrier mobility. Recently, a series of transition metal perovskite chalcogenides  $ABX_3$  ( $X = S, Se$ ;  $A, B = \text{metal}$ ) with low

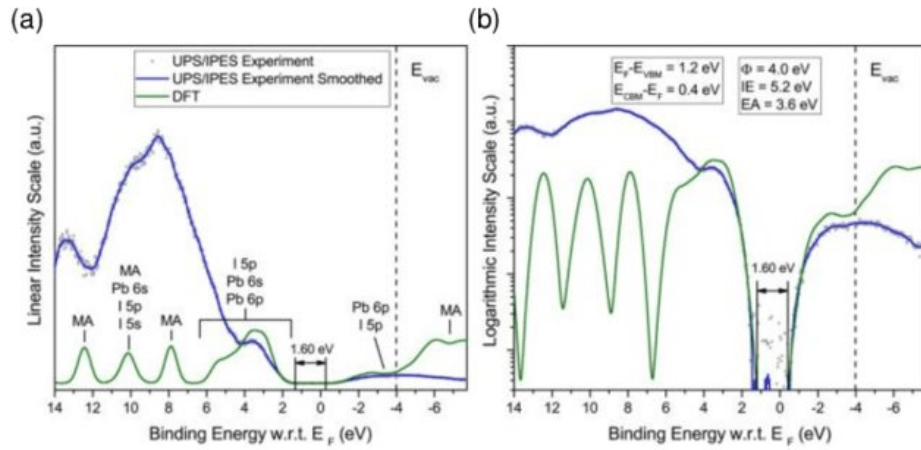


Figure 4.6: UPS/IPES spectrum of  $MAPbI_3$  in (a) linear (b) Semi-logarithmic graph. Compare this with the case density calculated by *DFT* [51].

band gap have been theoretically predicted by *DFT* calculation and experimentally synthesized the reported performance is summarized based on the configurations displayed in (Table.4.1). Some studies point out that most chalcogenides have the

Table 4.1: Summary of reported calculated band gap by computational of perovskite solar cell materials ( $ABX_3$ ,  $X= S, Se$ )

Materials	$E_g$ [eV] direct.	$E_g$ [eV] indirect	Methods of Study	References
$SrSnSe_3$	1.56	1.56	<i>DFT</i>	[54]
$SrSnS_3$	1.00	1.00	<i>DFT</i>	[58]
$BaZrS_3$	2.25	2.25	<i>DFT</i>	[55]
$BaZrSe_3$	1.44	1.01	<i>DFT</i>	[56]
$CaZrSe_3$	1.52	1.52	<i>DFT</i>	[57]
$LaYS_3$	1.79	1.79	<i>DFT</i>	[55]
$CuTaS_3$	1.3	1.3	<i>DFT</i>	[58]
$CsNbS_3$	1.47	1.47	<i>DFT</i>	[59]
$CaSnS_3$	1.58	1.67	<i>DFT</i>	[60]

best band gap; therefore, the band gap control is one of the keys to the stability of the perovskite device. Meng *et al.* [61] applied alloying and defect control in  $BaZrS_3$  by *DFT* method. Their calculations showed that a small Zr substitution by  $Ti(BaZr_{1-x}Ti_xS_3, x = 0.1)$  is able to reduce the bandgap from 1.76 eV to 1.47 eV. The theoretical *PCE* of  $BaZr_{1-x}Ti_xS_3$  is higher than those of well-known lead halide perovskites for the same thickness. They predicted that introducing compressive strain may be a plausible approach to stabilizing  $BaZr_{1-x}Ti_xS_3$  perovskite film. The

results show that some of the perovskite compounds are based on the calculated Goldschmidt tolerance coefficient, band gap value, light absorption spectrum, effective mass and phonon distribution [58], and are expected to be used in photo-voltaic applications. Also, pointed out that the element mixing strategy can be used to adjust the band gap and light absorption of the perovskite chalcogenide, and can be used to design tandem photo-voltaic devices [62]. The following section gives some details on methods that have been tried to improve the power conversion efficiency of perovskite solar cells through material modification.

## **4.8 Design/Fabrication Approaches**

Designing better perovskite electronic materials requires a comprehensive understanding of the electronic structure of these materials and the factors affecting it. By there systematically studying a series of materials, valuable information can be generated regarding the properties of the materials. There are two distinct methods used to study the properties of materials, experimental and computational. Here we give a short summary of both the experimental and computational approaches.

### **4.8.1 Experimental Approach**

Two major techniques employed in the fabrication of perovskite film are vacuum deposition and solution processing [63]. Solution casting methods have a favorable advantage over vacuum deposition because of the cost-effective and compatibility with large-scale device manufacturing. In both cases, researchers utilized a difference procedures in the preparation of the films that yielded difference in the quality of the film as well as in the reported power conversion tailored efficiency displayed in (Fig.4.7). The popular tailored approach used in vacuum deposition are one-step precursor deposition, sequential vapour deposition, two-source vacuum deposition processes (TSVD). Whereas in the solution deposition approach, one-step spin coating, two-step spin-coating, vapour-assisted solution deposition (VASD) and

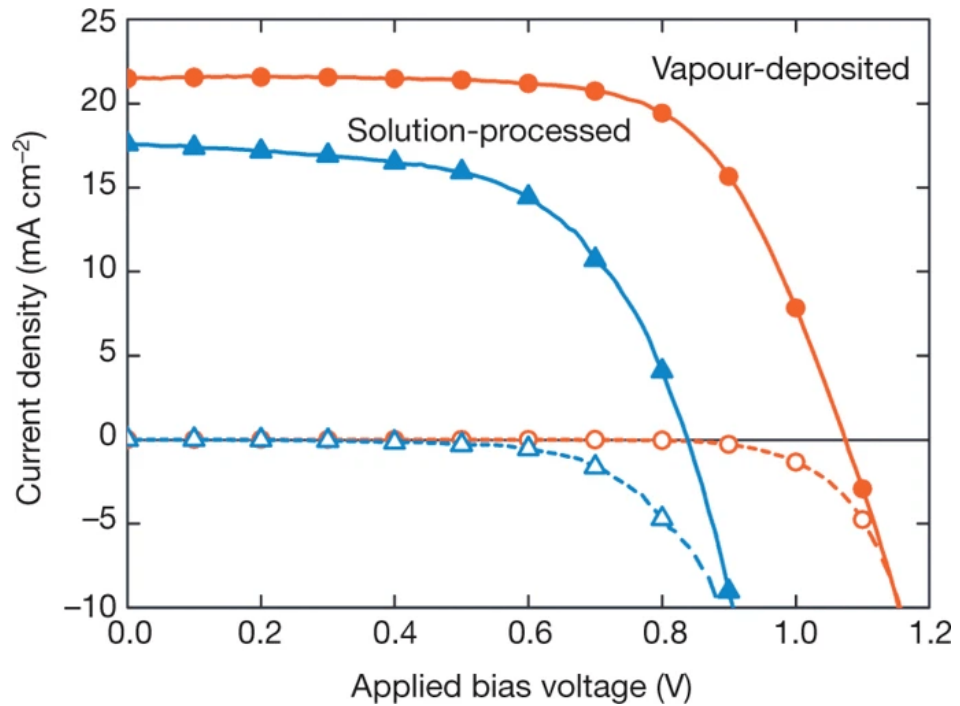


Figure 4.7: J-V characteristics produced by vapour deposition and solution deposition of the PSCs [3].

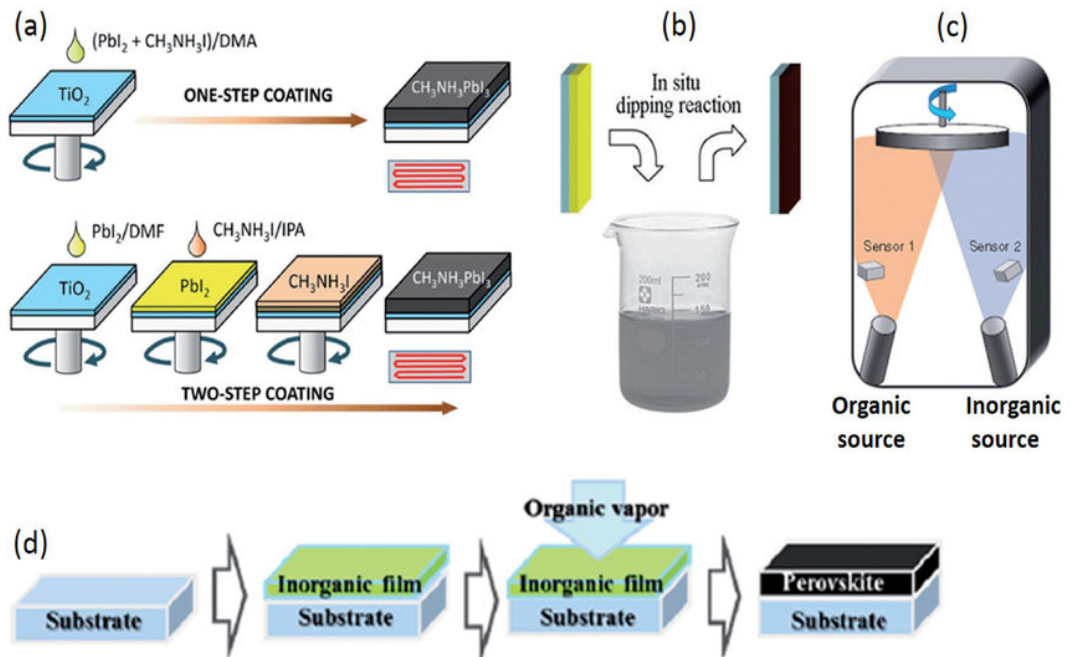


Figure 4.8: Different perovskite film preparation methods [81].

spray-coating are some of the familiarly used deposition approaches (Fig.4.8) [64]. Several experimental techniques such as X-ray diffraction [65], atomic force microscopy [66], electron diffraction [67] and polarized optical microscopy [68] have

been utilized to understand the bulk structure of polymers better. Nevertheless, the determination of conformations in a practical heterogeneous environment involving donor and acceptor regions remain beyond the reach of available experimental techniques [69]. *Ab initio* calculations are one of the most promising computational approaches to obtain detailed structural information of such molecules.

#### 4.8.2 Computational Approach

The computational approach is further divided into several disciplines, including Molecular Dynamics (MD), chemical dynamics, molecular approaches, *ab initio*, and semi-empirical approaches. A widespread disadvantage of the above methods is that they depend on external parameters or experimental results. For example, as long as a constant force field of interaction parameters is provided between atoms, molecular dynamics simulations can predict molecules structural evolution under temperature and kinetic properties [70]. Thus MD calculations strongly depend on *ab initio* calculation results, which assist into the improved force field and parameters necessary. Nowadays, MD successfully applied to the halide perovskites. Belugas *et al.* [74] employed the force field to study the vibration spectrum's temperature evolution and regenerated the essential characteristics of the vibration spectrum. The kinetic results of the MD simulation analysis show that the methylammonium lead iodide spectrum has a large temperature development, has the transformation of orthographic crystal to tetragonal crystal to cubic crystal, and strongly depends on the restriction and order of molecules. Taufique *et al.* [71] implemented a classic MD simulation to study the accumulation of PCBM, which forms a typical ETL on the surface of various perovskite crystals in the presence of solvents. There have been several reviews of the theoretical research into halide perovskites: reviews on optoelectronic properties [71], and Briefly reviews the nature of chemical bonds [72], and electronic as well as ionic motions [73], reviews focusing within MD simulations [72]. *Ab initio* quantum mechanical calculation, which does not depend on external parameters, is of great help since it can predict the structure, energy levels, and optical transition strength of compounds before synthesis [75, 76].

### 4.8.3 Density Function Theory

Over the decades since the introduction of the Schrödinger equation [77], many excellent methods have been developed for directly solving the electron structure problem, including configuration interaction, Moller-plesset perturbation theory, the coupled-cluster expansion and quantum Monte Carlo [71]. Nevertheless, the coupling between coordinates in the many-electron Schrödinger equation makes the computational cost of such methods significantly high or impossible [72]. The Density Functional Theory (*DFT*) which began in 1926 with the creation of the Thomas-Fermi theory [88], an approximate method for finding the electronic structure of atoms using just one electron ground state density  $\rho(r)$  came as a remedy to the problem of solving coupled coordinates, thus reducing the computational costs. Hohenberg and Kohn-Sham [99] laid a solid foundation of the theory by mathematically showing that an exact method based on the  $\rho(r)$  exists in principle, where  $\rho(r)$  is defined to be exactly that of the real system, currently *DFT* using the HK theorem [99]. the ground state energy can be written as;

$$E = T_s + U + V_{nuc} + E_{XC}[\rho] \quad (4.3)$$

Where  $T_s$  is the energy of the Kohn-Sham orbitals,  $U$  is the Hartree energy,  $V_{nuc}$  the core and its attraction to and  $E_{XC}[\rho]$  is everything else which makes the above exactly. In actual calculations, the *XC* contribution is approximate, and the result is only as good as the approximation used. The *XC* was first approximated using a theory called local density approximation (*LDA*) (Eqn.4.4) developed in the 1970's but had many shortcomings, Generalized Gradient Approximation (*GGA*) (Eqn.4.5) was later introduced to compensate for these shortcomings and hybrids were also submitted by Becke [80] leading to the well known and widely used exchange-correlation function called Becke's-three parameter Lee-Yang-Parr (*B3LYP*) [141].

$$E_{XC} = \int \epsilon_{xc}(n)n(\vec{r})d^3r \quad (4.4)$$

$$E_{XC} = \int (n, \nabla n)n(r)d^3r \quad (4.5)$$

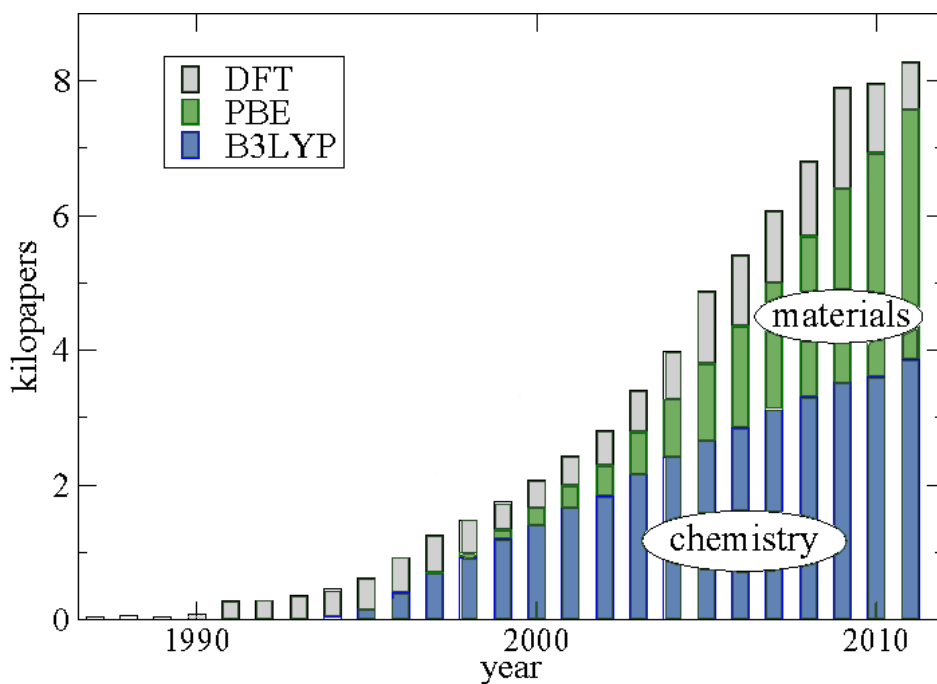


Figure 4.9: Number of *DFT* papers published based approximation function with citations [85].

Though *DFT* functionals were so well developed, until the 1990's they still could not treat Van der Waals interactions or yield correct long-range dispersion forces [92]. The reason was that the binding energy curves decay exponentially instead of  $-C_6/R^6$ , where  $R$  is the separation distance, and  $C_6$  is the Van De Waals coefficient [86]. Different strategies for solving this problem have proposed: (i) a completely scratch-based approach (i.e., a non-empirical approach); (ii) reparameterization of existing functions; and (iii) including empirical terms. Recently, the latter approach has been the subject of a renewed interest, and several attempts have been reported to use pair-wise attraction terms of the form  $-f(R)C_n/R_n$  ( $n=6,7,\dots$ ) for both molecular complexes and extended systems. The proposed corrections differ in the form of the damping function  $f(R)$  and the atom-atom dispersion coefficients  $C_n$ . David Langreth and Bengal Lundquist [87]. Developed an approximate non-local ground-state density functional called LL, with the right decay [89]. At the same time, with this development, Grimme [89] developed his DFT-D method that provides an empirical correction to the DFT results in a highly systematic and accurate fashion. The model has demonstrated to be successful in dealing with small molecular adducts,  $\pi$ -stacking, and large complexes (e.g., DNA base pairs)

of interest for biological systems and molecular crystals [91]. The use of DFT since its formalization has been steadily increasing, and better ways to treat chemical problems are emerging, as shown in (fig.4.9) shows a trend in the increase [85]. Up to this level, the success of DFT was only on ground state electron structure calculations, without considerations of the excited-state [93]. The need to develop methods that treat excited states lead to the development of methods like min-principle [94] and ensembles [103]. Later a time-dependent DFT (TDDFT) was developed and has become a robust and viral method. The method is based on the fact that all observables in a quantum problem are functional of the time-dependent density [95].

## 4.9 Stability of Perovskite Solar Cells

The primary challenge in realization perovskite solar cells today is the instability of the devices in a surrounding environment. Over the past few years, considerable effort have been made to improve perovskite-type solar cell devices, stability by adopting various device architectures, compositions, and manufacturing technologies. Stability and efficiency are essential parameters for commercial applications of perovskite solar cells. Perovskite devices have achieved high efficiency so far. However, the stability of the devices is still one of the problems facing the research community. Perovskite compounds with manufacturing processes can contain traps into the degradation of perovskites [96]. The exposure of these layers to UV light [97], humidity [98], oxygen [100], and temperature [101] affect the stability of PSC. Various experimental and computational studies were carried out to determine possible solutions to improve stability. Solving the instability of perovskite materials is a key strategy to increase long-term stability. The geometric factors limit the formation of stable 3-dimensional the perovskite structures. Stability structure of perovskite can be defined by Goldsmidt's called tolerance coefficient, as shown in Eq.(4.6) [102].

$$t = \frac{r_A + r_0}{\sqrt{2}(r_B + r_0)} \quad (4.6)$$

Where,  $r_A$ ,  $r_B$  and  $r_0$  are ionic radius for organic cation A, inorganic cation B and halide anion X, respectively. The ideal cubic perovskite structure would have a  $t=1$  and the cubic structure can only be acquired when  $0.89 < t < 1$  [103]. Low tolerance factor means lower symmetry and the perovskite would shift to an orthorhombic or tetragonal structure, which would give a negative effect on the opto-electronic properties of perovskite [104]. Most stable perovskite materials have to satisfy a  $0.8 < t < 1$  [106] and the most stable perovskite material is still  $MAPbI_3$ , which has a tolerance factor slightly higher than 0.9 [105]. The Computational approaches based on the Goldschmidt tolerance factor is used to estimate the geometric stability of the three-dimensional (3D) perovskite structure [3]. Filip and Giustino. [108] A theoretical combinatorial search based on density function theory was carried out on the entire periodic table. Korbel *et al.* [109] starting with over 32,000 possible 3D  $ABX_3$  compounds (Fig.4.10). Found suitable band gap values for 199 possible 3D  $ABX_3$  thermodynamically stable perovskites with cubic structure and photovoltaic applications. The result of these studies is that lead has the best photoelectric properties in 3D perovskite. Replacing the toxic  $Pb^{2+}$  and  $Sn^{2+}$ , while maintaining high performance is a grand challenge for the research community [110]. Recently, chemical composition engineering or alloying has proven to be an effective strategy that can be used to adjust the photoelectric and stabilizing performance of the perovskite-based solar cell [111]. However, for lead-free perovskite systems, this strategy has not been extensively studied. Further research may lead to the discovery of new 3D lead-free perovskites [111].

#### 4.9.1 Moisture instability

Instability of perovskite by moisture arises, from the effect the hygroscopic nature on amine salt [139].  $MAPbI_{3-x}Cl_x$  and  $MAPbI_3$  endure on a similar moisture-assisted degradation process, in which the methylamine group is lost due to sublimation, and  $PbI_2$  formed, leading to further degradation to  $CH_3$ ,  $NH_2$ , and  $HI$  [113]. However, recent experiments have shown that the formation of the hydrate phase of  $MAPbI_3$  is an integral part of the degradation mechanism [98]. Huang *et al.* [114]

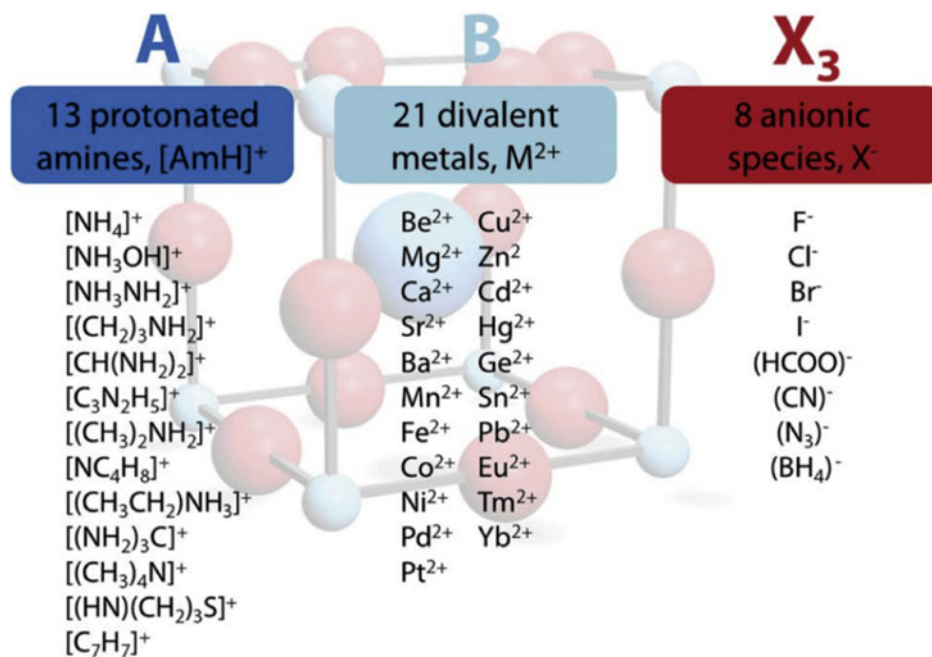


Figure 4.10: Calculated goldsmiths tolerance factor for some materials [112], Copyright 2015, The Royal Society of Chemistry

used pure inorganic 2D nanosheets exfoliated from montmorillonite as the photo-sensitive layer and added to the  $MAPbI_3$  perovskite precursor solution. As a result, the nanosheet is slowed down, and the crystallization rate is reduced, resulting in the formation of larger particles and shells on the surface of the perovskite film [114]. This shell effectively protected the perovskite against moisture, light, and even thermal degradation [114]. The color of the fresh film stored in a relatively humidity of 70% environment did not change, while the control completely turned to yellow (Fig.4.11)(a)), (Fig.4.11)(b) and (c), it can be clearly seen that the stability of the passivation device has been greatly improved under humidity and light. A moisture, induced recombination mechanism is also proposed to control moisture synthesis in planar geometry. Although the efficiency has increased to 19.3%, it quickly drops below 5% of the original performance when stored under ambient conditions [115]. The packaging technology developed for CIGS-based devices can effectively solve the humidity sensitivity of these devices [116]. Mosconi *et al.* [115] applied Ab initio molecular dynamics (AIMD) simulation to study the interaction between liquid water ends and the tetragonal  $MAPbI_3$  (001) surface with different terminations. Their results showed the interaction between Pb atoms and

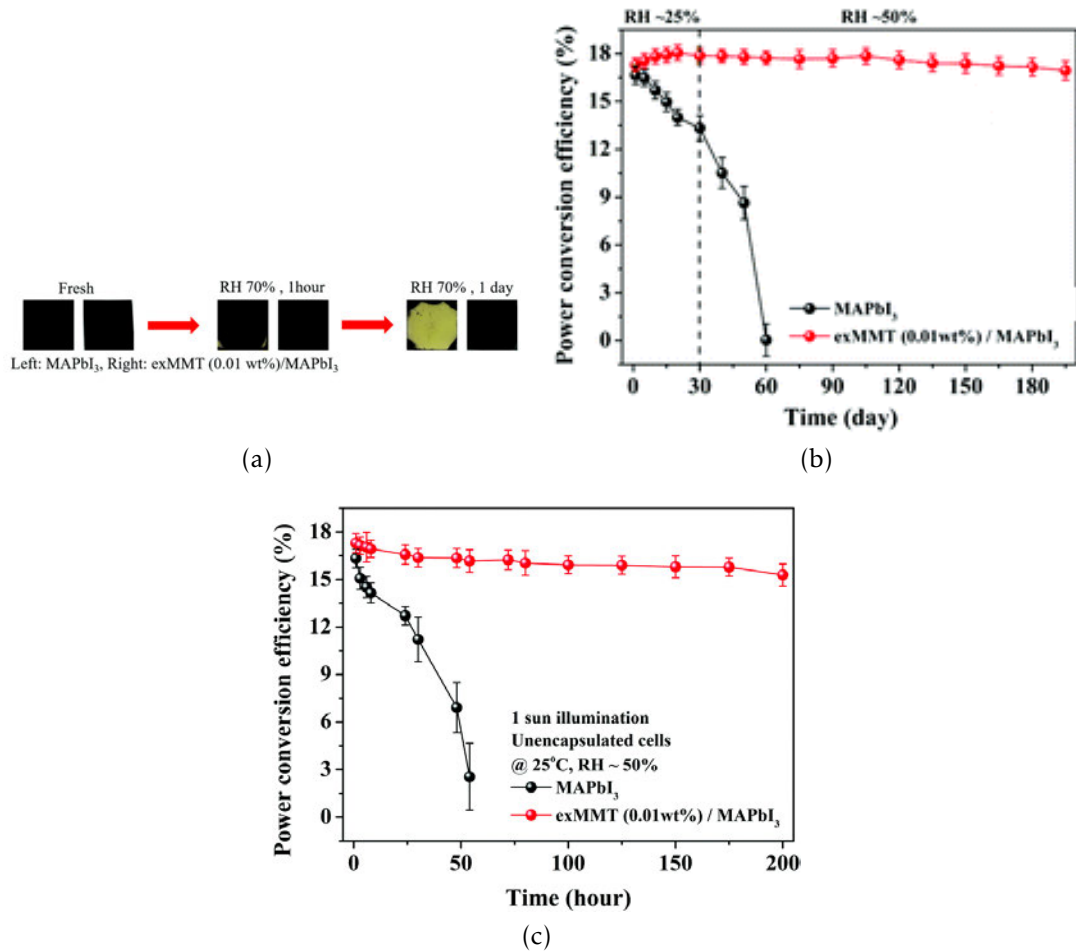
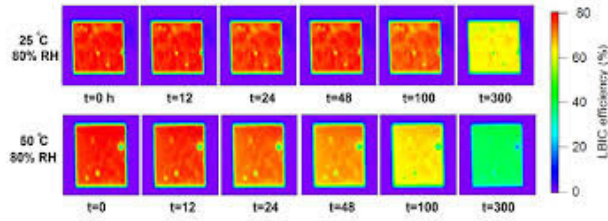


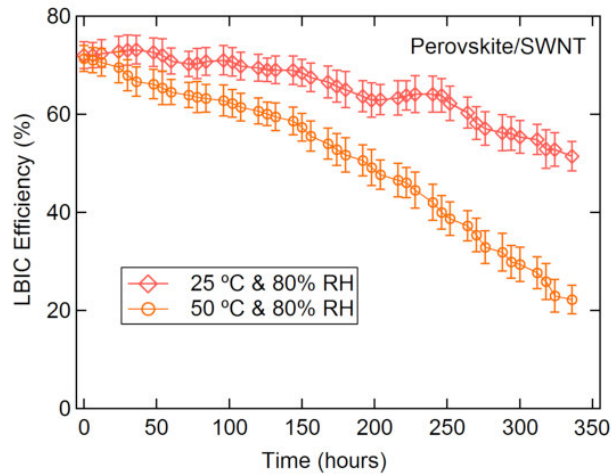
Figure 4.11: Exfoliated montmorillonite nanosheets to improve the environmental stability of  $MAPbI_3$  (b) Relative humidity of the  $MAPbI_3$  with the environmental condition around the film (c) Relative humidity of the  $MAPbI_3$  at room temperature with constant sunlight [114].

water molecules accelerate the release of I atoms, the surface of the MAI end is easy to dissolve, It was also found that, due to the stronger  $PbI$  bonds on these surfaces, the  $PbI^{-2}$  terminated surface is less sensitive to interfacial water, they also suggested that the incorporation of water molecules into the  $PbI_2$  exposed surface may be to the first step in the formation of an intermediate hydrated phase. Zhang *et al.* [116] performed AIMD and DFT calculations on  $MAPbI_3$  perovskite, the calculation results show that the light absorption attenuation caused by moisture is closely related to the formation of hydrated species, the electronic excitation in the exposed and water-adsorbed  $MAPbI_3$  nanoparticles tends to weaken the  $PbI$  bond, in the excited state where water molecules participate in the electronic excitation,

the bonding mode induced by light stimulation is reduced by up to 20%, which indicates the Accelerated decomposition of perovskite in the presence of sunlight and moisture. Long *et al.* [119] performed Ab Initio non-adiabatic molecular dynamics from scratch. Found that the tetragonal  $MAPbI_3$  can destroy the perovskite surface of a small amount of water adsorbed on the surface of the MAI end (001), so that the light-stimulated electrons are positioned close to the surface, and more importantly, the electron holes are reduced by avoiding deep electron traps overlap and increase the life span of the induced state. Some theoretical efforts have focused on the influence of water molecules on the stability of other perovskite materials, such as  $MAGel_3$  and  $FAPbI_3$  [120]. These studies also found that in  $MAPbI_3$ , water easily diffuses into the perovskite, structural destructions, the formation of hydrated intermediates, and the moisture-induced decrease in optical absorption observed in  $MAPbI_3$ . DFT-based calculations are used not only to study the mechanism of water degradation in perovskite solar cells but also to propose strategies to improve their water stability. Dong *et al.* [121] performed theoretical calculations on the corresponding molecular model of  $MAPbI_3$  and found that the hydrogen bond interaction between the inorganic  $PbI_3$  unit and the organic  $CH_3NH_3$  unit plays an important role in determining the stability of  $MAPbI_3$ . Computations show that due to the high polarity of water, the organic-inorganic structure will inevitably change in a humid environment. Based on these theoretical insights, they deposited an ultra-thin  $Al_2O_3$  film on the hole transport layer to improve the stability of the medium without significantly reducing efficiency. First-principles DFT calculations performed by Zhang and co-workers' in conjunction with AIMD showed that the  $PbI_2$  end (001) surface of  $MAPbI_3$  is more stable than the MAI-terminated  $PbI_2$  defect surface in a humid environment which is the same as Calculated by Mosconi *et al.* [117], Koocher *et al.* [122] found that water adsorption on the surface of  $MAPbI_3$  (001) is greatly affected by the orientation of  $CH_3NH_3$  (MA) cations near the surface. Water favorably adsorbs on in all positions on the  $PbI_2$  and MAI surfaces studied, water can be actively adsorbed and supports the existence of the experimentally observed hydrate state, which is a possible first step in the degradation process. The calculation results (including the implicit liberation model) show that higher water concentration can promote degradation by increasing lattice distortion. Heben



(a)



(b)

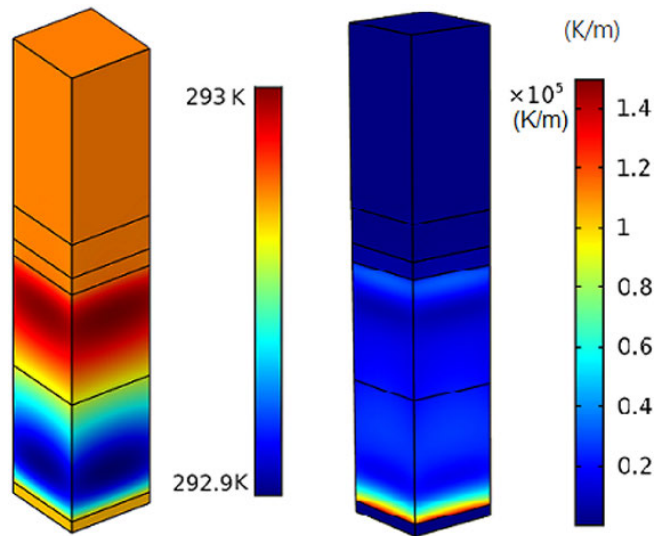
Figure 4.12: (A) LBIC mapping development of perovskite/SWCNT devices under high humidity conditions, (b) stability testing of perovskite/SWCNT devices under high humidity conditions [123].

*et al.* [123] studied the degradation mechanism of perovskite devices against moisture. They added an *SWCNT/PMMA* composite as an encapsulation layer. Due to this encapsulation layer improve the resistance to water. And the preliminary devices showed an average efficiency of around 7%. Due to the addition of the dielectric *PMMA*, the open-circuit voltage drops and the series resistance increases significantly. However, these devices exhibit better current collection uniformity and improved breakdown resistance (Fig.4.12). The addition of *SWCNT/PMMA* encapsulation enhanced the devices from 24 to 300 h for the high temperature and 52 to 700 h for the low-temperature condition. With the optimization of the production process and glass packaging application, the service life may improve. *SWCNT/PMMA* electrodes have high heat and humidity resistance and have great potential for perovskite-type solar cells long-term stability. Thermal instability of perovskite solar cells is a big issue for scientists community. When the device that

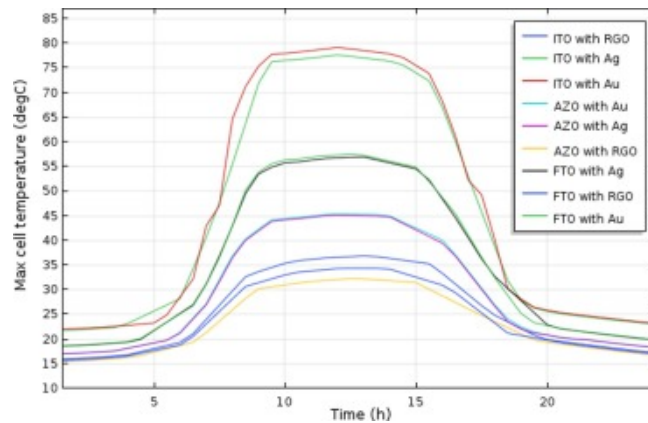
subjects to a high temperature causing the device's degradation. In this section, we discuss some of the numerical and experimental studies that have been conducted on the effect of the temperature on perovskite solar cells. As well as strategies developed to improve the thermal stability of these optoelectronic devices. As we know that the temperature has a great influence on the crystal structure and on the perovskite phase. It was previously reported on the studies on influence of temperature, that the tetragonal phase changed to the cubic phase at  $54\text{ C}^\circ$ -  $56\text{ C}^\circ$  [124]. The performance ( $\eta$ ) of the device is highly dependent on the operating temperature through the following relations reported in the literature (Eqn.4.7) [125].

$$\eta_c = \eta_{T_{ref}}[1 - \beta_{ref}(T_M - T_{ref})] \quad (4.7)$$

Where  $T$  and  $\eta$  are the temperature and  $PCE$ , respectively, and  $\beta_{ref}$  is the temperature coefficient of the  $PV$  module. It should be noted that these relations reported for traditional solar cell modules and the performance loss through the degradation of the device components have not been considered. Makableha *et al.* [126] use numerical simulation to investigate the effects of the thermal behavior, including solar radiation, Joule heating, and non-radiative recombination, for regular planar heterojunction perovskite solar cell consisting of indium tin oxide (ITO) as front contact and gold as back contact is conducted(Au). The result it has been found that solar radiation is the dominant source through which of maximised operating temperature of the cell reached  $74.5\text{ C}^\circ$  under the effect of Joule heating and non-radiative recombination is minor, and the maximum. Displayed in (Fig.4.13(b)) shown the influence of all heat sources, all combinations' thermal behavior. The results show that the structure with  $ITO/Au$  contacts will have a higher operating temperature reaching  $79\text{ C}^\circ$ . In comparison,  $ITO/Ag$  temperature will be slightly lower due to higher emission, going to  $77.7\text{C}^\circ$ . Then, the  $FTO/Au$  contact is reduced by about 27.5%, and almost the same percentage decreases the  $FTO/Ag$  contact. The higher temperature drop resulted in  $AZO$  use as front contacts and Au and Ag as back contacts, and the temperature reached  $45.3\text{ C}^\circ$  [126]. Gorji *et al.* [127] applied the *COMSOL* calculations on the heat conduction between the perovskite-type solar cell and graphene. The results indicated that the bottom layer (RGO) is less hot than the other layers, which are the contact acts as a heat sink and a greater



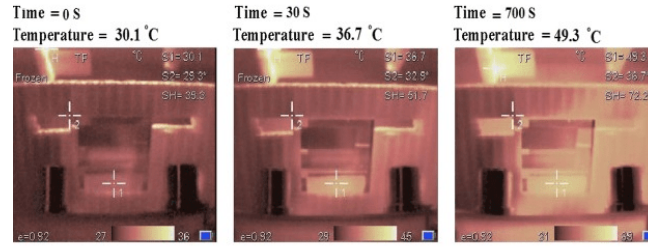
(a) Show thermal simulation results.



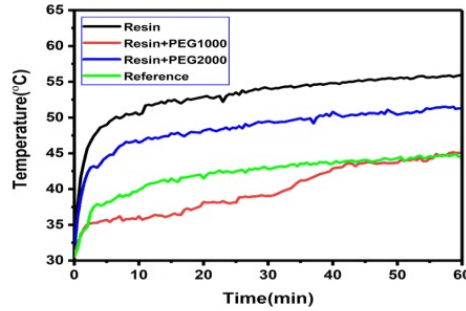
(b) The maximum working temperature of the PSC through one day due to all the heating sources

Figure 4.13: Simulation results of Thermal instability of PSCs [126, 127].

conductor with a higher area close to the air environmentS showing in (Fig.4.13(a)). These results refer to improve the thermal trends of the cell due to high thermal conduction and thin thickness of the RGO layer. Fumani *et al.* [129] did designed a polymer encapsulation layer both a flexible moisture-blocked and temperature-controlled were used as Cooling Agent. Results have proved that the resin encapsulation system commonly used in optoelectronic devices can be used as a barrier to heat release caused by light loss and electrical loss during devices operation. Also, they investigated the effect of the designed cooling system PSC temperature adjustment, by using four types of devices the reference cell encapsulated with resin cell only, encapsulated resin/PEG1000, and resin/PEG2000 system, one which is ther-



(a)



(b)

Figure 4.14: (a) operating device temperature curve, (b) a temperature-time graph under the sun [129].

mally controlled under sunlight (Fig.4.14). In all the examples studied, the trend of temperature increase(Fig4.14) (a), and (b). As observed, the maximum temperatures of the reference device, resin, resin/PEG1000, and resin/PEG2000 encapsulated devices are 41.2, 49.3, 36.6, and 46.9 C°, respectively. Compared with the unencapsulated resin/PEG1000 and resin/PEG2000 encapsulated devices, the pure resin encapsulated devices reached the highest temperature. As a result, a 2-year stable device is achieved, as confirmed by the electrical analysis that showed no significant changes in the recombination and transport resistances after 450 days of storage.

## 4.9.2 UV instability

*UV* light exposure is a very important factor that influencing the stability of perovskite solar cells. Like many solar cell technologies, illumination becomes the cause of degradation of perovskite solar cells. Degradation of perovskites by *UV*

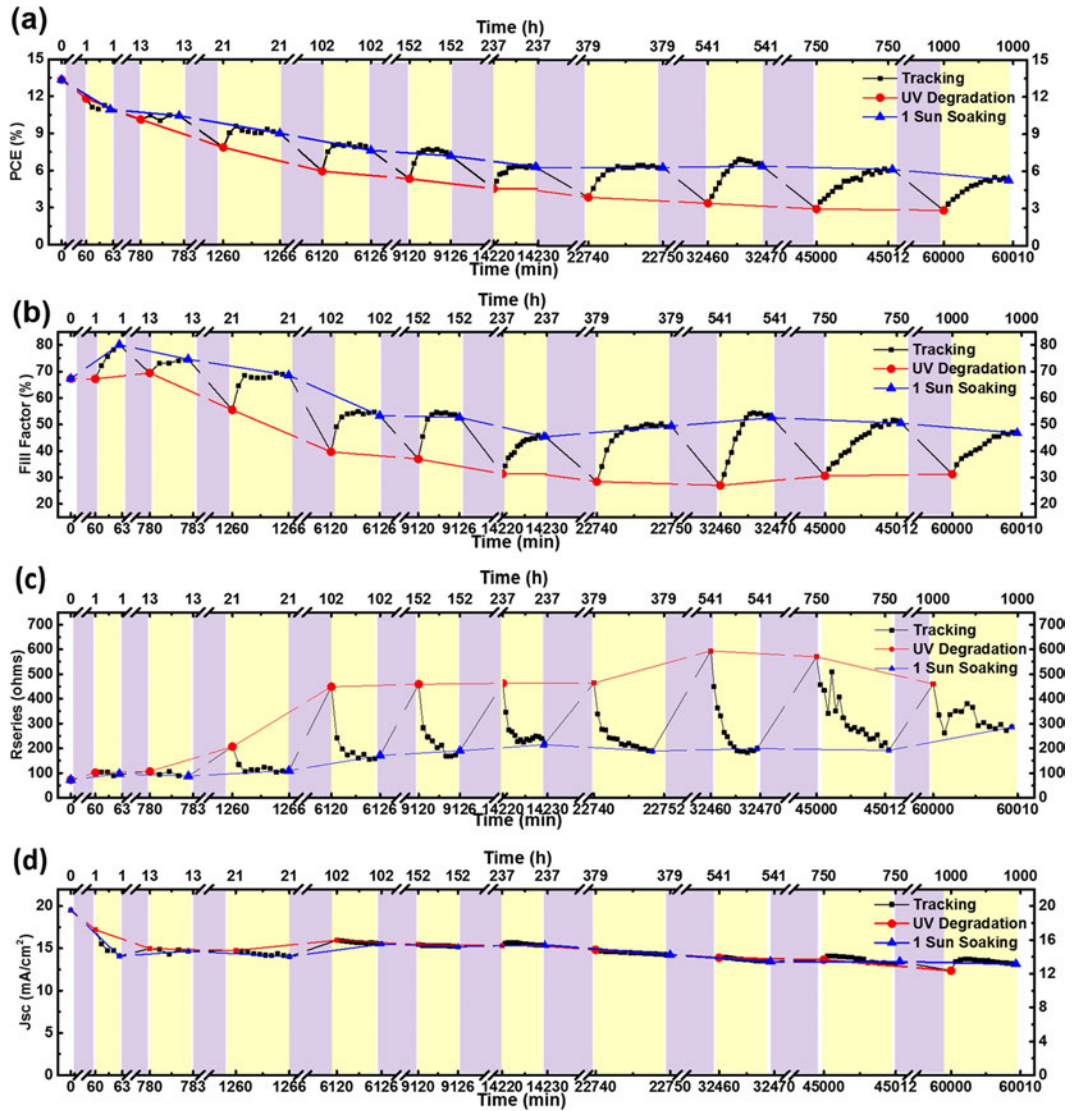


Figure 4.15: UV degradation/recovery cycle of perovskite device performance [141].

light attributed to the use of the  $TiO_2$  layer as a photosensitizer in  $PSC$ . With assistance from  $UV$  light,  $TiO_2$  could interact with  $I^-$  and form  $I_2$  as in typical  $DSSCs$ . Therefore, it could destroy the perovskite crystal structure and enhance the ionic reaction process of organic cations [130]. Leijtens *et al.* [2] was investigated by measuring 5h efficiency decay curve, measured under 1-sun A.M 1.5G illumination for devices with and without encapsulation and  $UV$  filter. The results showed that encapsulated devices decayed more rapidly than a nonencapsulated device, which indicated that the degradation not just starts from the active layer but also the meso- $TiO_2$  (Fig.4.1). Display their  $UV$  1-sun cycling illumination test results and possible mechanism. Ito *et al.* Reported observes that the inclusion of the  $Sb_2S_3$  layer in

the interface between the mesoporous  $TiO_2$  and the perovskite layer increased the stability due to the interruption of the iodide pair at this interface. Unfortunately, the UV-filter might trigger an unavoidable fabrication cost increasing due to extra materials cost [130]. It has also been reported that the presence of oxygen prevents the ultraviolet activation degradation at the  $TiO_2$  interface, which eliminates the surface state and passivates the trap sites at the interface, which is the titanium dioxide n-type semiconductor [132]. The use of aluminum silicate shells on titanium dioxide nanoparticles can increase stability [132]. With regards to (MSSC), the  $Al_2O_3$  scaffold is a more stable alternative to  $TiO_2$  [133]. However, alternative charged layers and electrodes, interface engineering, and packaging technologies must be sought to solve this problem. Various strategies have been reported to delay the UV-induced instability of PCS devices. Several groups have demonstrated the stability of about 1000 hours under a light with little or no degradation in performance [134].

## 4.10 Hysteresis Effects

The mechanism of hysteresis in perovskite devices is still unknown several hypotheses were established. one of these hypotheses ferroelectric polarization, widely discussed [135], and ion migration [136]. Hysteric behavior could be dependent on the ferroelectric polarization. Thus, it is interesting to investigate hysteresis, depending on the ferroelectric. Understanding the ferroelectric behavior is essential to improve efficiency and stability because it affects light-stimulated electron-hole matching and separation [137]. Snaith *et al.* [138] suggested the capacitance effect, the ferroelectric behavior of absorber, and defect density are the sources of the hysteresis behavior. If this effect not considered, it will result in a false comparison between the efficiency value and the stabilized output [139]. The hysteresis observed in the current-voltage ( $J - V$ ) curve is due to the ferroelectric domain under the applied electric field, and the same effect may cause ion migration or trapping of charge carriers [140]. Determine the existence of ion migration is dependent on the measure of the current-voltage  $J - V$  curve of the perovskite film in the lateral electrode

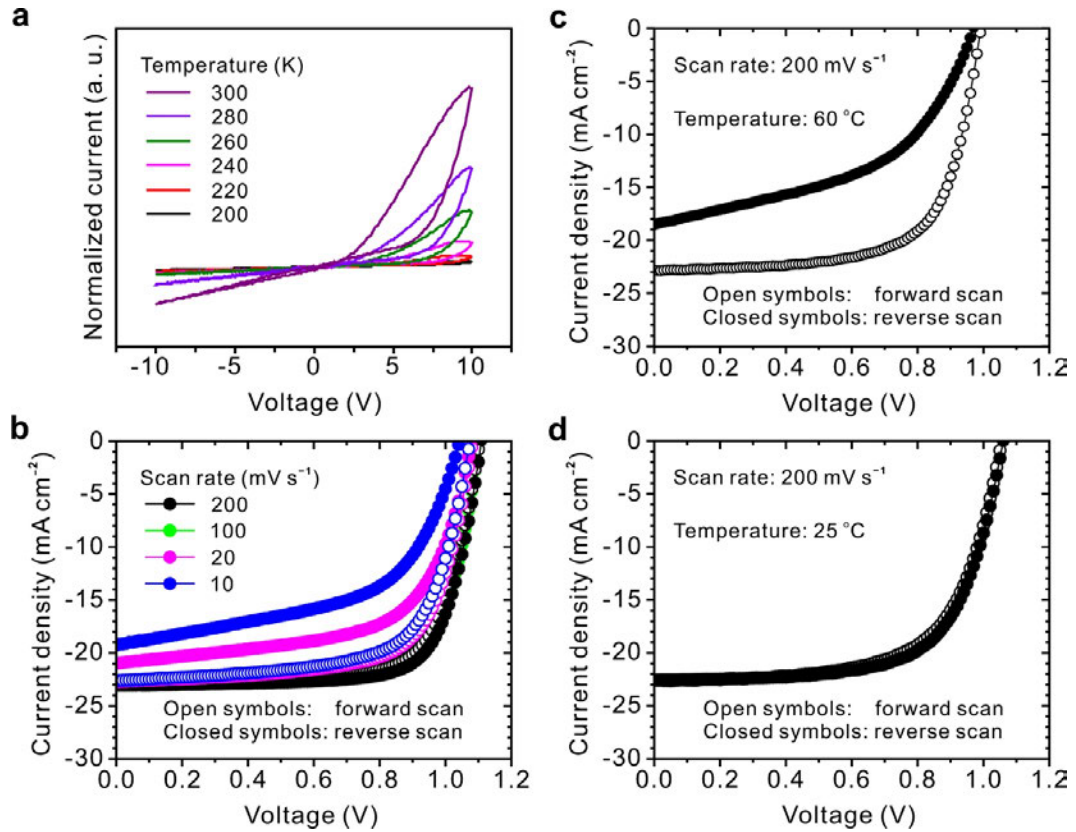


Figure 4.16: Diagram of ion migration in perovskites solar cells [141].

structure, by temperature-dependent conductivity electrical measurements. Ulzii *et al.* [141] used this design to ionic conduction, they find as ions would not contribute to the conductivity at low temperatures, but would help when the temperature was sufficiently high to provide the energy required to form mobile ions. Fig.4.16 shows  $J - V$  curves, (a) temperature-dependent conductivity measurements in a lateral structured perovskite film, (b) scan rate dependent current density-voltage curves of perovskite solar cells, c, d Effect of temperature on the hysteresis of perovskite solar cells at a fast scan rate of  $200 \text{ mV s}^{-1}$ . Current density-voltage curves measured at  $60 \text{ C}^\circ$  (c) and after cooling to room temperature (d), these results revealed that the hysteresis increased with increasing temperature [142]. Recent studies have begun to support that both ion migration and charge trapping could be the reasons  $J - V$  hysteresis [143, 144]. Understanding the disruptive phenomena that cause degradation in the perovskite device is critical to improving efficiency and is an open area of research. Physical optimization and theoretical simulation through trial and error will ensure stable efficiency and contribute to technology maturity.

## 4.11 Conclusions and perspectives

In this article, we've reviewed the developments and basic structures of perovskite-based solar cells. We also explained in detail the several computational and experimental attempts to address and understanding certain vital factors such as the optical properties, energy bandgap, and the stability of the perovskite materials limiting the development. The commonly used *Pb* element is highly toxic, and *TiO<sub>2</sub>* suffers from UV-induced instability, contributing to the short lifetimes of *PSC*. Suggested alternatives, such as *SnO<sub>2</sub>* and *ZnO*, have shown massive potential in the *PSC* community, with low-temperature fabrication. Moreover, replacing *Pb* with non-toxic ingredients will also prove beneficial in the future. We also introduce the perovskite-chalcogenide with narrow bandgap, which provides more light absorption, one of the promising aspects of perovskite solar cells.

Currently, the theoretical approaches to understanding the microscopic physical mechanism of perovskite solar cells are considered a viable means. It will be easier to provide ideas for improvement and develop materials and structures that are simpler and more efficient if researchers can develop a theoretical device to verify the complex composition of the perovskite. The instability issues of *PSC* are also still been debated, and more research is needed to full comprehension since this is a significant underlying problem of perovskite photovoltaic technology.

Many strategies are being developed to improve the stability of perovskite solar cells against moisture, temperature, oxygen, and ultraviolet light. The moisture and oxygen stability of the perovskite device can effectively improve through advanced packaging technology. Ultraviolet light and heat are unavoidable problems of perovskite devices during the operation. Given the rapid development and a vast number of publications on *PSC*, an investigation of newly designed strategies for improving the stability issues pushes its commercialization one step forward. Furthermore, more efforts should be made to the intrinsic and essential mechanisms of the degradation process. The main factors that affect the degradation of perovskite materials under the environmental atmosphere should be clarified to provide more scientific guidance to increase stability.

---

## References

- [1] A. Pal, L. K. Wen, C. Y. Jun, I. Jeon, *effects due to fullerene size, addends, and crystallinity on band structure, charge transport and optical properties*, *Physical Chemistry Chemical Physics* 19 (2017) 28330–28343.
- [2] H. Tanaka, M. Misono, *Advances in designing perovskite catalysts*, *Current Opinion in Solid State and Materials Science* 5 (2001) 381–387.
- [3] I. Warshaw, R. Roy, *Stable and metastable equilibria in the systems  $\text{y}_2\text{o}_2\text{-al}_2\text{o}_3$ , and  $\text{gd}_2\text{o}_3\text{ fe}_2\text{o}_3$* , *Journal of the American Ceramic Society* 42 (1959) 434–438.
- [4] S. Kazim, M. K. Nazeeruddin, M. Graetzel, S. Ahmad, *Perovskite as light harvester: a game changer in photovoltaics*, *Angewandte Chemie International Edition* 53 (2014) 2812–2824.
- [5] Y.K. Ren, X.H. Ding, Y.H. Wu, J. Zhu, T. Hayat, A. Alsaedi, Y.F. Xu, Z.Q. Li, S.F. Yang, S.Y. Dai, *Temperature-assisted rapid nucleation: a facile method to optimize the film morphology for perovskite solar cells*, *Journal of Materials Chemistry A* 5 (2017) 20327–20333.
- [6] M. Liu, M. B. Johnston, H. J. Snaith, *Efficient planar heterojunction perovskite solar cells by vapour deposition*, *Nature* 501 (2013) 395–398.
- [7] J. Duan, W. Sha, Y. Zhao, Y. Wang, X. Yang, Q. Tang, *Inorganic perovskite solar cells: an emerging member of the photovoltaic community*, *Journal of Materials Chemistry A* 7 (2019) 21036–21068.
- [8] Q. Wali, F. J. Iftikhar, M. E. Khan, A. Ullah, Y. Iqbal, R. Jose, *Advances in stability of perovskite solar cells*, *Organic Electronics* 78 (2020) 105590.
- [9] C. Gai, J. Wang, Y. Wang, J. Li, et al., *The low-dimensional three-dimensional tin halide perovskite: Film characterization and device performance*, *Energies* 13 (2019) 1–26.

- [10] D.Y. Son, J.W. Lee, Y. J. Choi, I.H. Jang, S. Lee, P. J. Yoo, H. Shin, N. Ahn, M. Choi, D. Kim, et al., *Selfformed grain boundary healing layer for highly efficient ch 3 nh 3 pbi 3 perovskite solar cells*, *Nature Energy* 1 (2016) 1–8.
- [11] A. K. Shukla, K. Sudhakar, P. Baredar, *A comprehensive review on design of building integrated photovoltaic system*, *Energy and Buildings* 128 (2016) 99–110.
- [12] M. A. Green, A. HoBaillie, *Perovskite solar cells: the birth of a new era in photovoltaics*, *ACS Energy Letters* 2 (2017) 822–830.
- [13] Z. Song, C. L. McElvany, A. B. Phillips, I. Celik, P. W. Krantz, S. C. Watthage, G. K. Liyanage, D. Apul, M. J. Heben, *A techno-economic analysis of perovskite solar module manufacturing with low-cost materials and techniques*, *Energy Environmental Science* 10 (2017) 1297–1305.
- [14] C. Battaglia, A. Cuevas, S. De Wolf, *High-efficiency crystalline silicon solar cells: status and perspectives*, *Energy Environmental Science* 9 (2016) 1552–1576.
- [15] F. Sani, S. Shafie, H. N. Lim, A. O. Musa, *Advancement on lead-free organic-inorganic halide perovskite solar cells: a review*, *Materials* 11 (2018) 1008.
- [16] M. I. H. Ansari, A. Qurashi, M. K. Nazeeruddin, *Frontiers, opportunities, and challenges in perovskite solar cells: A critical review*, *Journal of Photochemistry and Photobiology C: Photochemistry Reviews* 35 (2018) 1–24.
- [17] W. Ke, G. Fang, J. Wan, H. Tao, Q. Liu, L. Xiong, P. Qin, J. Wang, H. Lei, G. Yang, et al., *Efficient hole-blocking layer-free planar halide perovskite thin-film solar cells*, *Nature communications* 6 (2015) 1–7.
- [18] H. J. Snaith, A. Abate, J. M. Ball, G. E. Eperon, T. Leijtens, N. K. Noel, S. D. Stranks, J. T.-W. Wang, K. Wojciechowski, W. Zhang, *Anomalous hysteresis in perovskite solar cells*, *The journal of physical chemistry letters* 5 (2014) 1511–1515.
- [19] P. Tonui, S. O. Oseni, G. Sharma, Q. Yan, G. T. Mola, *Perovskites photovoltaic solar cells: An overview of current status*, *Renewable and Sustainable Energy Reviews* 91 (2018) 1025–1044.

- [20] N. Marinova, S. Valero, J. L. Delgado, *Organic and perovskite solar cells: Working principles, materials and interfaces*, *Journal of colloid and interface science* 488 (2017) 373–389.
- [21] H. S. Jung, N.-G. Park, *Perovskite solar cells: from materials to devices*, *small* 11 (2015) 10–25.
- [22] F. H. Alharbi, M. I. Hossain, N. Tabet, *Perovskite based solar cells: A milestone towards cheaper pv technology*, in: *3rd International Symposium on Environmental Friendly Energies and Applications (EFEA)*, IEEE, 2014, pp. 1–6.
- [23] T. Shi, W.-J. Yin, F. Hong, K. Zhu, Y. Yan, *Unipolar self-doping behavior in perovskite  $\text{CH}_3\text{NH}_3\text{PbBr}_3$* , *Applied Physics Letters* 106 (2015) 103902.
- [24] G. Boschloo, A. Hagfeldt, *Characteristics of the iodide/triiodide redox mediator in dyesensitized solar cells*, *Accounts of chemical research* 42 (2009) 1819–1826.
- [25] A. Kojima, K. Teshima, Y. Shirai, T. Miyasaka, *Organometal halide perovskites as visible-light sensitizers for photovoltaic cells*, *Journal of the American Chemical Society* 131 (2009) 6050–6051. 26. M. Graetzel, *The light and shade of perovskite solar cells*, *Nature materials* 13 (2014) 838.
- [26] H.S. Kim, C.-R. Lee, J.-H. Im, K.-B. Lee, T. Moehl, A. Marchioro, S.-J. Moon, R. Humphry-Baker, J.-H. Yum, J. E. Moser, et al., *Lead iodide perovskite sensitized all-solid-state submicron thin film mesoscopic solar cell with efficiency exceeding 9%*, *Scientific reports* 2 (2012) 591.
- [27] M. M. Lee, J. Teuscher, T. Miyasaka, T. N. Murakami, H. J. Snaith, *Efficient hybrid solar cells based on meso-superstructured organometal halide perovskites*, *Science* 338 (2012) 643–647.
- [28] O. Malinkiewicz, A. Yella, Y. H. Lee, G. M. Espallargas, M. Graetzel, M. K. Nazeeruddin, H. J. Bolink, *Perovskite solar cells employing organic charge-transport layers*, *Nature Photonics* 8 (2014) 128–132.
- [29] G. Dong, Y. Yang, L. Sheng, D. Xia, T. Su, R. Fan, Y. Shi, J. Wang, *Inverted thermal annealing of perovskite films: a method for enhancing photovoltaic device efficiency*, *RSC advances* 6 (2016) 44034–44040.

- [30] S. De Wolf, J. Holovsky, S.J. Moon, P. Loper, B. Niesen, M. Ledinsky, F.J. Haug, J.H. Yum, C. Ballif, *Organometallic halide perovskites: sharp optical absorption edge and its relation to photovoltaic performance*, *The journal of physical chemistry letters* 5 (2014) 1035–1039.
- [31] M. Saliba, T. Matsui, K. Domanski, J.-P. Correa-Baena, M. K. Nazeeruddin, S. M. Zakeeruddin, A. Hagfeldt, et al., *Cesium-containing triple cation perovskite solar cells: improved stability, reproducibility and high efficiency*, *Energy environmental science* 9 (2016) 1989–1997.
- [32] W. S. Yang, B.W. Park, E. H. Jung, N. J. Jeon, Y. C. Kim, D. U. Lee, S. S. Shin, J. Seo, E. K. Kim, J. H. Noh, et al., *Iodide management in formamidinium-lead-halide based perovskite layers for efficient solar cells*, *Science* 356 (2017) 1376–1379.
- [33] D. Zhao, C. Wang, Z. Song, Y. Yu, C. Chen, X. Zhao, K. Zhu, Y. Yan, *Four-terminal all-perovskite tandem solar cells achieving power conversion efficiencies exceeding 23%*, *ACS Energy Letters* 3 (2018) 305–306.
- [34] Q. Jiang, Y. Zhao, X. Zhang, X. Yang, Y. Chen, Z. Chu, Q. Ye, X. Li, Z. Yin, J. You, *Author correction: Surface passivation of perovskite film for efficient solar cells*, *Nature Photonics* 13 (2019) 500–500.
- [35] Shockley W. and Queisser H. J. *Detailed balance limit of efficiency of p-n junction solar cells*. *J. Appl. Phys*, 32:510–519, 1961.
- [36] F. Sahli, J. Werner, B. A. Kamino, M. Bräuninger, R. Monnard, B. Paviet-Salomon, L. Barraud, L. Ding, J. J. D. Leon, D. Sacchetto, et al., *Fully textured monolithic perovskite/silicon tandem solar cells with 25.2% power conversion efficiency*, *Nature materials* 17 (2018) 820–826.
- [37] A. N., B. V., *The future of energy supply: Challenges and opportunities*, *Angew. Chem. Int. Ed.* 46 (2007) 5266.
- [38] D. G., S. M. C., B. C. J., *Polymer-fullerene bulk-heterojunction solar cells*, *Adv. Mater* 46 (2009) 1323–1338.

- [39] K. Shen, H. L. Sun, G. Ji, Y. Yang, Z. Jiang, F. Song, *Fabrication and characterization of organic inorganic hybrid perovskite devices with external doping*, *Nanoelectronics and Materials Development* (2016) 95.
- [40] M. R. Filip, G. Volonakis, F. Giustino, *Hybrid halide perovskites: Fundamental theory and materials design*, *Handbook of Materials Modeling: Applications: Current and Emerging Materials* (2020) 295–324.
- [41] B. E., K. F. C., *Low band gap polymers for organic photovoltaics*, *Sol. Energy Mater. Sol. Cells* 91 (2007) 954985.
- [42] S. W., Q. H. J., *Detailed balance limit of efficiency of p-n junction solar cells*, *J. Appl. Phys* 32 (1961) 510–519.
- [43] Q. Zhu, X. Bao, J. Yu, D. Zhu, M. Qiu, R. Yang, L. Dong, *Compact layer free perovskite solar cells with a high-mobility hole-transporting layer*, *ACS applied materials interfaces* 8 (2016) 2652–2657.
- [44] S. Aharon, S. Gamliel, B. El Cohen, L. Etgar, *Depletion region effect of highly efficient hole conductor free ch<sub>3</sub>nh<sub>3</sub>pbi<sub>3</sub> perovskite solar cells*, *Physical Chemistry Chemical Physics* 16 (2014) 10512–10518.
- [45] B. Suarez, V. Gonzalez-Pedro, T. S. Ripolles, R. S. Sanchez, L. Otero, I. Mora-Sero, *Recombination study of combined halides (cl, br, i) perovskite solar cells*, *The journal of physical chemistry letters* 5 (2014) 1628–1635.
- [46] D. Liu, W. Zha, J. Chen, R. Sa, *Theoretical study of structural stability, electronic and optical properties of ma<sub>1-x</sub>cs<sub>x</sub>pbi<sub>3</sub> for photovoltaic applications*, *Applied Physics Express* 13 (2019) 011007.
- [47] R. Sa, M. Liu, W. Zha, *Effect of rubidium incorporation on the structural, electronic and properties of mapbi<sub>3</sub>*, *Chemical Physics Letters* 743 (2020) 137179.
- [48] A. Polman, M. Knight, E. C. Garnett, B. Ehrler, W. C. Sinke, *Photovoltaic materials: Present efficiencies and future challenges*, *Science* 352 (2016).
- [49] J. Even, L. Pedesseau, C. Katan, *Analysis of multivalley and multibandgap absorption and enhancement of free carriers related to exciton screening in hybrid perovskites*, *The Journal of Physical Chemistry C* 118 (2014) 11566–11572.

- [50] Y. Yang, D. P. Ostrowski, R. M. France, K. Zhu, J. Van De Lagemaat, J. M. Luther, M. C. Beard, *Observation of a hot-phonon bottleneck in lead-iodide perovskites*, *Nature Photonics* 10 (2016) 53–59.
- [51] Endres, D. A. Egger, M. Kulbak, R. A. Kerner, L. Zhao, S. H. Silver, G. Hodes, B. P. Rand, D. Cahen, L. Kronik, et al., *Valence and conduction band densities of states of metal halide perovskites: a combined experimental–theoretical study*, *The journal of physical chemistry letters* 7 (2016) 2722–2729.
- [52] R. Bhatta, M. Tsige, *Understanding the effect of heteroatoms on structural and electronic properties of conjugated polymers*, *Polymer* 56 (2015) 293–299.
- [53] S. Niu, H. Huyan, M. Yeung, K. Ye, L. Blankemeier, T. Orvis, D. Sarkar, D. J. Singh, R. Kapadia, et al., *Bandgap control via structural and chemical tuning of transition metal perovskite chalcogenides*, *Advanced Materials* 29 (2017) 1604733.
- [54] M.G. Ju, J. Dai, L. Ma, X. C. Zeng, *Perovskite chalcogenides with optimal bandgap and desired optical absorption for photovoltaic devices*, *Advanced Energy Materials* 7 (2017) 1700216.
- [55] K. Kuhar, A. Crovetto, M. Pandey, K. S. Thygesen, B. Seger, P. C. Vesborg, O. Hansen, I. Chorkendorff, K. W. Jacobsen, *Sulfide perovskites for solar energy conversion applications: computational screening and synthesis of the selected compound layers*, *Energy Environmental Science* 10 (2017) 2579–2593.
- [56] S. Kořbel, M. A. Marques, S. Botti, *Stability and electronic properties of new inorganic perovskites from high-throughput ab initio calculations*, *Journal of Materials Chemistry C* 4 (2016) 3157–3167.
- [57] Y.Y. Sun, M. L. Agiorgousis, P. Zhang, S. Zhang, *Chalcogenide perovskites for photovoltaics*, *Nano letters* 15 (2015) 581–585.
- [58] J. Heo, L. Yu, E. Altschul, B. E. Waters, J. F. Wager, A. Zunger, D. A. Keszler, *Cu<sup>2+</sup>: Intermetal d–d transitions enable high solar absorption*, *Chemistry of Materials* 29 (2017) 2594–2598.

- [59] H. Park, F. H. Alharbi, S. Sanvito, N. Tabet, F. El-Mellouhi, *Elucidating the impact of chalcogen content on the photovoltaic properties of oxychalcogenide perovskites:  $\text{NamO}_3\text{-}x\text{q}_x$  ( $m = \text{nb, ta}$ ;  $q = \text{s, se, te}$ ), *ChemPhysChem* 19 (2018) 703–714.*
- [60] R. Jaramillo, J. Ravichandran, *In praise and in search of highly-polarizable semiconductors, arXiv preprint arXiv:1907.04600* (2019).
- [61] J. W. Bennett, I. Grinberg, A. M. Rappe, *Effect of substituting of s for o: The sulfide perovskite  $\text{Ba}_2\text{S}_2\text{O}_7$  investigated with density functional theory, *Physical Review B* 79 (2009) 235115.*
- [62] W. Meng, B. Saparov, F. Hong, J. Wang, D. B. Mitzi, Y. Yan, *Alloying and defect control within chalcogenide perovskites for optimized photovoltaic application, *Chemistry of Materials* 28 (2016) 821–829.*
- [63] J. A'vila, C. Momblona, P. P. Boix, M. Sessolo, H. J. Bolink, *Vapor-deposited perovskites: the route to high-performance solar cell production?, *Joule* 1 (2017) 431–442.*
- [64] S. Shi, Y. Li, X. Li, H. Wang, *Advancements in all-solid-state hybrid solar cells based on organometal halide perovskites, *Materials Horizons* 2 (2015) 378–405.*
- [65] J. S., G. S., P. U., *X-ray structural and crystallinity studies of low and high molecular weight poly(3-hexylthiophene), *Physica Status Solidi Applied Research* 205 (2008) 488–496.*
- [66] R. Kline, D. DeLongchamp, D. Fischer, E. Lin, L. Richter, M. Chabinyc, M. Toney, M. Heeney, I. McCulloch, *Critical role of side-chain attachment density on the order and device performance of polythiophenes, *Macromolecules* 40 (2007) 7960–7965.*
- [67] R. S. Bhatta, Y. Y. Yimer, M. Tsige, D. S. Perry, *Conformations and torsional potentials of poly(3-hexylthiophene) oligomers: Density functional calculations up to the dodecamer, *Computational and Theoretical Chemistry* 995 (2012) 36–42.*
- [68] B. Ram, Y. Yeneneh, P. David, M. Tsige, *Improved force field for molecular modeling of poly(3-hexylthiophene), *J. Phys. Chem* 117 (2013).*

- [69] A. Mattoni, A. Filippetti, M. Saba, C. Caddeo, P. Delugas, *Temperature evolution of methylammonium trihalide vibrations at the atomic scale*, *The Journal of Physical Chemistry Letters* 7 (2016) 529–535.
- [70] M. Taufique, S. Mortuza, S. Banerjee, *Mechanistic insight into the attachment of fullerene derivatives on crystal faces of methylammonium lead iodide based perovskites*, *The Journal of Physical Chemistry C* 120 (2016) 22426–22432.
- [71] W.-J. Yin, J.-H. Yang, J. Kang, Y. Yan, S.-H. Wei, *Halide perovskite materials for solar cells: a theoretical review*, *Journal of Materials Chemistry A* 3 (2015) 8926–8942.
- [72] A. Walsh, *Principles of chemical bonding and band gap engineering in hybrid organic–inorganic halide perovskites*, *The Journal of Physical Chemistry C* 119 (2015) 5755–5760.
- [73] J. M. Frost, A. Walsh, *What is moving in hybrid halide perovskite solar cells?*, *Accounts of chemical research* 49 (2016) 528–535.
- [74] A. Mattoni, A. Filippetti, C. Caddeo, *Modeling hybrid perovskites by molecular dynamics*, *Journal of Physics: Condensed Matter* 29 (2016) 043001.
- [75] M. C. Zerner, *Semiempirical molecular orbital methods*, *Reviews in computational chemistry* 2 (1991) 313–365.
- [76] T. D. Crawford, M. C. Tam, M. L. Abrams, *The current state of ab initio calculations of optical rotation and electronic circular dichroism spectra*, *The Journal of Physical Chemistry A* 111 (2007) 12057–12068.
- [77] P. Suryanarayana, V. Gavini, T. Blesgen, K. Bhattacharya, M. Ortiz, *Non-periodic finite-element formulation of kohn–sham density functional theory*, *Journal of the Mechanics and Physics of Solids* 58 (2010) 256–280.
- [78] L. I.N, *Quantum Chemistry*, Prentice hall, 2008. Burke K. Burke, *Perspective on density functional theory*, *J. Chem. Phys.* 23 (2007) 542–548.
- [79] T. L.H, *The calculation of atomic fields*, *Math. Proc. Cambridge Philos. Soc.* 136 (1927) 150901. 81. F. E, *Eine statistische methode zur bestimmung einiger eigen-*

- schaften des atoms und ihre anwendung auf die theorie des periodischen systems der elemente, Physik 48 (1928) 73.*
- [80] P. Hohenberg, W. Kohn, *Inhomogeneous electron gas, Phys. Rev.* 136 (1964) B864–B871.
- [81] Mohammed Istafaul Haque Ansari, Ahsanulhaq Qurashi, and Mohammad Khaja Nazeeruddin. *Frontiers, opportunities, and challenges in perovskite solar cells: A critical review. Journal of Photochemistry and Photobiology C: Photochemistry Reviews*, 35:1–24, 2018
- [82] W. Kohn, L. J. Sham, *Self-consistent equations including exchange and correlation effects, Phys. Rev.* 140 (1965) A1133–A1138.
- [83] B. AD, *Density-functional thermochemistry. iii. the role of exact exchange, J. Chem. Phys* 98 (1993) 5648–5652.
- [84] C. Lee, W. Yang, R. G. Parr, *Development of the colle-salvetti correlation-energy formula into a functional of the electron density, Phys. Rev. B* 37 (1988) 785–789.
- [85] K. Burke, *Perspective on density functional theory, The Journal of chemical physics* 136 (2012) 150901.
- [86] R. O. Jones, O. Gunnarsson, *The density functional formalism, its applications and prospects, Rev. Mod. Phys.* 61 (1989) 689–746. 88. G. E. K. U., O. L. N., K. W., *Density-functional theory for ensembles of fractionally occupied states. i. basic formalism, Phys. Rev. A* 37 (1988) 2809–2820.
- [87] Y. Andersson, D. C. Langreth, B. I. Lundqvist, *van der waals interactions in density-functional theory, Phys. Rev. Lett.* 76 (1996) 102–105.
- [88] Thomas L.H. *The calculation of atomic fields. Math. Proc. Cambridge Philos. Soc.*, 136:150901, 1927
- [89] D. M., R. H., S. E., L. D.C., L. B. I., *Van der waals density functional for general geometries, Phys. Rev. Lett.* 92 (2004) 246401.
- [90] Stefan.Grimme, *Semiempirical gga-type density functional constructed with a long-range dispersion correction, J. Comp. Chem* 27 (2006) 1787–1799.

- [91] J. P. C. J., H. P., S. DR., *Density functional theory augmented with an empirical dispersion term. interaction energies and geometries of 80 noncovalent complexes compared with ab initio quantum mechanics calculations.*, *J Comput Chem.* 28 (2007) 555–569.
- [92] J. P., S. J., C. J., H. P., *Benchmark database of accurate (mp2 and ccSD(T) complete basis set limit) interaction energies of small model complexes, dna base pairs, and amino acid pairs*, *Phys. Chem. Chem. Phys* 8 (2006) 1985–93.
- [93] C. Van Caillie, R. D. Amos, *Geometric derivatives of density functional theory excitation energies using gradient-corrected functionals*, *Chemical Physics Letters* 317 (2000) 159–164.
- [94] O. L. N., G. E. K. U., K. W., *Density-functional theory for ensembles of fractionally occupied states. ii. application to the he atom*, *Phys. Rev. A* 37 (1988) 2821–2833.
- [95] R. Erich, G. E. K. U., *Density-functional theory for time-dependent systems*, *Phys. Rev. Lett.* 52 (1984) 997–1000.
- [96] A. Dualeh, T. Moehl, N. Te´treault, J. Teuscher, P. Gao, M. K. Nazeeruddin, M. Gratzel, *Impedance spectroscopic analysis of lead iodide perovskite-sensitized solid-state solar cells*, *ACS nano* 8 (2014) 362–373.
- [97] F. Bella, G. Griffini, J.-P. Correa-Baena, G. Saracco, M. Gra¨tzel, A. Hagfeldt, S. Turri, C. Gerbaldi, *Improving efficiency and stability of perovskite solar cells with photocurable fluoropolymers*, *Science* 354 (2016) 203–206.
- [98] J. Yang, B. D. Siempelkamp, D. Liu, T. L. Kelly, *Investigation of  $\text{CH}_3\text{NH}_3\text{PbI}_3$  degradation rates and mechanisms in controlled humidity environments using in situ techniques*, *ACS nano* 9 (2015) 1955–1963.
- [99] P. Hohenberg and W. Kohn. *Inhomogeneous electron gas*. *Phys. Rev.*, 136:B864–B871, 1964.
- [100] G. Niu, X. Guo, L. Wang, *Review of recent progress in chemical stability of perovskite solar cells*, *Journal of Materials Chemistry A* 3 (2015) 8970–8980.

- [101] R. Wang, M. Mujahid, Y. Duan, Z.-K. Wang, J. Xue, Y. Yang, *A review of perovskites solar cell stability*, *Advanced Functional Materials* 29 (2019) 1808843.
- [102] V. M. Goldschmidt, *Die gesetze der krystallochemie*, *Naturwissenschaften* 14 (1926) 477–485.
- [103] M. A. Green, A. HoBaillie, H. J. Snaith, *The emergence of perovskite solar cells*, *Nature photonics* 8 (2014) 506–514.
- [104] W. Li, Z. Wang, F. Deschler, S. Gao, R. H. Friend, A. K. Cheetham, *Chemically diverse and multifunctional hybrid organic–inorganic perovskites*, *Nature Reviews Materials* 2 (2017) 16099.
- [105] Z. Li, M. Yang, J.-S. Park, S.-H. Wei, J. J. Berry, K. Zhu, *Stabilizing perovskite structures by tuning tolerance factor: formation of formamidinium and cesium lead iodide solid-state alloys*, *Chemistry of Materials* 28 (2016) 284–292.
- [106] A. Amat, E. Mosconi, E. Ronca, C. Quarti, P. Umari, M. K. Nazeeruddin, M. Gratzel, F. De Angelis, *Cation-induced band-gap tuning in organohalide perovskites: interplay of spin–orbit coupling and octahedra tilting*, *Nano letters* 14 (2014) 3608–3616.
- [107] M. R. Filip, G. E. Eperon, H. J. Snaith, F. Giustino, *Steric engineering of metal-halide perovskites with tunable optical band gaps*, *Nature communications* 5 (2014) 1–9.
- [108] M. R. Filip, F. Giustino, *Computational screening of homovalent lead substitution in organic–inorganic halide perovskites*, *The Journal of Physical Chemistry C* 120 (2016) 166–173.
- [109] A. Babayigit, A. Ethirajan, M. Muller, B. Conings, *Toxicity of organometal halide perovskite solar cells*, *Nature materials* 15 (2016) 247.
- [110] L. K. Ono, E. J. Juarez-Perez, Y. Qi, *Progress on perovskite materials and solar cells with mixed cations and halide anions*, *ACS applied materials interfaces* 9 (2017) 30197–30246.

- [111] L. K. Ono, E. J. Juarez-Perez, Y. Qi, *Progress on novel perovskite materials and solar cells with mixed cations and halide anions*.7 (2010).
- [112] G. Kieslich, S. Sun, A. K. Cheetham, *An extended tolerance factor approach for organic–inorganic perovskites*, *Chemical science* 6 (2015) 3430–3433. Kwon Y. Kwon, J. Lim, H. Yun, Y. Kim, T. Park, *Energy environ. sci.* 7, 1454 (2014), 1009 .
- [113] H. Zhou, Q. Chen, G. Li, S. Luo, T.-b. Song, H.-S. Duan, Z. Hong, J. You, Y. Liu, Y. Yang, *Interface engineering of highly efficient perovskite solar cells*, *Science* 345 (2014) 542–546.
- [114] H.-H. Huang, Y.-C. Shih, L. Wang, K.-F. Lin, *Boosting the ultra-stable unencapsulated perovskite solar cells by using montmorillonite/CH<sub>3</sub>CH<sub>3</sub>PbI<sub>3</sub> nanocomposite as photoactive layer*, *Energy Environmental Science* 12 (2019) 1265–1273.
- [115] G. Longo, L. Gil-Escrig, M. J. Degen, M. Sessolo, H. J. Bolink, *Perovskite solar cells prepared by flash evaporation*, *Chemical Communications* 51 (2015) 7376–7378.
- [116] M. D. Kempe, A. A. Dameron, M. O. Reese, *Evaluation of moisture ingress from the perimeter of photovoltaic modules*, *Progress in Photovoltaics: Research and Applications* 22 (2014) 1159–1171.
- [117] C. Clegg, I. G. Hill, *Systematic study on the impact of water on the performance and stability of perovskite solar cells*, *Rsc Advances* 6 (2016) 52448–52458.
- [118] L. Zhang, M.G. Ju, W. Liang, *The effect of moisture on the structures and properties of lead halide perovskites: a first-principles theoretical investigation*, *Physical Chemistry Chemical Physics* 18 (2016) 23174–23183.
- [119] R. Long, W. Fang, O. V. Prezhdo, *Moderate humidity delays electron–hole recombination in hybrid organic inorganic perovskites: Timedomain ab initio simulations rationalize experiments*, *The journal of physical chemistry letters* 7 (2016) 3215–3222.
- [120] Y. Guo, C. Li, X. Li, Y. Niu, S. Hou, F. Wang, *Effects of rb incorporation and water degradation on the stability of the cubic formamidinium lead iodide perovskite surface: a first-principles study*, *The Journal of Physical Chemistry C* 121 (2017) 12711–12717.

- [121] X. Dong, X. Fang, M. Lv, B. Lin, S. Zhang, J. Ding, N. Yuan, *Improvement of the humidity stability of organic–inorganic perovskite solar cells using ultrathin al 2 o 3 layers prepared by atomic layer deposition*, *Journal of Materials Chemistry A* 3 (2015) 5360–5367.
- [122] N. Z. Koocher, D. Saldana-Greco, F. Wang, S. Liu, A. M. Rappe, *Polarization dependence of water adsorption to ch<sub>3</sub>nh<sub>3</sub>pb<sub>3</sub> (001) surfaces*, *The journal of physical chemistry letters* 6 (2015) 4371–4378.
- [123] Z. Song, S. C. Watthage, A. B. Phillips, G. K. Liyanage, R. R. M. J. Heben, *Investigation of degradation mechanisms of perovskite-based photovoltaic devices using laser beam induced current mapping*, in: *Thin Films for Solar and Energy Technology VII*, volume 9561, *International Society for Optics and Photonics*, 2015, p. 956107.
- [124] Y. Rong, L. Liu, A. Mei, X. Li, H. Han, *Beyond efficiency: the challenge of stability in mesoscopic perovskite solar cells*, *Advanced Energy Materials* 5 (2015) 1501066.
- [125] W. Charles Lawrence Kamuyu, J. R. Lim, C. S. Won, H. K. Ahn, *Prediction model of photovoltaic module temperature for power performance of floating pvs*, *Energies* 11 (2018) 447.
- [126] Y. F. Makableh, I. A. Awad, W. Hassan, G. Aljaiuossi, *Enhancement of the thermal properties of heterojunction perovskite solar cells by nanostructured contacts design*, *Solar Energy* 202 (2020) 204–209.
- [127] S. Zandi, P. Saxena, N. E. Gorji, *Numerical simulation of heat distribution in rgo-contacted perovskite solar cells using comsol*, *Solar Energy* 197 (2020) 105–110.
- [128] S. Lee, S. Kim, S. Bae, K. Cho, T. Chung, L. Mundt, S. Lee, S. Park, H. Park, M. Schubert, et al., *Uv degradation and recovery of perovskite solar cells sci*, *Rep* 6 (2016) 38150.
- [129] Nasibeh Mansour Rezaei Fumani, Farzaneh Arabpour Roghabadi, Maryam Ali-daei, Seyed Mojtaba Sadrameli, Vahid Ahmadi, and Farhood Najafi. *Prolonged lifetime of perovskite solar cells using a moisture-blocked and temperature-controlled*

- encapsulation system comprising a phase change material as a cooling agent. ACS omega*, 5(13):7106–7114, 2020.
- [130] T. Leijtens, G. E. Eperon, S. Pathak, A. Abate, M. M. Lee, H. J. Snaith, *Overcoming ultraviolet light instability of sensitized tio 2 with meso-superstructured organometal tri-halide perovskite solar cells*, *Nature communications* 4 (2013) 1–8.
- [131] S. Ito, S. Tanaka, K. Manabe, H. Nishino, *Effects of surface blocking layer of sb2s3 on nanocrystalline tio2 for ch3nh3pb3 perovskite solar cells*, *The Journal of Physical Chemistry C* 118 (2014) 16995–17000.
- [132] S. K. Pathak, A. Abate, T. Leijtens, D. J. Hollman, J. Teuscher, L. Pazos, P. Docampo, U. Steiner, H. J. Snaith, *Towards long-term photostability of solid-state dye sensitized solar cells*, *Advanced Energy Materials* 4 (2014) 1301667.
- [133] E. L. Unger, E. T. Hoke, C. D. Bailie, W. H. Nguyen, A. R. Bowring, T. Heumu¨ller, M. G. Christoforo, M. D. McGehee, *Hysteresis and transient behavior in current–voltage measurements of hybrid-perovskite absorber solar cells*, *Energy Environmental Science* 7 (2014) 3690–3698.
- [134] N. Arora, M. I. Dar, A. Hinderhofer, N. Pellet, F. Schreiber, S. M. Zakeeruddin, M. Gra¨tzel, *Perovskite solar cells with cusc n hole extraction layers yield stabilized efficiencies greater than 20%*, *Science* 358 (2017) 768–771.
- [135] H.-W. Chen, N. Sakai, M. Ikegami, T. Miyasaka, *Emergence of hysteresis and transient ferroelectric response in organo-lead halide perovskite solar cells*, *The journal of physical chemistry letters* 6 (2015) 164–169.
- [136] J. M. Azpiroz, E. Mosconi, J. Bisquert, F. De Angelis, *Defect migration in methylammonium lead iodide and its role in perovskite solar cell operation*, *Energy Environmental Science* 8 (2015) 2118–2127.
- [137] S. Liu, F. Zheng, N. Z. Koocher, H. Takenaka, F. Wang, A. M. Rappe, *Ferroelectric domain wall induced band gap reduction and charge separation in organometal halide perovskites*, *The journal of physical chemistry letters* 6 (2015) 693–699.

- [138] J. Wei, Y. Zhao, H. Li, G. Li, J. Pan, D. Xu, Q. Zhao, D. Yu, *Hysteresis analysis based on the ferroelectric effect in hybrid perovskite solar cells*, *The journal of physical chemistry letters* 5 (2014) 3937–3945.
- [139] H.-S. Kim, N.-G. Park, *Parameters affecting  $i-v$  hysteresis of perovskite solar cells: effects of perovskite crystal size and mesoporous  $\text{TiO}_2$  layer*, *The journal of physical chemistry letters* 5 (2014) 2927–2934.
- [140] Y. Shao, Z. Xiao, C. Bi, Y. Yuan, J. Huang, *Origin and elimination of photocurrent hysteresis by fullerene passivation in  $\text{CH}_3\text{NH}_3\text{PbI}_3$  planar heterojunction solar cells*, *Nature communications* 5 (2014) 1–7.
- [141] J.-W. Lee, Z. Dai, T.-H. Han, C. Choi, S.-Y. Chang, S.-J. Lee, N. De Marco, H. Zhao, P. Sun, Y. Huang, et al., *2d perovskite stabilized phase-pure formamidinium perovskite solar cells*, *Nature communications* 9 (2018) 1–10.
- [142] G. Tumen-Ulzii, T. Matsushima, D. Klotz, M. R. Leyden, P. Wang, C. Qin, J.-W. Lee, S.-J. Lee, Y. Yang, C. Adachi, *Hysteresis-less and stable perovskite solar cells with a self-assembled monolayer*, *Communications Materials* 1 (2020) 1–7.
- [143] W. Zhou, S. Chen, Y. Zhao, Q. Li, Y. Zhao, R. Fu, D. Yu, P. Gao, Q. Zhao, *Constructing  $\text{CsPbBr}_3$  cluster passivated-triple cation perovskite for highly efficient and operationally stable solar cells*, *Advanced Functional Materials* 29 (2019) 1809180.
- [144] J. Cao, S. X. Tao, P. A. Bobbert, C.-P. Wong, N. Zhao, *Interstitial occupancy by extrinsic alkali cations in perovskites and its impact on ion migration*, *Advanced Materials* 30 (2018) 1707350.

---

## CHAPTER 5

# Investigation of the structural and electronic properties of $Cs_2HfI_6$ using (DFT)

### 5.1 Abstract

Structure and electronic properties of the  $Cs_2HfI_6$  compound were studied based on density functional theory. The local density approximation (*LDA*) and generalized gradient approximations (*GGA*) for potential exchange-correlation. The density of state and structure of the electronic band was calculated. We obtained an indirect band-gap of 1.9 eV for  $Cs_2HfI_6$ , which increases its potential in the field of lead-free hybrid perovskite solar cells. the calculated energy band structure shows that the cubic perovskite  $Cs_2HfI_6$  is a semiconductor. The optical properties, the real and imaginary parts (dielectric function), refractive index, and absorptance coefficient were calculated.

### 5.2 Introduction

Perovskite solar cells show the most promising performance for power conversion efficiency (*PCE*) of the solar cell, more than 25.6% close to the Shock-ley–Queisser limit of 31.4% [1, 2]. However, the fast expansion of perovskite-based solar cells has two significant challenges: poor stability and toxicity [3, 4]. Pb-based perovskites

hold out as efficient structures in solar cells absorbs; thus, it remains essential to find suitable substitutes with excellent photoelectric properties and high stability [5, 6]. Regrettably, perovskites solar cells produced without lead show low efficiency [7]. Some progress has been reported on inorganic cells, and lead-free materials have been developed, such as (Sn, Ge) established perovskites, which exhibit photoelectric properties comparable to Pb-based materials [6]. The halide perovskite divalent metal cation-based oxidation from 2+ to 4+ state, but it is unstable due to phase transition [5]. In addition to the elements of trivalent metal ions of IVA group such as Bi or Sb as non-toxic substitution elements have garnered many studies with perfect stability but weak (*PCE*) when inserted into a perovskite device. Nowadays, new materials have been successfully synthesized both experimentally and computationally and they have been incorporated into solar cells, such as  $Cs_2Au_2I_6$  [8, 9] and  $Cs_2NaBiI_6$  [10]. At the same time, in the perovskite compounds, most tetravalent cations come from the transition metal (TM) elements, the cations in the B-site can also be in the 4+ state. An inclusive study of the TM based spatially required perovskites is helpful for the discovery of non-lead perovskites. Sakai *et al.* [8]  $Cs_2PdBr_6$  was synthesized by applying a solution method, and it shows a 1.6 eV optical band gap and good stability. Ju *et al* [7]. A theory study found a series of  $Ti^{4+}$  dependent on halide perovskite as Pb-free perovskite absorbers with appropriate bandgap, good absorption capacity, and long-term stability. In a similar work, Wang *et al* [11]. found an easy approach to synthesizing the big size single-crystal structure of  $Cs_2PtI_6$  good quality films. They showed an energy band gap of 1.37 eV, with a *PCE* of 0.73% [7]. This stability measurement that the *PSCs* without any encapsulation could retain almost 80% of their initial efficiency under various extreme conditions [12]. However, these studies mainly focused on a few select TM elements. Although double perovskites show high stability, they usually have a wide band gap  $> 1.5$  eV which dramatically reduces the photo-voltaic efficiency. Therefore, it is essential to improve lead-free, with tight energy gap materials for solar cells applications. The optical performance inspection of materials is essential for different purposes such as absorbs, transmission, refraction, reflectors and different optoelectronic equipment to know the material restraint to incident electromagnetic rays. We present a simple derivation of the dielectric function

which describes the linear relation between electrical displacement and the macroscopic electric field. Therefore, a dielectric function is calculated with the following Eq.(5.1) [12, 13]:

$$\varepsilon(\omega) = \varepsilon_1\omega + i\varepsilon_2(\omega), \quad (5.1)$$

where the real part represented by  $\varepsilon_1\omega$  and imagery part represent dielectric function by  $i\varepsilon_2(\omega)$ , the dielectric functional parts allow important properties parameters such as the refractive index is one of the optical properties ( $n(\omega)$  extinction coefficient  $k(\omega)$ , optical conductivity (real)  $\sigma_1(\omega)$  and (imaginary)  $\sigma_2(\omega)$ , refractive index  $R(\omega)$ , absorption coefficient  $\alpha(\omega)$  and loss function aspect to photon energy. As mentioned the refractive index  $n(\omega)$  is connected to the dielectric function  $\varepsilon(\omega)$  by Eq.(5.2):

$$\sqrt{\varepsilon(\omega)} = n(\omega) + i\kappa(\omega), \quad (5.2)$$

where  $i\kappa(\omega)$  is the extinction coefficient. Another important parameter is the absorption coefficient ( $\alpha$ ) which is described as the reciprocal of the depth of penetration of radiation into a bulk solid,

$$\alpha(\omega) = \frac{4\pi\kappa}{C}, \quad (5.3)$$

where  $4\pi\kappa$  is Extinction coefficient,  $C$  is a light constant. Dielectric function refractive index and absorption coefficient, they can be found by the equation as follows Eq.(5.4) and Eq.(5.5)

$$n(\omega) = \left[ \frac{1}{2}((\varepsilon_1(\omega)^2 + \varepsilon_2(\omega)^2) + (\varepsilon(\omega))) \right]^{\frac{1}{2}}, \quad (5.4)$$

$$\kappa(\omega) = \left[ \frac{1}{2}((\varepsilon_1(\omega)^2 + \varepsilon_2(\omega)^2) - (\varepsilon(\omega))) \right]^{\frac{1}{2}}. \quad (5.5)$$

In this work, we are utilizing the first principle (*DFT*) method, as implemented in quantum espresso, to investigate the electronic structure of cubic Cesium Hafnium iodide perovskite  $Cs_2HfI_6$ . Besides, to unravel the optical properties of these double perovskite materials.

## 5.3 Computational Details

### 5.3.1 Methodology

Computations were performed with (*DFT*). The simulation package (*QE*) software code was used for this purpose [14, 16]. Interaction of the Core-valence was expressed by using the Projector Augmented Wave (*PAW*) [17, 18]. The Generalized Gradient Approximation (*GGA*) was used with (*PBE*) exchange-correlation function [17]. The cut-off energy of plane-wave extending was set to 450 eV. The energy convergence of the total energy and force criterion was  $10^{-5}$  eV per atom during relaxation. The (*Scf*) calculation was done for the density of states calculation, and the (*nscf*) calculation, a K-point grid was set an  $8 \times 8 \times 8$  to achieve high accuracy. K-point a  $12 \times 12 \times 12$  was applied for the optical properties and electronic calculation of the  $Cs_2HfI_6$ . For  $2 \times 2 \times 2$  super-cell structure,  $3 \times 3 \times 3$  and  $4 \times 4 \times 4$  grids were performed of structural optimization and electronic calculation, respectively. The first brillouin zone was sampled using k-bath. We adopted *GGA* to calculate the band gap without considering the effect of spin-orbit coupling [19].

## 5.4 Results and Discussions

### 5.5 Geometric Structure

We started our *DFT* simulation  $Cs_2HfI_6$  with geometric optimization to ensure the accuracy of the calculation. The calculations were carried out of this cubic perovskite by the  $Pm\bar{3}m$  structure and crystal lattice constant of  $a = b = c = 8.3\text{\AA}$  [20]. The calculated lattice parameter of the  $Cs_2HfI_6$  are  $a = b = c = 7.42\text{\AA}$ ,  $\alpha = 59.9$

$\beta = 60.0001$   $\gamma = 59.9$ , and unit-cell volume =  $288.92\text{\AA}^3$ , this shows a decrease in the lattice parameter, which can be attributed to the smaller ionic of Hf.

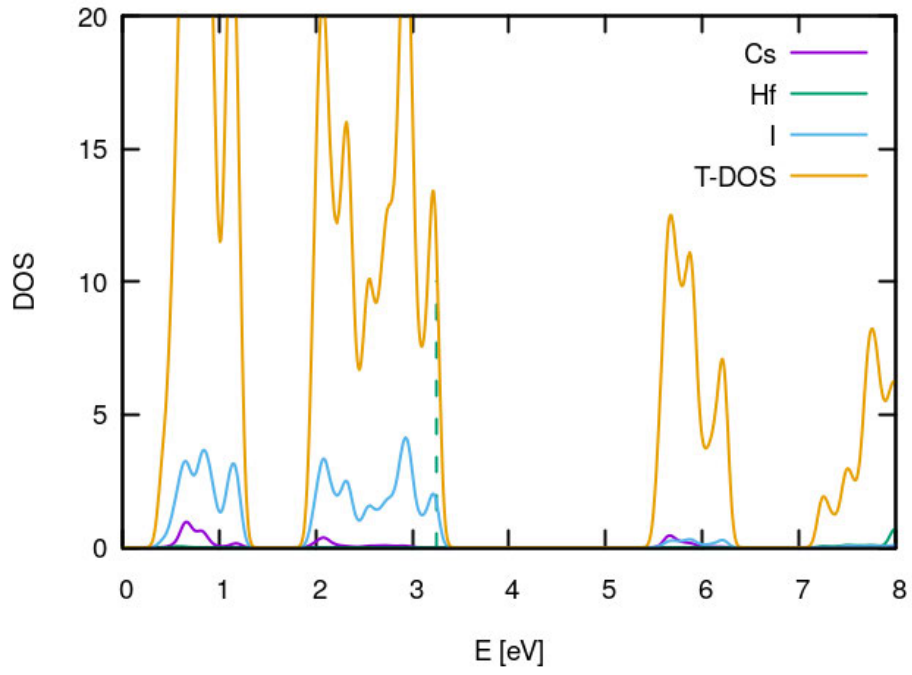


Figure 5.1: DOS and PDOS for  $Cs_2HfI_6$ .

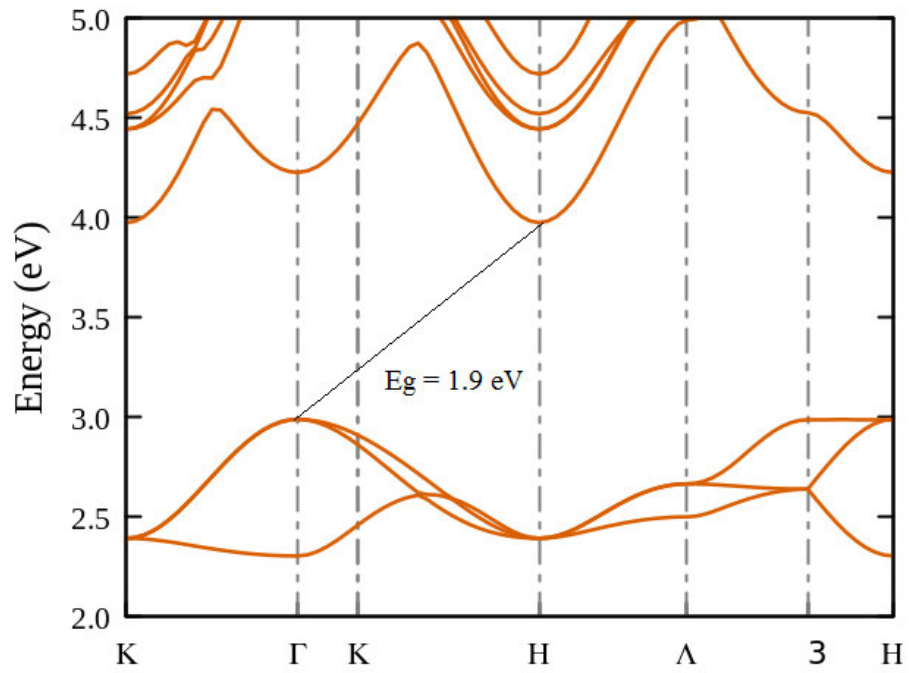


Figure 5.2: Band gap structure of  $Cs_2HfI_6$  perovskite.

## 5.6 Band structure of $Cs_2HfI_6$ and Density of State

One of the essential characteristics to be studied is the band gap of the materials, which plays a vital role in determining the behavior of the materials. Physical properties of solids state materials can be provided from electronic band structure as optical behavior can be explained successfully from the electronic band which form a foundation for solid-state devices as solar cells, etc. approximations of Density of state shown in (Fig.5.1). As shown in these figures, the wave vector for the valance band maximum (*VBM*) and the conduction band minimum (*CBM*) are similar, at the (0,0,0) point of the Brillouin zone, and hence,  $Cs_2HfI_6$  in the cubic phase has a direct band-gap at the Gamma ( $\Gamma$ ) point. A semiconductor is a material that has conductivity due to the flow of electrons, and its size is between a conductor and an insulator. For electronic excitation, it can be defined as a material whose energy ranges from zero to about 4 electron volts (eV) [21]. The band gap values from GGA approximations were calculated. This result shows that the band gap of 1.9 eV obtained is a semiconductor material. So far, no earlier published theoretical and experimental works compare with this calculated result for  $Cs_2HfI_6$ . The electronic density of states (*DOS*) defines as the number of electronic energy states per unit energy at each energy level that is available to be occupied by the electrons. The total electronic density of states of  $Cs_2HfI_6$  at zero pressure is shown in Fig.5.2 which can be used to describe the electronic structure.

## 5.7 Optical Properties of $Cs_2HfI_6$

Optical behavior of the  $Cs_2HfI_6$  was calculated from the complex dielectric function. We used one direction for the calculation of the coefficients using  $x = y = z$  due to its cubic structure. High dielectric constants are ideal for photo-voltaic applications because of a dielectric constant of 10 eV. the dielectric function imaginary part was calculated in the long-wavelength  $q \rightarrow 0$  limits, as displayed in Fig.5.3. A high absorption coefficient is desired in solar cell applications. The calculated

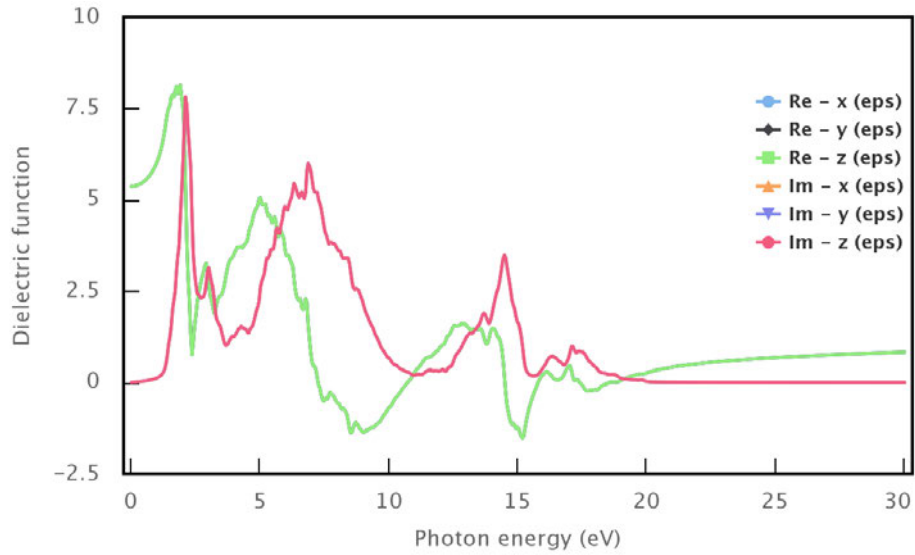


Figure 5.3: The real and imaginary parts of dielectric function of  $Cs_2HfI_6$  perovskite as a function of Photon energy.

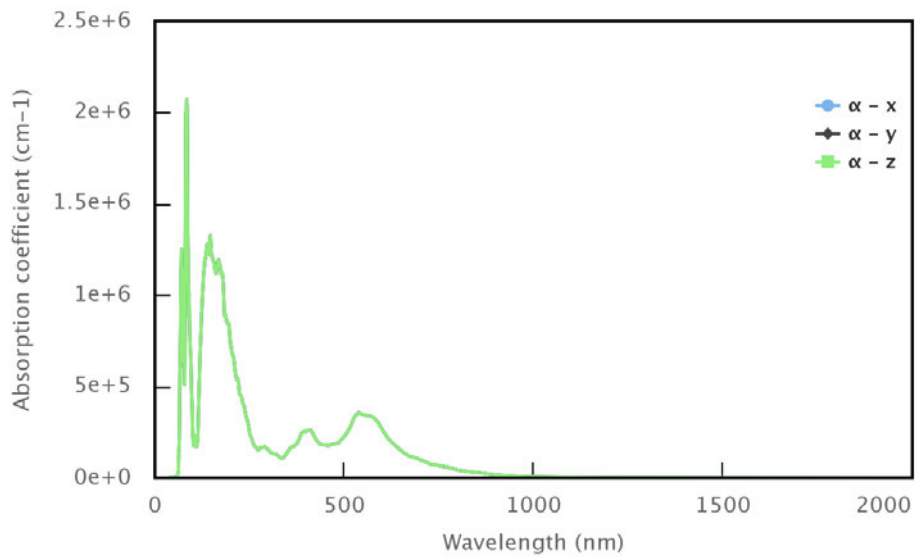


Figure 5.4: The absorption coefficient of  $Cs_2HfI_6$  perovskite as a function Photon energy.

absorption coefficient as a function of photon energy shown in Fig.5.4 shows the absorption curves of  $Cs_2HfI_6$  in the 400-900 nm domain, referred to as the relative band-gap value of its strong optical absorption. . The calculated other optical properties, such as Refractive index  $n(\omega)$  Fig.(5.5, Fig.5.6) were around 1.9 eV, which is close to the band energy calculated. Reflectivity index shown in (Fig.5.6))

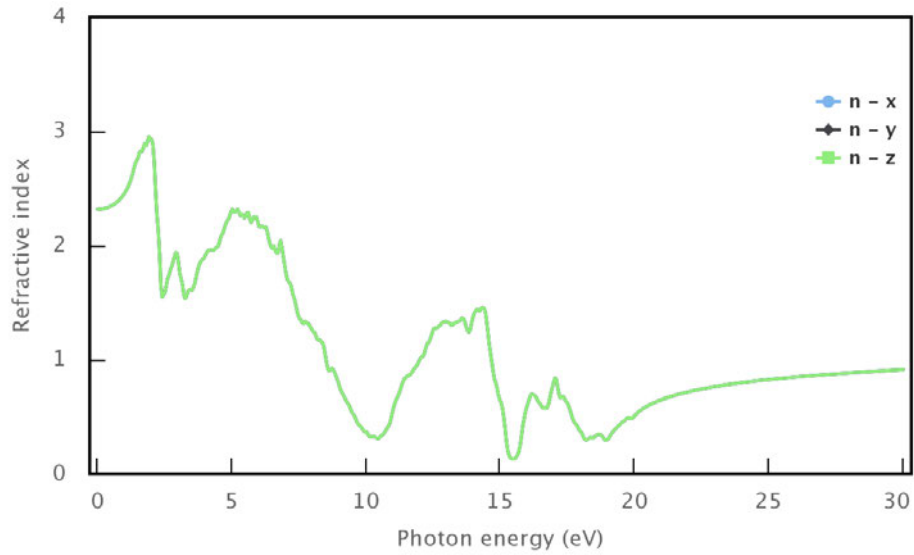


Figure 5.5: Refractive index real part of  $Cs_2HfI_6$ .

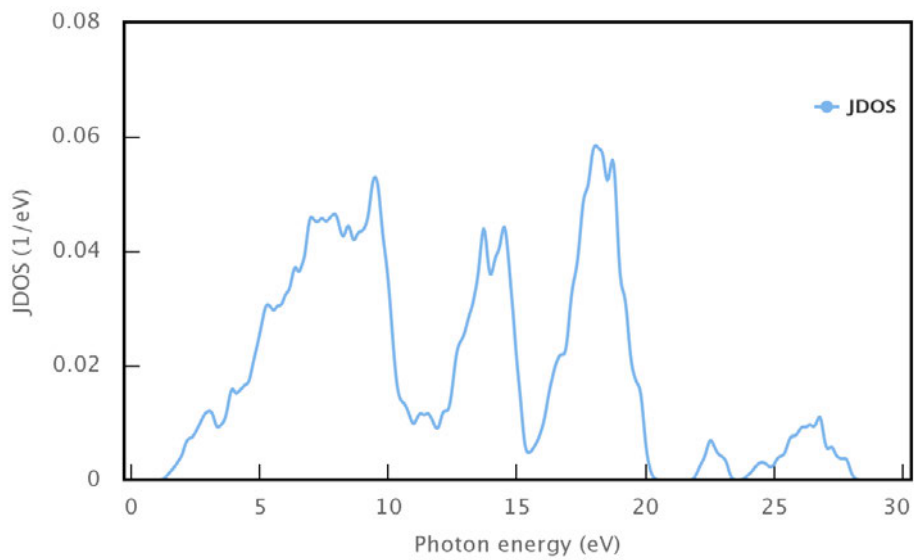


Figure 5.6: Reflectivity index of  $Cs_2HfI_6$ .

is a suitable optical band gap energy and loss function in the solar radiation energy range. It indicates that  $Cs_2HfI_6$  may be a promising candidate for light-absorbing materials in lead-free perovskite solar cells.

## Conclusion

This paper systematically studied the electronic structures and optical properties of the perovskite  $Cs_2HfI_6$  compound using the density-functional theory. Our results show that  $Cs_2HfI_6$  may be an excellent choice to use in perovskite photo voltaic devices. We have calculated a band gap of around 1.9 eV. Therefore, a *DFT* calculation could help to develop material for possible applications of the perovskite solar cell.

---

# References

- [1] W.Jian Yin, J. Hui Yang, Joongoo Kang, and Su-Huai Wei. *Halide perovskite materials for solar cells: a theoretical review*. *Journal of Materials Chemistry A*, 3(17):8926–8942, 2015.
- [2] S. Hsiang Chan, M. Chung Wu, Yi-Ying Li, Kun-Mu Lee, Yang-Fang Chen, and Wei-Fang Su. *Barium doping effect on the photovoltaic performance and stability of  $\text{MA}_{0.4}\text{FA}_{0.6}\text{BAPb}_{1-x}\text{YCl}_{3-y}$  perovskite solar cells*. *Applied Surface Science*, page 146451, 2020.
- [3] Henry J Snaith. *Present status and future prospects of perovskite photovoltaics*. *Nature materials*, 17(5):372–376, 2018.
- [4] A. Kumar Jena, Ashish Kulkarni, and Tsutomu Miyasaka. *Halide perovskite photovoltaics: background, status, and future prospects*. *Chemical reviews*, 119(5):3036–3103, 2019.
- [5] Alexander D Jodkowski, Daily Rodr'iguez-Adr'on, Rafael Luque, and Gustavo de Miguel. *Alternative perovskites for photovoltaics*. *Advanced Energy Materials*, 8(21):1703120, 2018.
- [6] Tsutomu Miyasaka, Ashish Kulkarni, Gyu Min Kim, Senol Oz, and Ajay K Jena. *Perovskite solar cells: Can we go organic-free, lead-free, and dopant-free*. *Advanced Energy Materials*, 10(13):1902500, 2020.
- [7] Julie Euvrard, Xiaoming Wang, Tianyang Li, Yanfa Yan, and David B Mitzi. *Is  $\text{Cs}_2\text{TiBr}_6$  a promising pb-free perovskite for solar energy applications*, *Journal of Materials Chemistry A*, 8(7):4049–4054, 2020.
- [8] Min Chen, Ming-Gang Ju, Alexander D Carl, Yingxia Zong, Ronald L Grimm, Jiajun Gu, Xiao Cheng Zeng, Yuanyuan Zhou, and Nitin P Padture. *Cesium ti-*

- tanium (iv) bromide thin films based stable lead-free perovskite solar cells. *Joule*, 2(3):558–570, 2018.
- [9] Chu Zhang, Liguao Gao, Siowhwa Teo, Zhanglin Guo, Zhenhua Xu, Shuai Zhao, and Tingli Ma. Design of a novel and highly stable lead-free  $\text{cs}_2\text{nabii}_6$  double perovskite for photovoltaic application. *Sustainable Energy Fuels*, 2(11):2419–2428, 2018.
- [10] CuncunWu, Qiaohui Zhang, Ganghong Liu, Zehao Zhang, DuoWang, Bo Qu, Zhi-jian Chen, and Lixin Xiao. From pb to bi: A promising family of pb-free optoelectronic materials and devices. *Advanced Energy Materials*, 10(13):1902496, 2020.
- [11] Lamjed Debbichi, Songju Lee, Hyunyoung Cho, Andrew M Rappe, Ki-Ha Hong, Min Seok Jang, and Hyungjun Kim. Mixed valence perovskite  $\text{cs}_2\text{au}_2\text{i}_6$ : A potential material for thin-film pb-free photovoltaic cells with ultrahigh efficiency. *Advanced Materials*, 30(12):1707001, 2018.
- [12] Shuzhang Yang, Liang Wang, Shuai Zhao, Anmin Liu, Yi Zhou, Qianji Han, Fengyang Yu, Liguao Gao, Chu Zhang, and Tingli Ma. A novel lead-free material  $\text{cs}_2\text{pti}_6$  with narrow bandgap and ultra-stable for its photovoltaic application. *ACS Applied Materials Interfaces*, 2020.
- [13] NWAshcroft and ND Mermin. *Solid state physics* (saunders, new york, 1976) p. 515; c. kittel. *Introduction to Solid State Physics*, pages 260–262, 2004.
- [14] P. G. O. Andreussi, T. Brumme, O Bunau, M Buongiorno Nardelli, M Calandra, R Sabatini, B Santra, MSchlipf, A P Seitsonen, A Smogunov, I Timrov,. *Advanced capabilities for materials modelling with quantum espresso. Journal of Physics: Condensed Matter*, 29(46):465901, 2017.
- [15] G. Kresse, J. Furthmüller, and J Hafner. Theory of the crystal structures of selenium and tellurium: the effect of generalized-gradient corrections to the local-density approximation. *Physical Review B*, 50(18):13181, 1994.
- [16] Peter Schwerdtfeger. The pseudopotential approximation in electronic structure theory. *ChemPhysChem*, 12(17):3143–3155, 2011.

- [17] *John P Perdew, Kieron Burke, and Matthias Ernzerhof. Generalized gradient approximation made simple. Physical review letters, 77(18):3865, 1996.*
- [18] *Yunkai Zhou, Yousef Saad, Murilo L Tiago, and James R Chelikowsky. Parallel self-consistent-field calculations via chebyshev-filtered subspace acceleration. Physical Review E, 74(6):066704, 2006.*
- [19] *M. Atikur Rahman et al. A review on semiconductors including applications and temperature effects in semiconductors. American Scientific Research Journal for Engineering, Technology, and Sciences (ASRJETS), 7(1):50–70, 2014.61.*
- [20] *Anubhav Jain, Shyue Ping Ong, Geoffroy Hautier, Wei Chen, William Davidson Richards, Stephen Dacek, Shreyas Cholia, Dan Gunter, David Skinner, Gerbrand Ceder, and Kristin a. Persson. The Materials Project: A materials genome approach to accelerating materials innovation. APL Materials, 1(1):011002, 2013.*
- [21] *Md Atikur Rahman et al. A review on semiconductors including applications and temperature effects in semiconductors. American Scientific Research Journal for Engineering, Technology, and Sciences (ASRJETS), 7(1):50–70, 2014.*

---

## CHAPTER 6

# Summary and future work

### 6.1 Summary

This work aims to study the various properties of the perovskite material compounds  $Cs_2HfI_6$  and  $Li_2TiO_3$  to provide helpful information of their applications in solar cells. The investigation is based on the calculation tool of density functional theory (DFT). We studied the perovskite material's structural, electronic and optical properties of the  $Cs_2HfI_6$  material. We estimated the efficiency of its solar cell based on the Shockley Quisel efficiency limit and the maximum efficiency limit of the spectroscopy. We calculated this approximation to estimate the electronic and optical properties of DFT and GW levels. GGA PBEsol calculates the band structure and PDOS. Our results are consistent with the available experimental data for  $Li_2TiO_3$ .

We hope that our prediction of  $Cs_2HfI_6$  will be experimentally confirmed in the nearest future. This project also reviewed the instability issues of perovskite solar cells. More research is needed to fully comprehend since perovskites photovoltaic technology is facing this significant problem. We have also reviewed strategies to improve the stability of perovskite solar cells against moisture, temperature, oxygen, and ultraviolet light. In addition, we have discussed the developments and basic structures of perovskite-based solar cells and explained several computational and experimental approaches to investigating the properties of these devices.

## 6.2 Future work

The conclusions from this research show that utilizing computational approaches to study properties of perovskites materials based on solar cells Increases the possibility of finding nontoxic materials with high efficiency.

The transition metals are promising candidates to decrease the toxicity and environmental stabilization of *PSCs* equipment, which are significant challenges in perovskites solar cells. In addition, the research on the optical properties of the materials and their applications in *PSC* devices also represents a fantastic direction in the future of solar energy.

Perovskite solar cells materials properties are motivated enormous potential to study. Many calculations by *DFT* can produce other properties not covered in this study as the mechanical properties, thermodynamic, magnetic and chemical properties. In addition, a good piece of work one can get interested in is comparing computational results with the experimental results of perovskite to accelerate the investigation of perovskite properties.